LUND UNIVERSITY

Turbo Charged Low Temperature Combustion - Experiments, Modeling and Control

Aulin, Hans

2011

Turbo Charged Low Temperature Combustion
Experiments, Modeling and Control

Turbo Charged Low Temperature Combustion
Experiments, Modeling and Control

Hans Aulin

Division of Combustion Engines
Department of Energy Sciences
Lund University
Lund, March 2011

To my Grandfather

Division of Combustion Engines
Department of Energy Sciences
Lund University
Box 118
SE-221 00 LUND
Sweden

Abstract

Both the global economy and the society in general are dependent on the availability of reliable transportation. Most transportation technology involves the use of internal combustion engines in one way or another. Because of the large numbers of internal combustion engines in use around the world, their emissions have a significant environmental impact. Therefore, considerable efforts have been invested into developing more sophisticated engine control systems and improving engine combustion behavior and post-treatment systems. These efforts have resulted in significant reductions in NO_x, CO, HC, and particulate matter emissions and further improvements can be expected. Emissions of the green house gas CO_2 were once unregulated, but has recently become the focus of considerable attention because of its role in global warming. The formation of CO_2 in an internal combustion engine is directly dependant on its efficiency. This, together with the fact that the Earth's oil resources are finite and rapidly diminishing, means that there remains a need for improvements in engine efficiency. Homogeneous Charge Compression Ignition (HCCI) and Partially Premixed Combustion (PPC) are "low-temperature" combustion techniques that can, if implemented correctly, allow for the development of engines with improved efficiency and low emissions of particulate matter and NO_x.

The objective of the work described in this thesis was to obtain insights into how these low temperature combustion processes can be controlled so as to achieve a high degree of combustion stability, low noise, and reliable transient performance. A set of control-oriented models of HCCI engines were developed. These models capture the engines dynamic behavior and have been used to design controllers that were tested on a real Turbo Negative Valve Overlap (NVO) HCCI Engine. Engines using these controllers exhibited improved transient performance compared to engines using a more conventional controller design.

A number of difficulties relating to load range and controllability were encountered in the studies on HCCI engines; it was suggested that PPC engines might suffer less from these problems. PPC represents a significant advance on HCCI in terms of controllability. However, in order to satisfy modern emissions criteria, it is necessary to operate PPC engines with extensive Exhaust Gas Recirculation (EGR). This presents some challenges relating to excessive rates of pressure increase during transient load increases. This problem was solved using a dual-injection strategy and model-based control.

Low-load PPC operation is difficult with high octane fuels. Various methods for extending the load tolerated by PPC were proposed; some, such as

switching to SI mode, were evaluated experimentally. To the best of the author's knowledge, these experiments were the first instances in which the mode of operation of an active engine was changed from SI to PPC and back.

In both PPC and HCCI, combustion is highly sensitive to environmental conditions. Some of these are not easy to measure or understand with sufficient accuracy to predict their impact. Some kind of combustion event feedback is therefore necessary. To this end, piezo-electric pressure sensors, an ion current sensor and a high precision torque sensor were evaluated as feedback sensors that could potentially provide this data.

The piezo-electric pressure transducer was found to be superior to the alternatives. Its readings are precise and provide accurate feedback on combustion timing. The ion current sensor was found to be a useful alternative at high and intermediate loads; unfortunately, at low loads, the signal-to-noise of the ion current signal is poor. An algorithm was proposed to improve the detection of the ion current, and was somewhat successful. Using a novel technique, data from the torque sensor was used in conjunction with combustion and black box models to obtain information on the combustion phasing.

Acknowledgments

I have many people to thank for getting this thesis written. First of all I would like to thank my supervisor, Per Tunestål. He is a very sympathetic man who in some way knows almost everything about everything.

I would also like to thank my co-supervisor, Bengt Johansson and my colleagues at SAAB for doing everything to figure out a solution for the continuation of the project.

Krister Olsson has provided for extremely fast computer support and fruitful discussions. All my colleagues at the departments deserve special thanks but in particular I want to mention Claes-Göran Zander, Sasa Trajkovic, Mehrzad Kaiadi, Magnus Lewander, Martin Algotsson, Patrick Borgqvist, Clement Chartier, Ulf Aronsson and Guillaume Lequien. You deserve special thanks for simply making things more fun. It is a shame that I didn't get to know some of you earlier! Martin Algotsson deserves a extra thanks for help with proof-reading.

Also the technicians, Tom Hademark, Bertil Andersson, Kjell Jonholm, Tommy Peterssen and Mats Bengtsson deserve special thanks for providing me with support with projects both on and off work.

Last but not least I want to thank my family and friends for their encouragement and support. Especially I want to mention my brother for help with the proof-reading.

To those not mentioned, I am not less grateful!

Hans

Contents

1

Introduction

1.1 Context

The global economy and society in general are greatly dependant on the availability of reliable transportation. However, modern transportation technology is highly reliant on internal combustion engines (ICE), most of which consume fossil fuel during operation. The planet's oil resources will not last forever, and the price of oil has increased substantially over the last decade. Moreover, there is increasing concern about the environmental impact of ICE, from both global and local points of view.

The main emissions from combustion engines are carbon monoxide (CO), ydrocarbons (HC), carbon dioxide (CO_2), nitrogen oxide (NO_x) and particulate matter (PM), all of which impact the environment in different ways. CO is a highly toxic gas for humans. HC is known to cause cancer and promotes the formation of ground level ozone together with NO_x. CO_2 is a green house gas and has been the focus of much concern in recent years because of its role in global warming. NO_x causes acid rain. PM consists primarily of soot, which is in turn composed of a number of different chemical species. Together with NO_x, it is considered to be the most harmful emission produced by combustion engines.

Currently, there are no realistic alternatives that could fully replace the internal combustion engine. Electric vehicles and hybrids will be suitable for some short range journeys and may allow for reduced fuel consumption in general, respectively. However, the volumetric and gravimetric density of modern batteries is still inferior to that of any fuel used in any ICE (see Fig. 1.1 for comparison). The ICE will therefore continue to play a major role in transportation around the world for several decades or maybe even centuries to
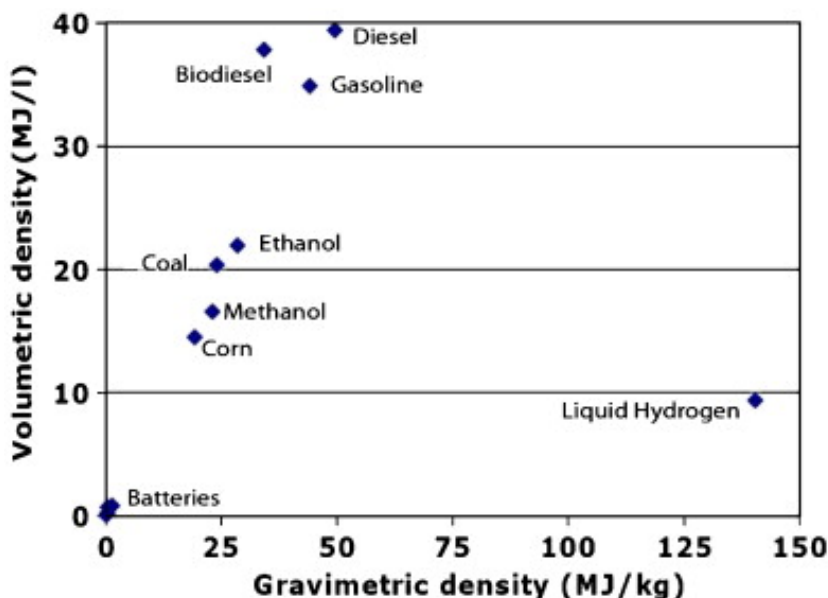
Figure 1.1 Caloric energy density of batteries and liquid fuels, Figure taken from [1].

come. Because of this, every effort must be made to reduce its emissions and improve its efficiency.

Emissions are subject to strict legislation. In order to comply with this legislation, considerable effort has been invested into the development of improved engine control and after-treatment systems such as Selective Catalytic Reduction (SCR), Particulate Filters, and three way catalysts (TWC). However, these after-treatment systems are expensive, and so it would be more convenient if the combustion process could be controlled in such way as to eliminate or minimise the emissions where they are formed.

The production of CO_2 is greatly affected by the engine efficiency. Compression Ignition (CI) engines are highly efficient and thus have relatively modest CO_2 emissions, making CI attractive for future internal combustion engine designs. However, conventional CI engines often generate high NO_x and soot emissions. Soot is formed when the air-fuel mixture is too rich and the temperature is around 1900K. NOx is formed at temperatures above 2200K. Fig. 1.2 shows how the formation of these species depends on the conditions in the combustion chamber. The blue arrows show the path for a fuel droplet

2
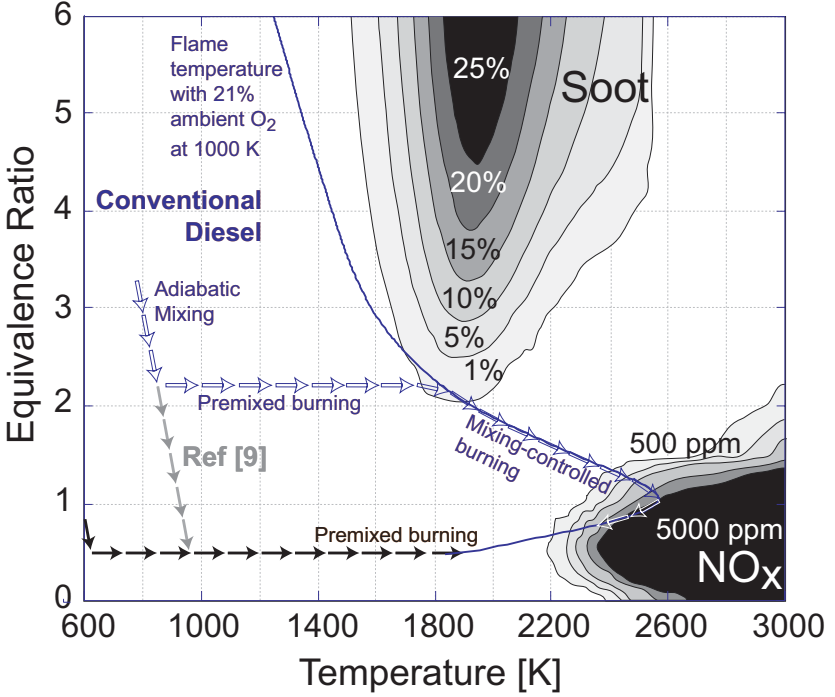
Figure 1.2 Equivalence ratio versus temperature plot describing the regions where soot and NOx is formed for a diesel-like fuel. It is likely that the behavior is similar for gasoline. Figure taken from [2].

that has been injected directly into hot compressed air (as would be the case during typical diesel combustion). Three different phases can be identified: adiabatic mixing, premixed burning and mixing-controlled burning.

Soot and NO_x are formed when the fuel encounters conditions corresponding to their formation zones as shown in the figure - that is to say, soot and NOx formation can be minimised by ensuring the fuel does not encounter conditions corresponding to their formation zones. This can be achieved by operating under HCCI, in which case the conditions encountered by the fuel are shown by the black arrows. In HCCI, the fuel is injected during the intake stroke. This means that the composition of the air-fuel mixture is uniform and the equivalence ratio is constant. Because the mixture is lean and uniform, the peak temperature is low and the NOx and soot formation zones are avoided.

PPC is intended to work in a similar way but the injection occurs at a later stage, resulting in partially-premixed combustion. The conditions encountered by the fuel in this case are shown by the grey arrows, which eventually merge with the black ones. Combustion concepts of this kind, which give low peak temperatures, are referred to as Low Temperature Combustion (LTC) concepts [3, 4, 5]. Experiments, modeling and control of these kind of concepts is what this thesis is all about

1.2 Contribution of Thesis

This thesis describes two different projects. The first project was a continuation of the work started by Jari Hyvönen [6] and Göran Haraldsson [7], and focused on Turbo HCCI using Negative Valve Overlap (NVO). The project was conducted in collaboration with Thomas Johansson. Thomas was responsible for the development of the hardware and the combustion concept. The author was responsible for the work on controls and electronics. The objective of the project was to extend the viable operating range of turbocharged NVO HCCI engines and to develop controllers to accomplish this goal. The knowledge gained from this first project and parallel projects conducted at the Lund testing facility prompted the second project, which became known as the combined combustion concept (CCC) project. On the basis of the observation that different combustion modes have different strengths and weaknesses, the objective of the CCC project was to develop an engine that could switch between the SI, PPC, and and conventional CI (Diesel) combustion modes so as to always operate in the optimal mode for the conditions and requirements at hand. The experiments and conceptual/theoretical work pertaining to CCC discussed in the thesis were conducted by the author. Thomas Johansson assisted with the operation of the test-cell for two weeks while some of the steady-state experiments were being performed. In both projects, Per Tunestål acted as the primary supervisor while Bengt Johansson was the co-supervisor. This thesis is divided into three parts, focusing on "Combustion Sensing for Closed Loop Engine Control", "Turbo NVO HCCI," and "CCC".

Combustion Sensing for Closed Loop Engine Control

The author's work on combustion feedback sensors is discussed in the section on Combustion Sensing for Closed Loop Engine Control.

Without combustion feedback, reliable HCCI or PPC combustion would be difficult to achieve. Three different sensors were evaluated as potential sources of feedback.

The first section deals with cylinder pressure transducers. Sensors of this kind are arguably the best of those evaluated because they are placed in the cylinder and provide real-time information about events within it. Using in-cylinder pressure readings and the first law of thermodynamics, it was possible to make precise crank-angle-resolved estimates of the energy released. However, the cost for this kind of sensor is very high.

The second section deals with ion current sensors. During combustion, different ions are produced. These ions can be detected by applying a voltage over the spark gap; this causes the ions to produce a current that can be detected. The magnitude of the current depends on the ions present, which in turn depends on the properties of the combustion in the cylinder. Therefore, by looking at the ion current shape one can obtain insights into the progress of combustion in the cylinder. Using sensors of this kind, it was shown that Closed Loop Combustion Control (CLCC) is viable for mid to high loads in a light duty HCCI engine. The matched filter approach to determine the combustion phasing that is developed in this thesis enables closed loop HCCI control in operating points that are not possible with other ion current based methods.

The third section deals with an ABB torductor high precision torque sensor. This is a non-contact sensor that measures changes in the magnetic properties of an axle placed between the crankshaft and the flywheel. A new algorithm was developed to reconstruct in-cylinder pressure traces on the basis of measured values of the crank shaft torque. The results obtained demonstrate that it is possible to extract information about the combustion phasing using this approach.

The last section describes how instantaneous cylinder individual air charge estimation can be achieved by using cylinder pressure transducers. The method is over transient's superior compared to sensors commonly used for estimating mass air flow.

Turbo NVO HCCI

The author's work on HCCI is discussed in the section on Turbo NVO HCCI.

The first three sections deal with the main actuator control means for controlling the combustion and describes the design of a HCCI cylinder-balancing controller. At high load, the margins for stable combustion are decreased and cylinder balancing is vital to avoid subjecting any cylinder to heavy knock or misfires. The first experimental feedback controllers that were implemented were PID controllers. Map-based feed-forward was implemented

to improve the controller's transient performance; nonlinear compensation was also introduced. The experiments discussed in this chapter constitute the first combustion-feedback-controlled experiments ever performed using a turbocharged negative valve overlap engine.

The section, "Turbo NVO HCCI Dynamics", describes experiments performed to investigate the dynamics and the behavior of the engine. The sensitivity of the engine is highlighted along with the way in which its stability is highly sensitive to the boost pressure, temperature, speed, and load point. Understanding these dynamics is important when designing controllers.

The section entitled "A HCCI Combustion Model for Controller Design" discusses the development of a thermodynamic model of the engine. This model provided new insights into the dynamics of the Turbo HCCI engine. In particular, the model provided explanations for some of the results discussed in the chapter on "Turbo NVO HCCI Dynamics". The model uses a cycle-to-cycle approach to estimate the residual mass, cylinder air charge, and temperature at the start of combustion. Controllers of this kind had not previously been used with a turbocharged NVO HCCI engine.

The section on "Model Based Controller Design and Results" discusses the use of the model developed in the previous chapter to design a Kalman state estimator and an LQG feedback controller. In addition, the nonlinear combustion model is inverted to provide feedforward. The results obtained using the different controllers are compared to examine how the different controller strategies and hardware setups affect engine behavior.

Combined Combustion Concepts

It was demonstrated how a modified diesel engine was able to operate according to multiple different combustion concepts - Diesel, SI and PPC. To the author's knowledge, the multi mode engine concept articulated in this chapter has no predecessors elsewhere.

It is preferable to operate the engine with large amounts of EGR in PPC mode. However, this means that transient load steps can give rise to excessive combustion noise if action is not taken to mitigate the time delay associated with the movement of the exhaust through the long-route EGR system. The approach adopted for solving this problem involves using double injections during transients. These double injections are managed by an internal model controller that applies just enough double injection in order to limit the fuel penalty associated with it. Using this controller, the engine was able to handle load transients smoothly and without excessive or disturbing combustion noise.

Strategies for switching the engine's mode of operation from SI to PPC and back were tested. These are the first such switches ever reported in the literature.

1.3 Publications

The thesis is based in part on the following publications:

- H.Aulin, P.Bentioulis, P.Tunestål, B.Johansson, Improving Ion Current Feedback for HCCI Engine Control, *SAE Paper No. 2007-01-4053*

  The first author wrote and presented the paper. The first author performed the experiments and evaluated the data in collaboration with the second author, and discussed the work extensively with the third author.

- H.Aulin, T.Johansson, P.Tunestål, B.Johansson, Thermodynamic modeling and control of a turbo HCCI engine, *Iasted Controls and application*, 2009.

  The first author designed and performed the experiments, evaluated the data, and wrote and presented the paper. The second author was responsible for setting up the hardware. The work was discussed extensively with the third author.

- H.Aulin, T.Johansson, P.Tunestål, B.Johansson, Control of a Turbo Charged Engine Using a Model based Approach, *ECoSM 09, Rueil-Malmaison, France* , 2009

  The first author designed and performed the experiments, evaluated the data, and wrote and presented the paper. The second author was responsible for setting up the hardware. The work was discussed extensively with the third author.

- H.Aulin, T.Johansson, P.Tunestål, B.Johansson, Extracting Cylinder Individual Combustion Data from a High Precision Sensor, *ASME ICEF*, 2010

  The first author designed and performed the experiments, evaluated the data, and wrote and presented the paper. The second author dimensioned the torque sensor. The work was discussed extensively with the third author.

Other Relevant publications

- T.Johansson, H.Aulin P.Tunestål, B.Johansson, HCCI Operating Range in a Turbo-charged Multi Cylinder Engine with VVT and Spray-Guided DI, *SAE Paper No. 2009-01-0494*

  T.Johansson did the experiments, evaluated the data and wrote the paper. T.Johansson designed and modified the experimental apparatus. H.Aulin made the control system.

- T.Johansson, H.Aulin P.Tunestål, B.Johansson, The Effect of Intake Temperature in a Turbocharged Multi Cylinder Engine Operating in HCCI mode, *SAE Paper No. 2009-24-0060*

  T.Johansson did the experiments, evaluated the data and wrote the paper. T.Johansson designed and modified the experimental apparatus. H.Aulin made the control system.

- T.Johansson, H.Aulin P.Tunestål, B.Johansson, HCCI Heat Release Data for Combustion Simulation, based on Results from a Turbocharged Multi Cylinder Engine, *SAE Paper No. 2010-01-1490*

  T.Johansson did the experiments, evaluated the data, performed the engine simulation, and wrote the paper. T.Johansson designed and modified the experimental apparatus. H.Aulin made the control system. P. Borgqvist did the optimization of the Wiebe constants.

- T.Johansson, H.Aulin P.Tunestål, B.Johansson, Turbocharging to extend HCCI operating Range in a Multi Cylinder Engine - Benefits and Limitations, *Fisita technical Paper No. F2010-A037*

  T.Johansson did the experiments, evaluated the data and wrote the paper. T.Johansson designed and modified the experimental apparatus. H.Aulin made the control system.

2

Combustion Engine Fundamentals

This chapter provides some basic background information on the combustion engine that must be understood in order to follow the discussion in the subsequent chapters of this thesis.

The Four Stroke Cycle

Most engines in modern vehicles uses the four stroke cycle [8]. The four strokes correspond to the *intake, compression, expansion* and *exhaust* events, and are illustrated in Fig. 2.1

Different Combustion Modes

The working fluid in a reciprocating internal combustion engine is ignited somewhere around top dead center. How this mixture is ignited and how the energy is released differ depending on what combustion concept is being used. Most engines in use today use either the Otto (SI) or the Diesel (CI) combustion concept. In recent years, considerable research effort has been devoted to the development of Low Temperature Combustion (LTC) using HCCI or PPC. The following sections provide a brief introduction to these different combustion concepts.

Otto Fuel and air are mixed during the intake stroke. The charge is compressed and later ignited by a spark plug. Conventional Spark Ignition (SI) engines should be operated at an equivalence ratio of 1. The fuel may be port injected or Direct Injected (DI). In recent years, DI has been favoured. DI makes it possible to operate using a stratified mixture, meaning that the fuel is injected in such a way that the mixture around the spark plug is sufficiently rich for combustion while the outer regions are lean. This makes it possible to open up the throttle and thereby reduce throttling losses. SI engines using a
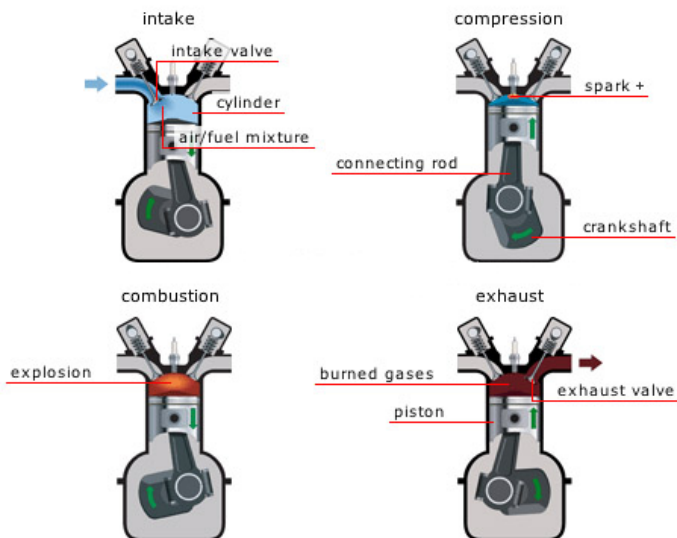
Figure 2.1 Graphical illustration of the four strokes *intake, compression, expansion and exhaust*. Modified from [9].

three way catalyst can achieve very clean emissions profiles. The combustion duration is highly dependent on engine speed, and typically lasts between 20 and 45 degrees. This makes it possible to operate an Otto engine at high speed and hence achieve a high specific power output.

Diesel   Diesel or conventional CI combustion typically proceeds under lean conditions. Air is inducted during the intake stroke and compressed. Then the fuel is injected and a diffusion flame is initiated when it starts to mix with the hot compressed air. The diffusion flame has locally-rich high temperature zones that can give rise to large quantities of NOx and Particulate Matter (PM) (see Fig. 1.2). The duration of this diffusion combustion is largely independent of the engine speed, which imposes limits on the maximum engine speed attainable.

Homogeneous Charge Compression Ignition   HCCI is often described as being an intermediate between CI and SI combustion because the fuel is injected during the intake stoke as in the SI engine and then ignited by compression as in the diesel engine. The concept is known for its high efficiency and promising emissions profile. Unfortunately, it is also known to be difficult to control and to have some other undesirable properties. Whereas ignition

is triggered by the spark in an SI engine and by injection in a Diesel engine, HCCI engines lack a direct ignition trigger. Instead, the timing of combustion is dictated by the conditions at the intake valve closing (IVC) event. If the combustion timing is too early, the pressure increases at an unsustainably high rate, a poor emissions profile is obtained, large CA50 fluctuations are observed, and a lot of noise is generated. Conversely, late combustion causes misfires, instability, and low efficiency. Precise control of the conditions at IVC and thus of the combustion timing is therefore vital.

Since the mixture is well mixed when combustion is initiated, the temperature and equivalence ratio in the combustion chamber are relatively uniform compared to the situation in a Diesel engine. This avoids the formation of localized "hotspots" where NOx and soot are formed in large quantities (see Fig. 1.2).

The combustion of a HCCI engine can be four to five times faster than for typical SI and Diesel combustion. This short duration of combustion limits its utility under high load. This gives the engine a very characteristic mechanical "ringing" noise. The peak load is limited by the rate at which the pressure in the combustion chamber rises. This limitation can to some extent be suppressed by diluting the mixture using a turbo charger [10, 11, 12], but even if this is done, the engine's power density will be less than that of a comparable Diesel or SI engine. Moreover, the use of a turbocharger necessitates the use of more sophisticated controllers [13].

Partially Premixed Combustion   In the same way that HCCI can be seen as an intermediate between CI and SI combustion, PPC can be regarded as being an intermediate between HCCI and CI. The difference between PPC, HCCI and CI is the ignition delay, which is defined as the time between the end of injection and the start of combustion. PPC is achieved if the ignition delay is greater than zero [14]. The precise location of the boundary between PPC and HCCI is not well-defined. However, the definition in this thesis is that combustion proceeds via HCCI if the ignition delay is so long that the fuel is injected during the intake stroke and via PPC if the fuel is injected during the compression stroke. The shorter the ignition delay, the more readily-controlled the combustion process; consequently, PPC is more controllable than HCCI.

Combined Combustion Concepts   Because the various combustion modes have different strengths and weaknesses, it has been suggested that it might be possible to maximize engine performance and efficiency by using an engine that can switch from one mode to another as appropriate. This approach

has been termed Combined Combustion Concepts (CCC). PPC alone cannot provide a sufficiently large operating range. Thus, if an engine operating under PPC were to be subjected to a significant increase in load (and hence in the amount of fuel injected), the ignition delay would decrease to the point that the combustion process would more closely resemble conventional CI mode. Conversely, if the load were significantly decreased, it would become impossible to further increase the ignition delay to maintain combustion, and so it would be necessary to switch to the Otto combustion mode.

Engine Out Emissions

The main engine out emissions from combustion engines are CO, HC, CO_2 and NO_x; all of these species form under different conditions. CO is formed in situations where there is insufficient oxygen to form CO_2; its formation is generally not a problem during lean combustion. CO is converted to CO_2 at temperatures above 1500 K. HC is formed if incomplete combustion occurs, as would be the case during rich combustion or if the combustion temperature was too low. CO_2 was previously unregulated but concerns about global warming have led to the introduction of regulations stipulating that all new cars must achieve average CO2 emissions below 130 g/km for the European driving cycle by 2015 [15]. CO_2 emissions are highly dependent on engine efficiency, which is why there is intense interest in research into compression ignition engines, which are highly efficient. NO_x is mainly formed at temperatures above 1800 K (see Fig. 1.2). NO_x formation halts when the temperature of the mixture within the combustion chamber decreases during the expansion stroke. However, all NO_x formed during combustion will survive until the exhaust valves open. Therefore, the only way to minimize NO_x formation is to avoid the occurrence of high in-cylinder temperatures. EGR can be used to decrease the in-cylinder temperature and hence decrease NO_x emissions. However, this can lead to increased soot formation, and so a compromise must be made. Particulate Matter, PM, consists primarily of soot, which in turn consists of a number of different species whose individual levels are not easily measured. Soot is formed due to a lack of oxygen; it is formed throughout the combustion process, but can also be consumed by oxidation.

3

Experimental Setup

The experiments were performed using three different engine types. These are the $SAAB\,L850$ engine, the $GM\,mule\,1$ engine and the $SAAB\,A20\,DTH$ diesel engine. The basic properties of these engines are shown in Table. 3.1

Test Engine	SAAB L850 HCCI	GM Mule1	SAAB A20DTH
Displacement	$1998cm^3$	$2198cm^3$	$1956cm^3$
Number of Cylinders	4	4	4
Compression Ratio	$Modified\ 18:1$	$11.75:1$	$16.5:1$
Bore x Stroke	$86mm$ x $86mm$	$86mm$ x $86mm$	$83mm$ x $90mm$

Table 3.1   The geometry of the different engines used.

SAAB L850

The SAAB L850 engine was used for the ion current experiments. It is a four-cylinder 2.0 liter engine that had been used by [6, 7] in a previous project. The compression ratio was increased from 9.5:1 to 18:1 by changing the pistons; in addition, the inlet cam was changed to one that closes 15 degrees earlier than the production camshaft. The combustion timing was controlled using fast thermal management, a technique for adjusting the intake temperature (and hence the combustion timing) by being able to take in either cool ambient air or air pre-heated by contact with the hot exhaust, and using throttles to rapidly adjust the proportion of the two in the intake.
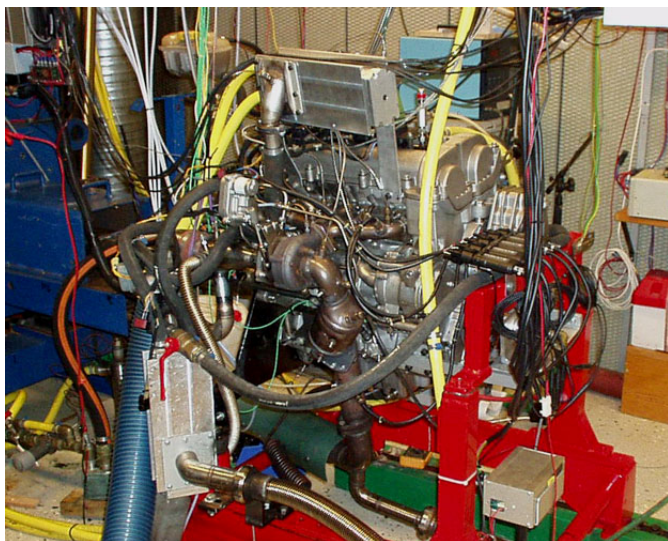
Figure 3.1   The mule1 HCCI engine installed in the testbed.

GM mule1

The Mule 1 GM HCCI engine (Fig. 3.1) was used in a number of different configurations. It is a 2,2 L engine that uses spray-guided direct injection. The engine was equipped with two different low lift and short duration camshafts. These were timed for Negative Valve Overlap (NVO), the phasing of which could be adjusted using hydraulic cam phasers (50° for each camshaft). The engine was tested with two different turbo chargers and two different exhaust camshafts with either 125 or 155 degrees of duration. There were two intake throttles connected to the intake, which were used to control the intake temperature by drawing in air directly from the compressor or cooled air taken from an intercooler path. The control system measured the temperature and pressure at all the positions of significance both upstream and downstream of the engine intake and exhaust manifolds. Significant effort was invested into building and maintaining the engine's electrical equipment and control systems. Two different turbochargers were used (B&W BV35 and KP31)

SAAB A20DTH

The SAAB A20DTH (Fig. 3.2) is a diesel engine modified with spark plugs. This was done by machining the glow plug holes to accommodate small moped
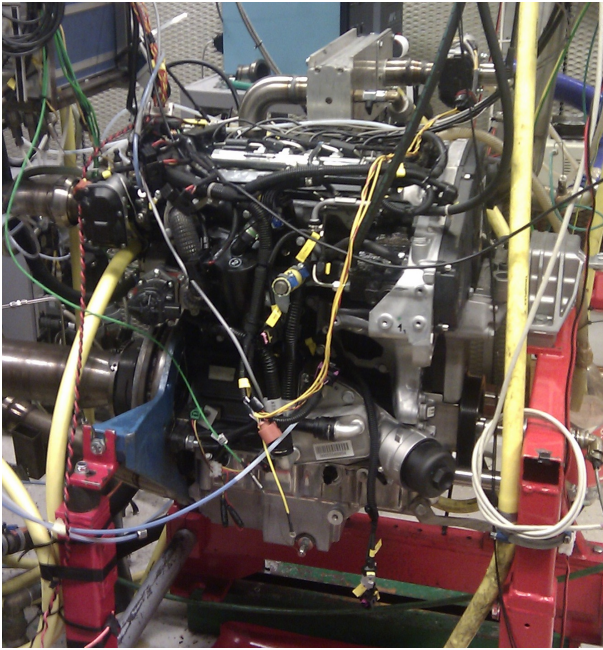
Figure 3.2   The A20DTH engine installed in the testbed.

spark plugs. Additional machining was applied to accommodate cylinder pressure transducers. The engine was equipped with both short and long route EGR, a VGT turbo, and temperature and pressure sensors at all the positions of significance both upstream and downstream of the engine intake and exhaust manifolds. Significant effort was invested into modifying the control system and into building and installing the engine and its electrical system.

The Engine Control Unit and Test Cell Setup

The L850 engine was operated using a Delphi based control system developed in-house. This system was later replaced by a dSpace MicroAutoBox and a dSpace Rapid Pro system which was subsequently used throughout the project

The MicroAutoBox is the master of the two dSpace systems; it performs the main combustion related algorithms and controls the data acquisition of in-cylinder pressure. The Rapid pro unit functions as an extension of the MicroAutoBox. It takes care of most of the signal conditioning for the sensors
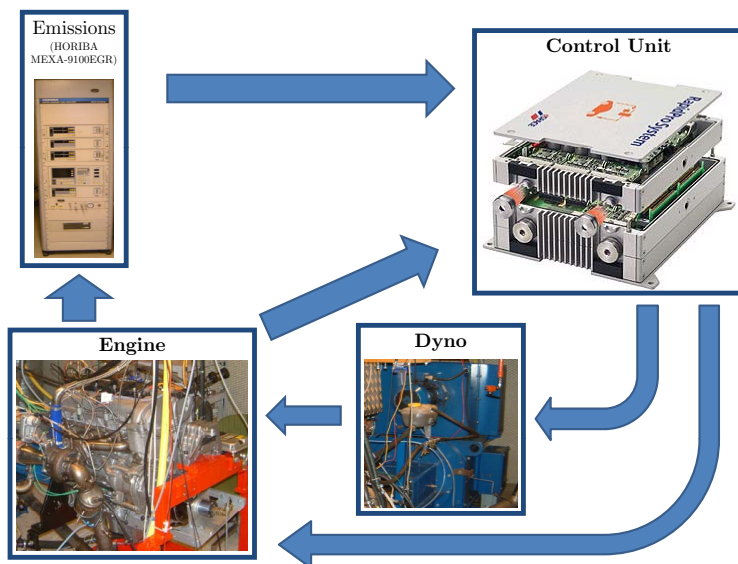
Figure 3.3   Brief overview of the test cell's structure. The control system communicates with the emissions systems, reads the engine outputs, and controls the engine actuators and the dyno speed according to the user's demands.

and power drivers for the engine's actuators. It is also configured to take care of the low-level tasks necessary for the engine's operation, such as controlling the throttles, fuel pressure, cam phasing, ignition and injection, etc.

The control system was also configured to be able to control the dyno and to collect data from the emissions monitoring system. The general layout of the test cell structure is shown in Fig. 3.3.

The ultimate goal in Engine Control Management (ECM) is to exercise control over the injection and ignition events so as to achieve optimal combustion.

Realtime Tasks

The ECM makes "decisions" on the basis of a number of inputs, the most important of which are the cylinder pressure and the crank angle position.
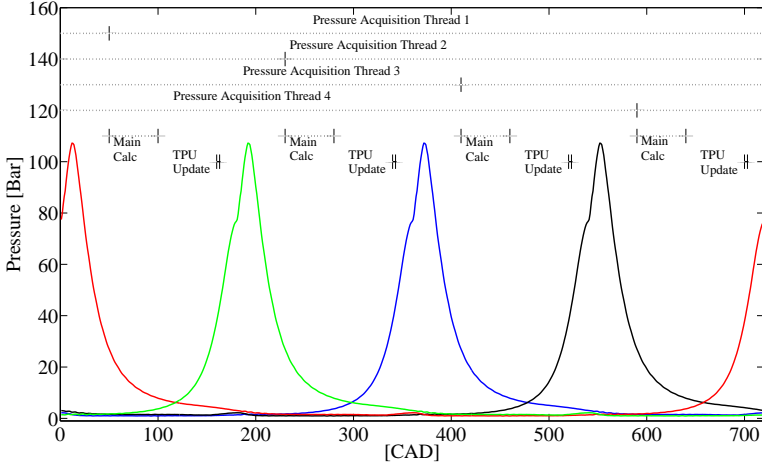
Figure 3.4 The cylinder pressure of the four cylinders and a timing diagram describing the most important threads working in the system. Four threads are continuously triggered for each crank angle degree the crankshaft rotates. These collect the pressure from each cylinder in cyclic buffers. The content in the buffer is sent forward as soon as combustion can be assumed to have ended. The main calculation thread processes the pressure data in order to determine what control actions should be taken. These control actions are then implemented when the TPU update thread is initiated.

Four threads are continuously triggered for each crank angle degree the crankshaft rotates. Their task is to store the pressure of each cylinder in a cyclic buffer. The timing of the tasks is shown in Fig. 3.4. The content of the buffer is sent forward as soon as the combustion is assumed to have ended, about 60 degrees after top dead center.

After the end of each combustion event, the main calculation thread is triggered. This takes care of all the combustion control related calculations. It consists of the blocks between *Virtual Sensors* and *Cylinder Balancing* in Fig. 3.5, which outlines the structure of the primary controller. The *Angle Based Inputs* block in the figure refers to the pressure acquisition tasks described above. The *Timer Based Inputs* block collects data from the various AD converters such as the pressure, temperature, and lambda sensors, etc. It is sampled with a frequency of 400 Hz.

The most important task for the *Virtual Sensors* block is to process the buffered cylinder pressure data obtained during the preceding engine cy-
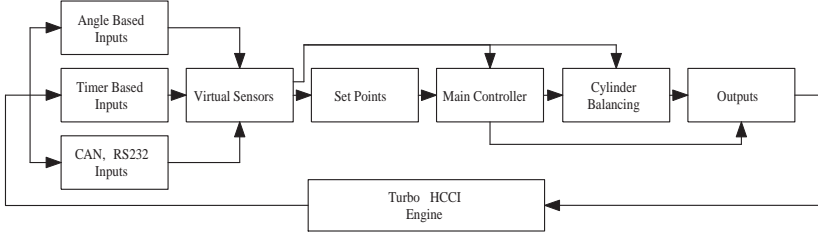
Figure 3.5 The flow of signals from engine input to output in the ECM. *Angle Based Inputs* refers to the cylinder pressure acquisition threads. The main calculation thread (see Fig. 3.4) takes care of all the combustion control related calculations. It consists of the blocks between *Virtual Sensors* and *Cylinder Balancing*.

cle. This data is processed to generate data on heat release, NMEP, RI and dP/dCa, and is used to calculate the CA50 and so on. This block also accommodates various observers and filters.

The *Set Points* block uses the processed data for map- or model-based feedforward control of actuators to regulate injection timing, combustion phasing requests etc. The feedforward is sent to the *Main Controller* which regulates the main combustion feedback controller. The feedback controller acts on the mean data for all of the cylinders and sends out a global request for all the cylinders. The *Cylinder Balancing* block then takes the main controller's injection signals as feed forward but balances each cylinder to maintain equal phasing and load.

The *Output* block contains different threads that update the settings of the Time Processing Unit, TPU so as to achieve the desired ignition and injection timing. The TPU update events are initiated 90 crank angles before the combustion reaches TDC. The controllers that regulate the throttles, fuel pump, cam phasing, and water pump etc. according to the demands of the ECM are also governed by the output block. This thread is triggered with a frequency of 400 Hz.

The same basic control flow structure was used for all engine types. Most of the engine-specific modifications were made in the setpoints and main controller parts of the ECM.

4

Combustion Sensing for Closed Loop Engine Control

The vast majority of the engines used in modern vehicles use some kind of closed loop combustion control. For example, SI engines use lambda control in order to maintain a lambda value of approximately 1, which allows the engine to operate with high efficiency and minimizes emissions. The closed loop control systems described in this thesis are reliant on measurements of the total load, combustion phasing, noise, and other important parameters from each combustion event. The longer the ignition delay an engine operates with, the harder it will be to know what combustion phasing the different cylinders are working at. The combustion phasing will to a large extent depend on the intake temperature, pressure, wall temperature, effective compression ratio, residual ratio. It is extremely difficult to predict precisely how these factors will affect the phasing. Some kind of feedback on the combustion phasing is therefore crucial to maintain adequate control.

This chapter discusses different sources of feedback. The first source considered is the piezoelectric cylinder pressure transducer. These are state of the art sensors, but are costly and exhibit poor reliability. However, it is possible to obtain a comprehensive picture of the energy release during combustion from the in-cylinder pressure readings together with the first law of thermodynamics. This provides useful information on the combustion process that can be used to obtain information on the burn rate profile and the combustion phasing.

The second way of obtaining feedback that is considered involves using the spark plugs as ion current sensors. During combustion, different ions are produced. These ions can be detected by applying a voltage over the spark gap. The voltage makes the ions produce a current that can be detected. The current depends on the ions present, which in turn depends on the progress of

combustion in the cylinders. Therefore, by looking at the ion current shape, one can get an indication of the combustion phasing in each cylinder. This technique has been used for quite some time to detect knock and misfires in SI engines; in most cases, the spark plug is used as the measurement probe. Closed loop HCCI combustion phasing control based on ion current measurements is demonstrated to be feasible.

The third and the last sensor considered is the ABB Torductor high precision torque sensor. This is a non-contact sensor that measures changes in the magnetic properties of an axle placed between the crankshaft and the flywheel. The torque measurements obtained from sensors of this kind can potentially be used to reconstruct combustion-related information.

4.1 The Use of Cylinder Pressure to Characterize Engine Operation

The industry standard method for analyzing combustion processes involves the use of pressure sensors; this section discusses some of the most important standardized state and feedback parameters. The most commonly used sensor is the piezoelectric pressure sensor. Sensors of this kind outperform the alternatives, and the information obtained from them can be considered to accurately reflect the real in-cylinder values. As such, data from sensors of this kind were used as a reference when evaluating the performance of the alternative sensors used in the work described herein.

Piezoelectric pressure sensors exhibit an excellent high frequency response. However, their steady state and low frequency behavior is less satisfactory because they are prone to current leakage under such conditions, and this must be compensated for. There are two commonly-used methods for this. The first involves an extra sensor placed in the inlet manifold. This is used to identify the offset error by comparing the difference between the piezo sensor and the ordinary manifold sensor at a point before the intake valves are closed. The drawback of using this method is that the pressure in the cylinders is not necessarily equal to that in the manifold because there may be pressure waves between the two volumes. Alternatively, one can use a least-squares fit of a polytropic compression model to the measured pressure [16]. However, to obtain reliable results using this approach, the polytropic exponent (see the section on Heat-release Calculations) must be known. The state of the art method is described in [17]. This method, estimates both the polytropic exponent and the pressure offset using a least squares procedure. This is implemented in the control system.
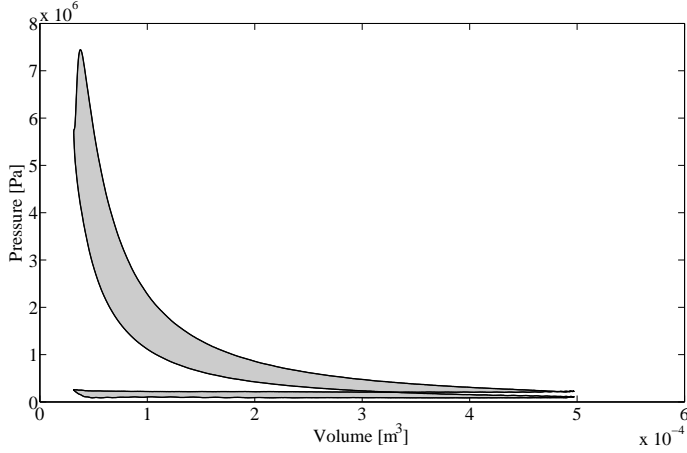
Figure 4.1   Pressure - Volume diagram. The work done can be described by the integral of the pressure in respect to volume.

Definition of state and feedback parameters

Below follows the definition of some of the most important combustion engine control feedback parameters

Cylinder pressure data from a complete cycle can be used to calculate the useful work transferred to the piston. The total work, W is given by the area enclosed by a $p-V$ diagram such as that shown in Fig. 4.1 . The useful work done is calculated using the following expression [18]:

$$W = \int_a^b p(\Theta)dV(\Theta) \tag{4.1}$$

Here, $p(\Theta)$ is the cylinder pressure and $V(\Theta)$ is the cylinder volume for a specific crank angle, Θ. a to b spans Θ over a complete cycle corresponding to 720°. A more useful measure for relative engine performance is the Net Mean Effective Pressure, $NMEP$ which can be described as the ratio of the delivered net work to the cylinder volume displaced per cycle, V_d [18].

$$NMEP = \frac{1}{V_d} \int_a^b p(\Theta)dV(\Theta) \tag{4.2}$$

The Ringing Index (RI) is a measure of how the engine's noise is perceived. Combustion noise inevitably goes hand in hand with higher efficiency and
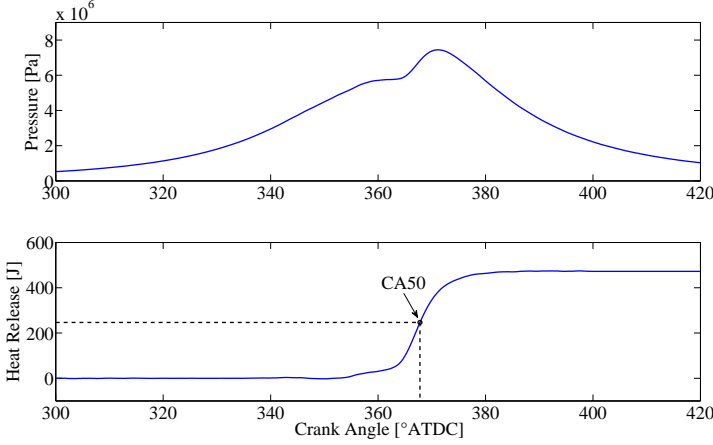
Figure 4.2   A pressure trace and the corresponding accumulated heat-release. The CA50 is given by the position at which 50% of the energy has been released.

so it is important that it is measured and accounted for by Engine Control Management (ECM) systems. The RI is described by

$$RI = \beta \frac{\left(\frac{\mathbf{dP}}{\mathbf{dt_{max}}}\right)^2}{p_{max}} \qquad (4.3)$$

where β is a calibration factor and p_{max} is the highest cylinder pressure for the treated cycle.

The combustion phasing is a very important feedback parameter. This is often discussed in terms of the CA50, which denotes the crank angle by which 50% of the fuel has been burned. This is a vital feedback parameter because its timing provides a wealth of information on the stability and efficiency of the combustion process. In order to calculate the CA50, it is necessary to have a reliable burn or heat release profile. This data can be obtained in a variety of ways, the most important of which are discussed in the following section on Heat-release Calculations. A typical heat-release profile and the corresponding CA50 are shown in Fig. 4.2

Heat-release Calculations

The heat-release profile is an important tool for understanding what is happening inside the cylinder. Much of the work in this project focused on using CA50 estimated from calculated heat-release profiles. The heat-release profile is also useful for monitoring the burning of the fuel in terms of when it starts

burning, the duration and efficiency of the combustion process. Heat-release profiles can be obtained using a variety of different methods; all of them are based on the first law of thermodynamics, which is the source of the following expression [18]:

$$\frac{dQ}{d\theta} = \frac{1}{\gamma - 1} V(\Theta) \frac{dp}{d\theta} + \frac{\gamma}{\gamma - 1} p(\theta) \frac{dV}{d\theta} + \frac{dQ_{ht}}{d\theta} + \frac{dQ_{Cr}}{d\theta} \tag{4.4}$$

Here, dQ is energy released through combustion, dQ_{ht} is the heat transfer, dQ_{cr} is the crevice losses, γ is the polytropic coefficient, and θ is the crank angle. Two different methods for calculating the heat-release are described below.

Rassweiler & Withrow   This method does not provide any information on the amount of energy that is released ($Q(\theta)$)but gives a burn rate profile ($mfb(\theta)$) that is suitable for determining the CA50. Computationally, this method is very undemanding and is therefore suitable for implementation in realtime control systems. By rearranging Eq. 4.4 and assuming that the mass is constant and the heat losses are zero, the following expression is obtained:

$$\frac{dp}{d\theta} = \frac{(\gamma - 1)}{V(\theta)} \frac{dQ}{d\theta} - \frac{\gamma p(\theta)}{V(v)} \frac{dV}{d\theta} \tag{4.5}$$

This expression shows that the change in total pressure, $dp(\theta)$ can be regarded as the sum of the pressure changes due to combustion, $dp_c(\theta)$, and those due to volume changes, $dp_v(\theta)$

$$dp(\theta) = dp_c(\theta) + dp_v(\theta) \tag{4.6}$$

The change in pressure caused by combustion, $dp_c(\theta)$, can be described by comparing the measured pressure, p_m, to the pressure that would be observed if the compression were to occur isentropically (i.e. without combustion):

$$dp_c(\Theta) = p_m(\Theta + 1) - p_m(\Theta) \left(\frac{V(\Theta)}{V(\Theta + 1)} \right)^{\gamma} \tag{4.7}$$

The mass fraction burnt (or equivalently, the the burn profile), $mfb(\Theta)$, is calculated as follows:

$$mfb(\Theta) = \frac{\int_a^{\Theta} dp_c(\Theta)}{\int_a^b dp_c(\Theta)} \tag{4.8}$$

Here, the values taken by the indices a and b should typically be 20-30 degrees before and after the angles at which combustion is assumed to occur, respectively, in order to ensure that the entirety of the combustion event is

captured. The term $\left(\frac{V(\Theta)}{V(\Theta+1)}\right)^{\gamma}$ should be tabulated as a vector to decrease the computational demands of this step.

Apparent Heat Release   By using Eq. 4.4 and assuming that the mass is constant and the heat losses are zero, the following expression is obtained:

$$\frac{dQ}{d\theta} = \frac{1}{\gamma - 1} V(\theta)\frac{dp}{d\theta} + \frac{\gamma}{\gamma - 1}p(\theta)\frac{dV}{d\theta} \tag{4.9}$$

The cumulative heat release profile can then be described by

$$Q(\theta) = \int_{a}^{\theta} dQ(\theta) \tag{4.10}$$

The index a should take a value prior to the start of combustion.

4.2 Concluding Remarks

The two methods are equal in accuracy when it comes to extracting the combustion phasing. If this is the primary objective, the Rassweiler-Withrow technique is preferred because it is the least computationally-intensive. However if the heat-release is to be used for some kind of analysis of combustion efficiency, the apparent heat release or even better, the self tuning method would be preferred [17].

## 4.3 Ion Current Measurements for Combustion Feedback

The aim of this section is to illustrate how the ion current behaves in HCCI engines. It also illustrates that CA50 can be extracted from the ion current which is successfully used for closed loop combustion control experiments by using ion current instead of pressure transducers. Also, an algorithm for detecting the ion current which maximizes the signal to noise ratio is shown. The algorithm is based on the fact that the shape of the signal is similar from cycle to cycle.

The second feedback sensor evaluated was the ion current sensor. Different ions are produced when combustion occurs. A voltage applied across an electrode in the combustion chamber will cause these ions to produce a detectable current. The current depends on the ions present and the ions present depend on the combustion process. Therefore, by looking at the ion current signal from a combustion event, one can draw certain conclusions about the combustion event's progress. This technique is used by some car manufacturers to detect knock and misfires in SI engines [19]. The spark plug is often used as a convenient measurement probe. The objective of the study described in this section was to determine whether the ion current could also be used to detect the HCCI-combustion phasing or CA50 as suggested by [20], and if so, to use it for closed loop combustion phasing control.

Current is carried by electrons and positive or negative ions [21]. The ions present in a combustion engine originate primarily from *chemical ionization* and *thermal ionization*. The first is caused by chemical reactions while the latter is caused by the high kinetic energy of individual species in the combustion chamber. The most abundant ions in the reactions are formed by the following reaction:

$$CH + O \rightarrow CHO^+ + e \qquad (4.11)$$

the product of which participates in a very fast reaction:

$$CHO^+ + H_2O \rightarrow H_3O^+ + CO \qquad (4.12)$$
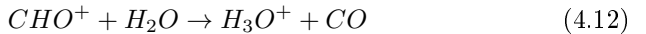
The molecular species finally reform:

$$H_3O^+ + e \rightarrow H_2O + H \qquad (4.13)$$

This process is much much slower than the first two, Thus there is a high concentration of H_3O^+ during combustion [22].

The extent of thermal ionization provides a measure of the temperature in

the combustion chamber. It can be regarded as a chemical reaction with only one reactant:

$$M \leftrightarrow M^+ + e \qquad (4.14)$$

Thermal energy causes the ionization of the arbitrary neutral species M to M+ with the concomitant release of an electron [22]. The species that contribute most heavily via this process are those with the lowest ionization energies, assuming their concentrations are not too low [22]. Different chemical species have different ionization energies. The presence of metallic additives in the fuel or in the air increases the extent of thermal ionization because these species have low ionization energies; this is particularly true for sodium (Na) and potassium (K). Introducing additives to the fuel can therefore improve the ion current signal strength.

Experimental Measurement Setup

Experiments were performed using the SAAB L850 engine modified to operate under HCCI (see Chapter 3). The center electrodes of the sparkplugs were used as measurement probes. A spark plug with an integrated pressure transducer was placed in cylinder 3. The other cylinders were equipped with NGK R (BCPR9ES) plugs. The coils used were made by Mecel, model Delphi 19005240.

An ion current measurement system was built (See Fig. 4.3). It consists of a capacitor and resistor placed in series between ground and the positive side of the secondary coil. The spark plug is placed between ground and the negative side of the secondary coil. When the discharge goes off, the spark plug can be regarded as a short circuit that produces high current going in an anti clockwise direction (See Fig. 4.3). The current will charge the capacitor until a 450V zener diode placed in parallel redirects the current through itself. When ions are produced around the electrode, the voltage of the capacitor will cause a current to flow in the clockwise direction. This current can then be measured as a voltage over the resistor. To prevent build-up of high voltage over this resistor, a high voltage diode is connected in parallel. The voltage over the resistor was amplified using an operational amplifier to suppress noise and better exploit the resolution of the A/D converter. The control system was modified to handle realtime data acquisition from the A/D converter for each cylinder.

The Influence of the Operating Conditions on the Ion Current Signal

A series of experiments were performed to investigate how the signal amplitude and shape of the ion current signal behave and how it is affected by different operating conditions. These experiments involved tests at different
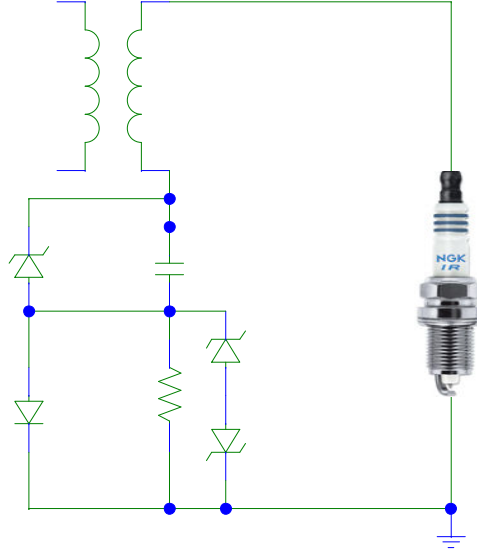
Figure 4.3 The ion current measurement setup.

values of lambda, fueling levels, engine speeds and combustion phasings. The data reported for each testpoint represents an average of 310 cycles. All of the signals reported were filtered using a first order Butterworth low pass filter.

Ion Current Amplitude Tests were conducted at 1000 and 2000 RPM. A lambda sweep was performed by increasing the amount of EGR at fuel levels from 380 to 500 J/(Cycle & Cylinder). The position of the ion current peak amplitude, CA_{IonMax} was that of Maximum Brake Torque (MBT). A plot of the peak ion current amplitude against total fuel consumed is shown in fig. 4.4 . The results show that the peak ion current amplitude increases significantly when lambda drops below 1.3 for all fueling levels. It is likely that this is due to higher peak temperatures in the combustion chamber, caused by the higher inlet air temperature required to maintain constant combustion phasing with the increased amount of EGR. When the ion current amplitude drops below 0.1 µA, the signal to noise ratio is so low that it is difficult to distinguish the actual signal. The behavior of the signals is similar at 1000 RPM but the amplitudes are slightly lower.

Ion Current Shape Influence of EGR, fuel and speed Figures 4.5 through 4.8 depict the ion current traces obtained when varying the amount
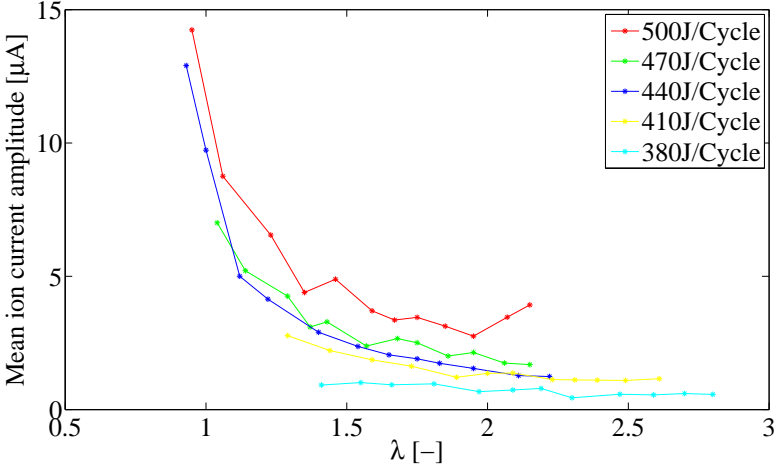
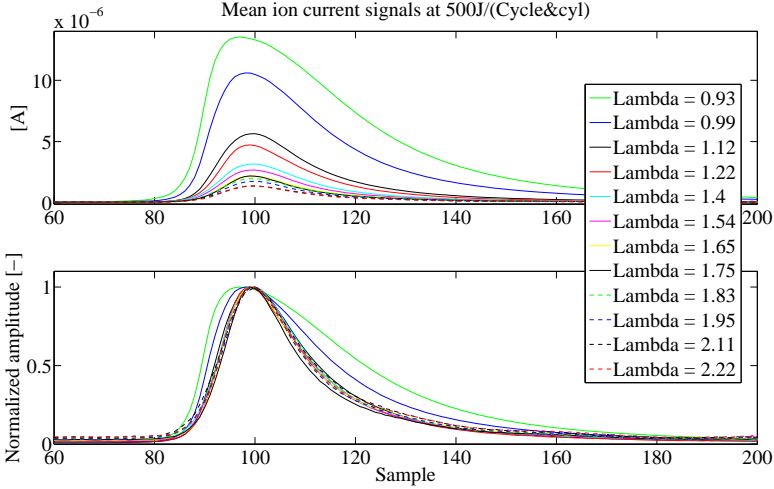**Figure 4.4** Mean ion current amplitude vs. λ at 2000 RPM.

Figure 4.5 Upper subplot: Ion current traces obtained at different values of lambda. Lower subplot: Normalized versions of the traces in the upper subplot.

EGR, fuel, speed and combustion timing. Fig.4.5 depicts the trace obtained with a constant amount of injected fuel (500 J/Cycle) . The ion current timing, CA_{IonMax}, was held at 10 crank angle degrees after top dead center, and the value of lambda was adjusted by controlling the amount of EGR. The
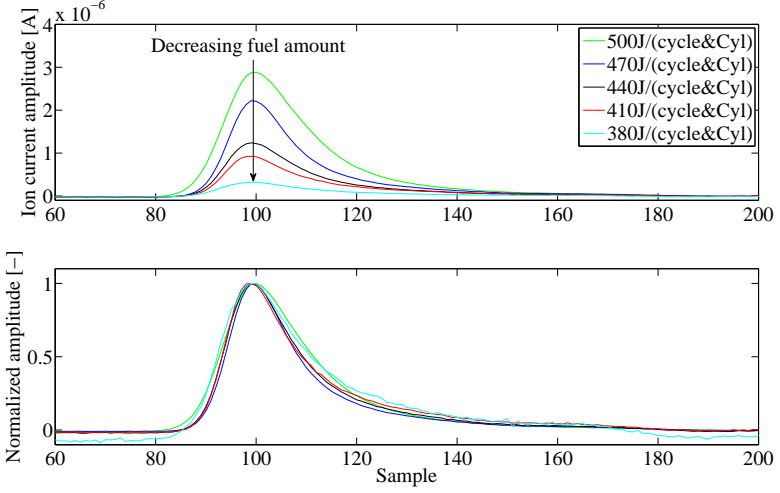
Figure 4.6 Upper subplot: Ion current traces obtained by varying the amount of fuel injected. Lower subplot: normalized versions of the same traces. All traces were acquired at a constant engine speed of 1000 RPM.

figure shows the raw signals in the upper subplot and the normalized mean signals in the lower subplot. The results in the lower subplot indicate that EGR has little or no influence on the shape of the trace under lean conditions. However, when running rich (i.e. when lambda is less than 1), the shape of the signal changes, as can be seen by comparing the blue and green traces in the figure. This is probably a consequence of slower combustion due to the lack of oxygen.

Fig.4.6 shows the traces obtained when varying the amount of fuel injected. As before, the combustion timing was maintained at MBT. The shape of the normalized signal is more or less unaffected by the changes in the amount of injected fuel, but the current amplitude increases as more fuel is injected. The injection of more fuel generates higher temperatures in the combustion chamber, resulting in a greater degree of ionization.

Fig.4.7 shows the traces obtained at different engine speeds. CA_{IonMax} was maintained at 10 CAD ATDC and no EGR has been used. Once again, the shape of the traces was unaffected by changing the engine speed. It should be noted that the time between samples at low engine speeds is longer than is the case at higher speeds. This indicates that reaction rates are more reliant on the crank angle position than the time derivative.
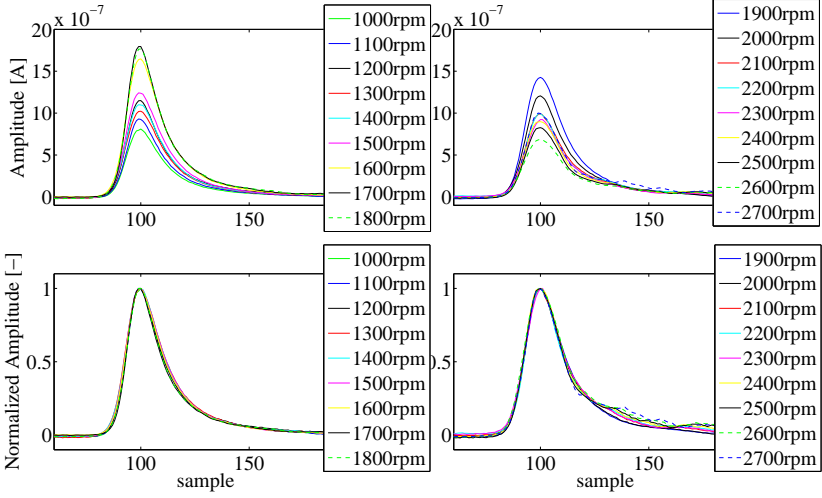
Figure 4.7   Upper subplots: Ion current traces obtained at different engine speeds. Lower subplots: The same traces after normalization.

Fig.4.8 shows the mean signals observed at different values of CA_{IonMax}. In these experiments, the amount of fuel injected and the air/fuel ratio were kept constant. The ion current timing was swept from 8 to 14 CAD ATDC. The test was conducted at 1000 RPM. Early combustion timing gives high peak temperatures and high temperatures give more ions. The higher the temperature, the faster the combustion; consequently, earlier timing gives rise to narrower traces.

In all of these experiments, the shape of the trace was unaffected by any of the changes save for changes in the combustion timing. This information on the behavior of the ion current signal is useful in determining how it should be treated in order to maximize the Signal To Noise Ratio (SNR).

The Ion Current Timing vs the CA50 from Heat Release

The relationship between the $CA50$ calculated from the heat-release and CA_{IonMax} was investigated for different loads at 1000 and 2000 RPM. Two kinds of parameter sweeps were done. In the first sweep, the amount of fuel injected was kept at 500 J/Cycle and lambda was changed by varying the amount of EGR. The results of a linear regression between CA_{IonMax} and $CA50$ for each EGR point are shown in Fig.4.9 . The speed was kept at 2000 RPM. The figure shows that the relationship between $CA50$ and CA_{IonMax}
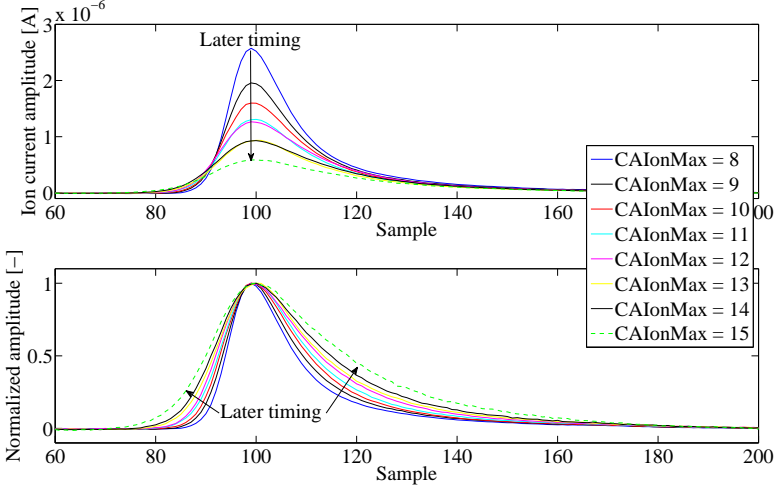
Figure 4.8   Ion current traces obtained by varying the timing position.

is more or less unaffected by the EGR-ratio. The mean line of the curves in Fig.4.9 is given by the equation:

$$CA_{IonMax} = 1.14CA50 - 0.02 \qquad (4.15)$$

Fig.4.10 shows the relationship between ion current timing and CA50 when the amount of fuel injected is varied; these experiments were performed at 1000 RPM

The high correlation between the ion current and the CA50 is encouraging and suggests that it may be possible to replace pressure-based measurements with ion-current sensors provided that the SNR is strong enough

Algorithms used to extract CA50

The ion current is obviously a promising source of combustion feedback, but its low signal to noise ratio is a problem that will affect its usability. The engine could be operated under heavy throttling and with high amounts of EGR to maximize the signal power at low load. However, this is not generally desirable because it will affect engine-out efficiency. Methods for extracting as much information as possible from the signal are therefore required. Two different methods for extracting CA50 from the ion current data were proposed, tested and evaluated. These methods are referred to as the peak algorithm and matched filter algorithm.
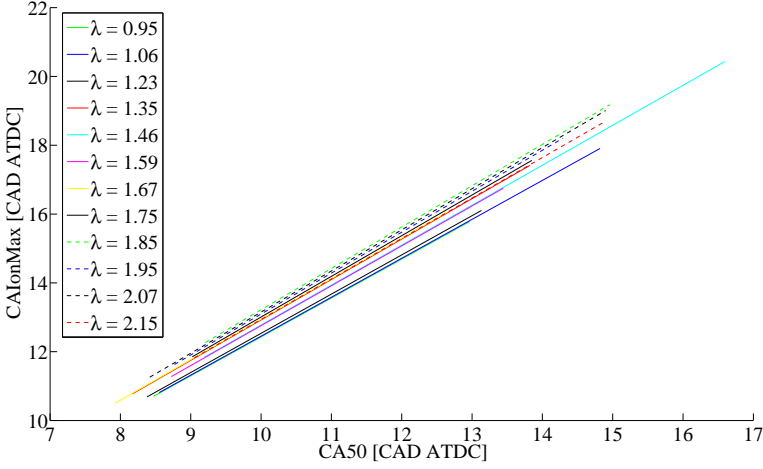
31

Figure 4.9   The relationship between ion current timing and CA50 for different amounts of EGR.

Peak Algorithm

The motivation for using the peak algorithm is its simplicity. First, the signal is smoothed using an IIR low pass filter. The algorithm then locates the peak. The search is made 10 CAD BTDC to 30 CAD ATDC. The method can fail when the SNR is low or when operating the engine in spark-assisted mode, which introduces an additional peak that sometimes is higher than the post peak. While there are more sophisticated and better methods than this, it provides a useful point of reference for comparative purposes.

Matched Filter Algorithm

Because the ion current signal is known to be similar from cycle to cycle, the SNR can be maximized by using a matched filter [23]. Matched filters have the same shape as the signals they are designed to isolate; the filter used in this instance was designed through ensemble averaging of several measured signals. Filtering takes the form of a convolution between the filter parameters and the signal according to

$$r(n) = \int_{-\infty}^{\infty} f(n)g(n - \tau)d\tau \qquad (4.16)$$

Note that the convolution between the signal and a time-reversed signal is the same as the auto-correlation of the signal. The idea behind the matched filter method is not to restore the signal but to detect it. The highest peak of the
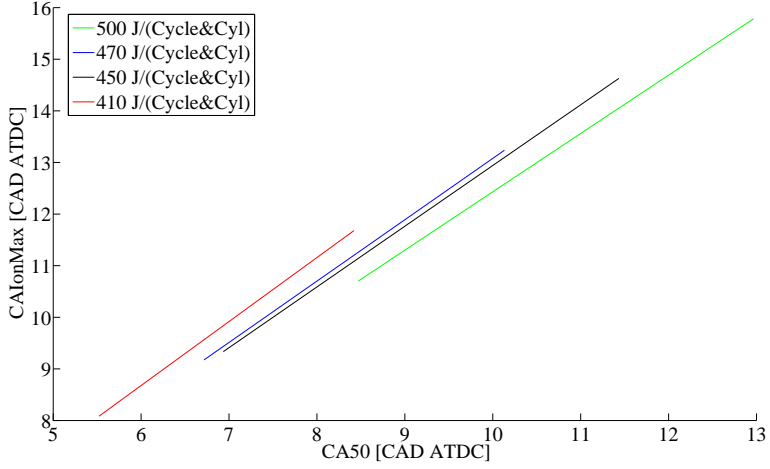
Figure 4.10   The relationship between ion current timing and CA50 when the amount of fuel injected is varied at 1000 RPM.

Method\Fuel	500J	470J	440J	410J	380J
Peak algorithm	0%	0%	0%	3%	16%
Matched filter algorithm	0%	0%	0%	0%	2%

Table 4.1   Comparison of the two algorithms. The tabulated values in table indicate the percentage of mismatches obtained with each method.

resulting signal, $r(n)$ indicates the point at which the filter, $f(n)$ most closely resembles the signal, $g(n)$. This kind of algorithm reduces noise that is not within the bandwidth of the filter. Fig. 4.11 depicts a graphical representation of the method. The figure shows how the filter "slides" over the noisy traces during the convolution process. When the filter reaches the "black star" as seen in the picture, the resemblance between it and the trace is at a maximum. Once the maximum of the filtered signal has been located, the CA_{IonMax} can be located.

Comparing the Peak Algorithm To the Matched Filter Algorithm
The performance of the matched algorithm at different fueling levels is compared to that of the peak algorithm in Tab. 4.1 . The percentage values indicate the ratio of miss-detections. The matched method outperforms the peak algorithm but is not perfect. At a fuel load of 410 J/Cycle, the accuracy of the peak method begins to decline; at 380 J/Cycle, that of the matched
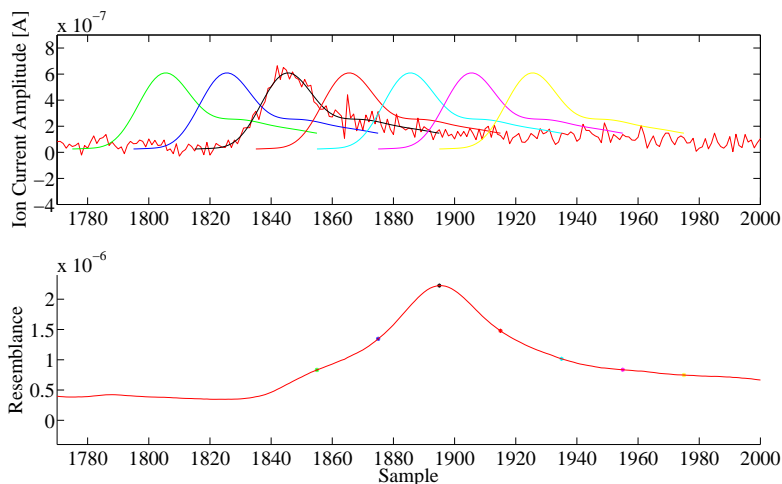
Figure 4.11 Example showing how the matched filter slides over the signal, above. The signal below shows the result from the convolution. The resemblance attains its maximum at the black star.

filter method also starts to flag, with mismatches being obtained in 2% of the cases examined, compared to 16% for the peak method.

Ion Current Sensing for HCCI Combustion Feedback

The peak algorithm was implemented in the engine control system and the predicted values of CA_{IonMax} were used as combustion feedback by the combustion controller. The feedback signal was ultimately processed by a PID controller that controlled the two throttles used to mix cold and hot intake air in order to maintain the desired combustion phasing. The step response of the system was investigated by changing the set point for CA_{IonMax} and monitoring how it and the heat-release-based $CA50$ changed during the transient. The results are taken from cylinder 3, which had been retrofitted with a spark plug with an integrated pressure sensor. The other cylinders used standard spark plugs. Both the center and ground electrode on the standard spark plugs were wider than that of the spark plug with the integrated pressure sensor. The steps are presented for load cases where the amount of fuel injected was 380J/(Cycle & Cylinder) and 500J/(Cycle & Cylinder). The SNR of the ion current for the cylinder with the combined spark plug/pressure sensor was lower than that from the other cylinders, being only half or less of that obtained with standard spark plugs. This imposed restrictions on the range of the load region that could be investigated. Fig.4.12 and Fig.4.13 show the step responses for the two fueling levels. It is readily apparent that
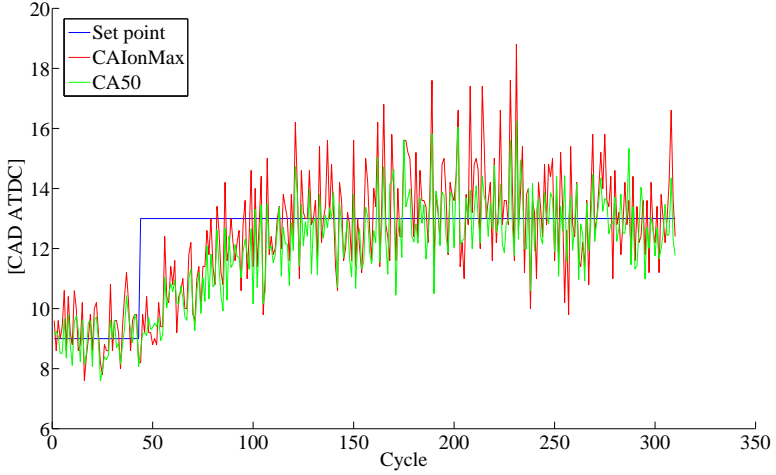
Figure 4.12 CA_{IonMax}-controlled step response. CA_{IonMax} and CA50 follow the set point. The fueling level is 470 J/Cycle.

the CA_{IonMax} and the real $CA50$ follow each other closely. Detection problems become apparent at fueling levels of around 380 J/cycle as can be seen in Fig. 4.13, but the combustion timing control still performs well. This is probably due to the higher SNR from the other cylinders.

Discussion

A difference between the pressure sensor and the ion current sensor is that the first measures the global pressure while the ion current only measures local conditions around the gap of the sparkplug. The reason for the good correlation between the ion current signal and the combustion timing is that HCCI combustion is initiated simultaneously (+- 1-3 degrees) throughout the entire cylinder. In spark-assisted HCCI, there is a flame front that has a pronounced influence on the signal shape. In this case, the ion current signal exhibits three peaks as shown in Fig 4.14. The figure illustrates 10 spark assisted cycles with the ignition fired at 40 CAD BTDC. The first peak between 40 to 25 CAD BTDC is due to the ignition and does not contain any useful information about the combustion. The second peak represents the flame front started by the ignition. The flame front starts the global combustion, which gives rise to the third peak (at approximately 5 - 15 CAD), which corresponds to the signal obtained in conventional HCCI. For some cycles, there is only one peak. This occurs when the mixture is too lean, resulting in large cycle to cycle variations in the flame front. These cycle to cycle variations make it
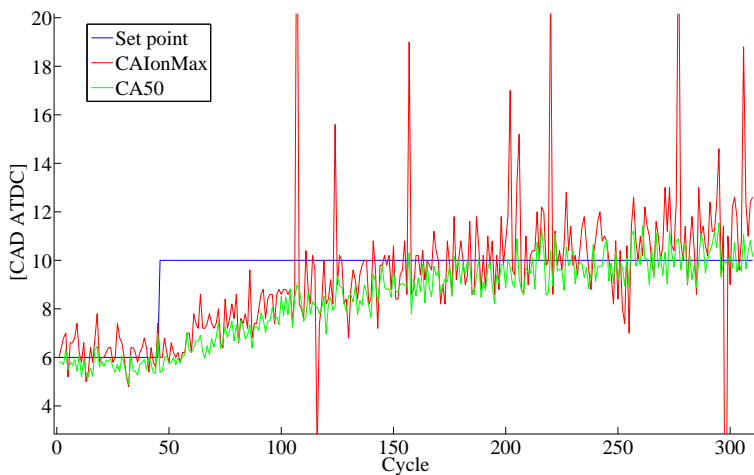
Figure 4.13 CA_{IonMax}-controlled step response. CA_{IonMax} and CA50 follow the set point, but there are some mismatches. The fueling level is 380 J/Cycle.
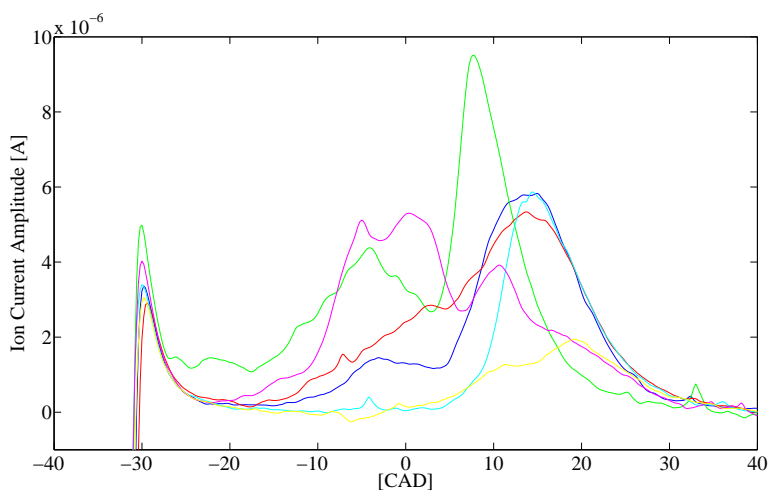

Figure 4.14   The ion current signal obtained over 10 consecutive cycles in spark-assisted HCCI mode. Spark assistance introduces an additional peak from the flame front initiated by the ignition.
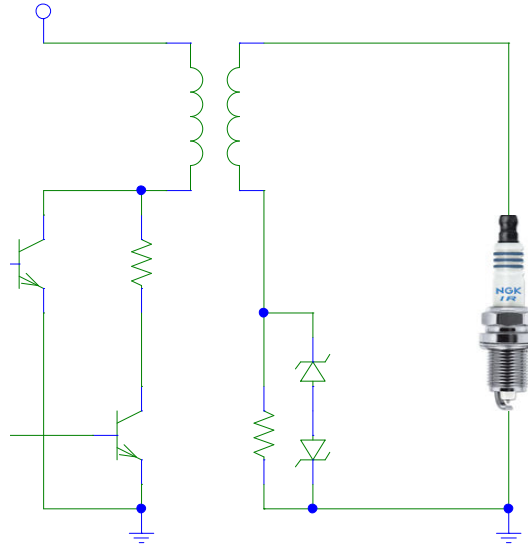
Figure 4.15 The primary side of the coil is switched at the desired carrier frequency using the lower transistor. In this way it is possible to produce very high measurement voltage on the secondary side. The upper transistor is used for controlling the ignition pulses.

more difficult to extract the combustion phasing from the measurements .

Other measurement approaches were also tried. A frequency analysis of the signals recorded using the measurement system as described in Fig 4.3 showed disturbances in the same frequency range as the the signal of the ion current. By performing an Amplitude Modulation (AM) of the current, the signal could be moved up in frequency to a point where disturbances are lower. Different AC sources, with frequencies of up to 100 kHz and approx 400V were built. The latest configuration of the AM measurement system is shown in Fig. 4.15 . This solution would be convenient since no extra hardware except for a transistor and some resistors and diodes are needed. To create the AC signal, the primary side of the coil is switched (the lower transistor) at the desired carrier frequency. The size of the left resistor determines how much energy is stored in the coil; by changing this, almost any desired AC voltage could be achieved on the secondary side. The measurements are made over the lower right resistor in the figure. The zener diodes in the figure are used to protect the measurement equipment during the spark discharges. Unfortunately, this approach proved to be a step in the wrong direction since currents

were obtained even when no combustion occurred. This may be because the air or the mixture in the spark gap can act as a capacitor; capacitors tend to conduct at high frequencies. Because of these problems, this approach was abandoned.

Summary

The ion current signal can serve as a source of combustion feedback. When the peak amplitude is high enough, ion current feedback is nearly as good as combustion phasing feedback derived from cylinder pressure-based heat release methods. The general behavior of the signals and how they are affected by different factors such as EGR, fuel amount and engine speed has been examined. When running without spark assistance, the shape is mostly affected by changes in timing. Changes in the amount of EGR, engine speed and amount of fuel injected primarily affect the amplitude rather than the shape of the signal. On-line ion current analysis for closed-loop combustion control has been performed with the "peak algorithm" . Off-line analysis established that when running without spark assistance the cycle to cycle similarity of the trace makes it possible to use a matched filter to detect the signals. This method improves the ratio of successful CA50 detections. Ion current is suitable as a feedback source for closed loop HCCI combustion control in the medium-to-high load (above 2.4 bar BMEP) region where HCCI is possible.

4.4 Extracting Cylinder Individual Combustion Data using a Torque Sensor

The aim of this section is to present a method which can be used to extract the combustion phasing from torque measurements.

The third combustion feedback sensor examined was the high precision ABB Torductor torque sensor [24] (see Fig. 4.16). This is a non-contact sensor that measures the changes in the magnetic flux that occur when the sensor axle is exposed to a torque. These changes correlate well to the changes in the torque. A typical torque trace and the corresponding pressure for each cylinder can be seen in Fig. 4.17.

Torque Sensing for Combustion detection

A method for detecting combustion phasing by using a torque sensor, named "torque ratio concept" was introduced by [25]. The authors have by using that method shown good results in detecting combustion phasing for both SI and diesel combustion. The method was also sucessfully tested in real time for closed-loop combustion phasing control of an SI engine [26]. The same type of sensor is used in this work but the combustion concept, Negative Valve Overlap (NVO) HCCI, differs in terms of its short combustion duration which typically lasts in between 4 to 7 crank angle degrees with a timing close to Top Dead Center (TDC).

Combustion around TDC causes problems since, the structure of the engine and hence the equations describing it makes it difficult to extract precise combustion related information. Another complication is the NVO meaning that for a four cylinder engine, there are two simultaneous in-cylinder events, combustion and re-compression, that have a significant impact on the torque.

The torque ratio concept relates the measured torque to a motored torque trace. This yields a signal correlating to the burn rate profile. The approach taken here is quite different compared to the torque ratio concept since the aim is to extract the combustion phasing by rebuilding the pressure trace. The method utilizes a physics-based torque model combined with data driven crankshaft flex models derived using least squares methods in the frequency domain.

Experimental Conditions and Experiments

The 2.3 liter four cylinder gasoline spray guided NVO Mule 1 engine is used. The engine is equipped according to the description in Chapter 3. Above that it is also equipped with the ABB Torductor torque sensor. The engine

Figure 4.16   The Torductor-s torque sensor [24].
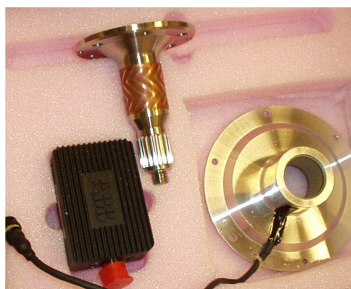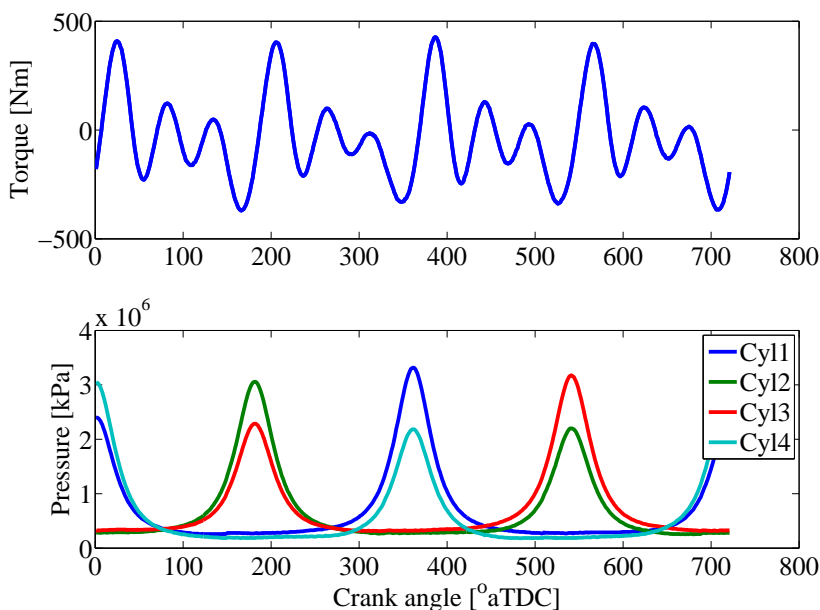

Figure 4.17   Typical torque trace and the corresponding pressure traces from the four cylinders.

was operated at 3 bar NMEP and the crank angle of 50% energy release, CA50, was swept from 3 to 8 Crank Angle Degrees, CAD, after top dead center, ATDC. The data from this single sweep was used for evaluation and development of the algorithms and results that are shown below.
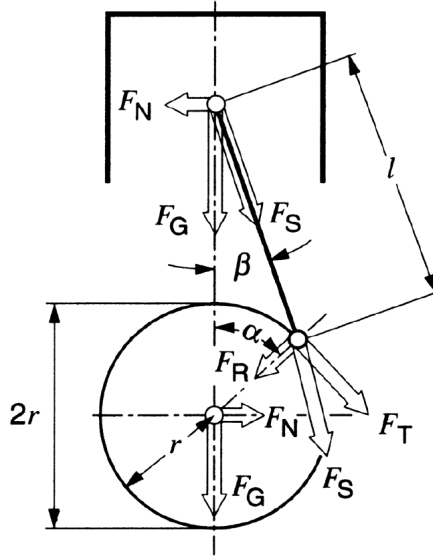
Figure 4.18 Variable notation for different components of the crankshaft mechanism. picture taken from[27].

Designing a Pressure to Torque model

The torque that the Torductor measures on the crankshaft can be seen as a sum of different contributions that originate from the cylinder pressure, mass forces and twisting of the crankshaft. The contributions of the first two are described by physical models. The twisting is described by the use of a black box model. Fig. 4.18 introduces a variable notation that should be used as a reference for understanding the discussion that follows.

Mass Forces The contribution of mass forces from each cylinder can be calculated if the complete engine geometry and the mass of the reciprocating parts are known. The derivation of formulas describing this can be found in [28]. The acceleration, a, of the reciprocating masses is possible to estimate using

$$a = r\omega^2(\cos\alpha + \lambda\cos 2\alpha) \qquad (4.17)$$

which describes the first and the second orders of oscillation. Higher orders of oscillation are neglected since they have, in comparison, low impact. r is the crank radius, ω the angular velocity, α the crank angle and λ the crank radius to con-rod length ratio. Since the accelerations of the masses are known (from Eq. 4.17), the engine speed induced inertial forces, F_m can be calculated using

Newtons second law,

$$F_m = ma \tag{4.18}$$

Gas Forces   The gas forces can be calculated using

$$F_G = PA_p \tag{4.19}$$

where P is the cylinder pressure and A_p is the projected area of the piston top. The total force, F_p, is then

$$F_p = F_m + F_G \tag{4.20}$$

Torque   The length of the torque lever can be described as

$$L = \frac{\sin(\alpha + \beta)}{\cos\beta} r \tag{4.21}$$

where β is given by.

$$\beta = \arccos(\sqrt{1 - \lambda^2 \sin^2 \alpha}) \tag{4.22}$$

The torque, t, generated by the force, F_p, can be calculated according to

$$t = F_p L \tag{4.23}$$

Converting measured pressure traces for each cylinder by using Eq. 4.23 to their corresponding torque traces and summing up the results, yields an estimate of the total torque that is caused by inertial and gas forces. The result of an experiment using the presented equations is shown in Fig. 4.19 where each cylinder individual torque contribution is shown in the upper subplot and the sums of these are displayed in the lower subplot. This plot also shows the Torductor measurements. The simulation shows that the mathematical model is able to estimate the trends of the torque, but the Torductor torque trace shows an oscillation superimposed on the physical model. This superimposed oscillation is caused by flexing of the crankshaft. This flexing must also be modeled in order to extract combustion related information from the Torductor sensor signals.

Crankshaft Flex Model   There are two possible strategies to model the flexibility of the crankshaft: physics based modelling and data driven modelling (system identification). The latter has, due to it's simplicity, been chosen here. The torque at the crankshaft that the Torductor is exposed to is considered as a sum of different torque contributions that are lead through cylinder individual weighting functions (H_1 to H_4 in the frequency domain).
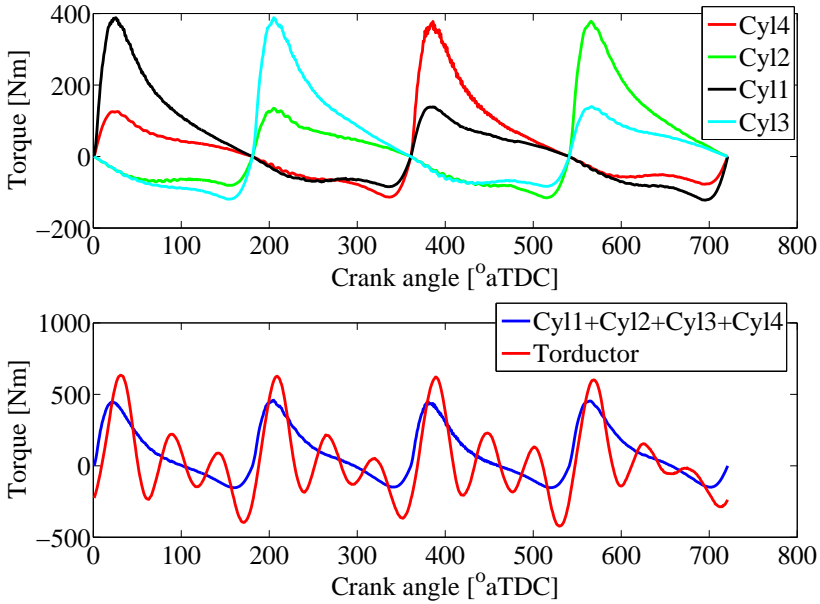
Figure 4.19   Each cylinder individual torque contribution is shown in the upper subplot and the sums of these are displayed in the lower subplot. This plot also shows the Torductor measurements. These shows an oscillation superimposed on the physical model. The oscillation is caused by flexing of the crankshaft.

The task is to estimate the filter parameters of these functions. If enough experimental data is available, the problem of doing so can be solved in a least squares sense. The method uses the fact that convolution in the time domain corresponds to multiplication in the frequency domain. The first step of the system identification process is therefore to convert each modeled torque trace and Torductor measurement trace, for each cycle that is used for the identification purpose, to the frequency domain using a discrete Fourier transform according to

$$T_x = \mathcal{F}\{t_x\} \tag{4.24}$$

where t_x is the measured or estimated (from the pressure sensors or the Torductor) time-discrete torque samples. The mathematical description of the dynamics can in the frequency domain be described as.

$$T_q = H_1 T_1 + H_2 T_2 + H_3 T_3 + H_4 T_4 \tag{4.25}$$

Where T_q and T_1 to T_4 are the discrete Fourier spectra of the Torductor torque trace and the torque calculated for each cylinder respectively. The

coefficients of the spectra are now redefined as $T_{n,k}(m)$ and $Tq_n(m)$, were m denotes a specific sample of the spectrum from cycle n and cylinder k. The following relations, taken from Eq. 4.25 hold for each specific sample, m.

$$
\begin{bmatrix}
T_{1,1}(m) & . & . & T_{1,k}(m) \\
. & . & . & . \\
. & . & . & . \\
T_{n,1}(m) & . & . & T_{n,k}(m)
\end{bmatrix}
\begin{bmatrix}
H_1(m) \\
. \\
. \\
H_k(m)
\end{bmatrix}
=
\begin{bmatrix}
Tq_1(m) \\
. \\
Tq_n(m)
\end{bmatrix}
\tag{4.26}
$$

If enough individual cycles/spectra, n, are available the coefficients of $H_1(m)$ to $H_4(m)$ can be estimated for each m using the pseudo inverse [29] for least squares estimation according to

$$
X = \left(A^T A\right)^{-1} A^T Y \tag{4.27}
$$

Where X corresponds to the second matrix in Eq. 4.26, A the first and Y the third matrix. This least squares procedure is performed for all samples, m. In this way, a complete model for simulating the crank shaft flex is available. By combining the pressure to torque model with the flex model, a complete pressure to "flywheel torque" model is obtained. A comparison between simulation and measurement can be seen in Fig. 4.20. The similarity between the two signals is obvious.

Designing a Torque to Pressure model

The previous section demonstrated that a physical torque model combined with a data driven flex model can be used to convert from in cylinder pressure to torque measured between the crankshaft and the flywheel. The intention is, however, to go in the opposite direction from torque to pressure.

Inverting the Flex model   The first step for reconstructing pressure traces by using Torductor measurements is to invert Eq. 4.25 for going from the measured torque sensor signal to a cylinder individual torque estimate. The equation can be rearranged and transformed to the discrete time domain according to

$$
t_1 = \mathcal{F}^{-1}(H_1^{-1}(T_q - (H_2 T_2 + H_3 T_3 + H_4 T_4))) \tag{4.28}
$$

Eq. 4.28 describes how torque of cylinder one, t_1, relates to the spectra from the Torductor and the other cylinder torques. The equation clearly states that it is impossible to rebuild the torque for any cylinder if the torque of the others are not known. This is not a large problem since only one combustion event occurs at a time. The cylinders that are not currently firing can be simulated if
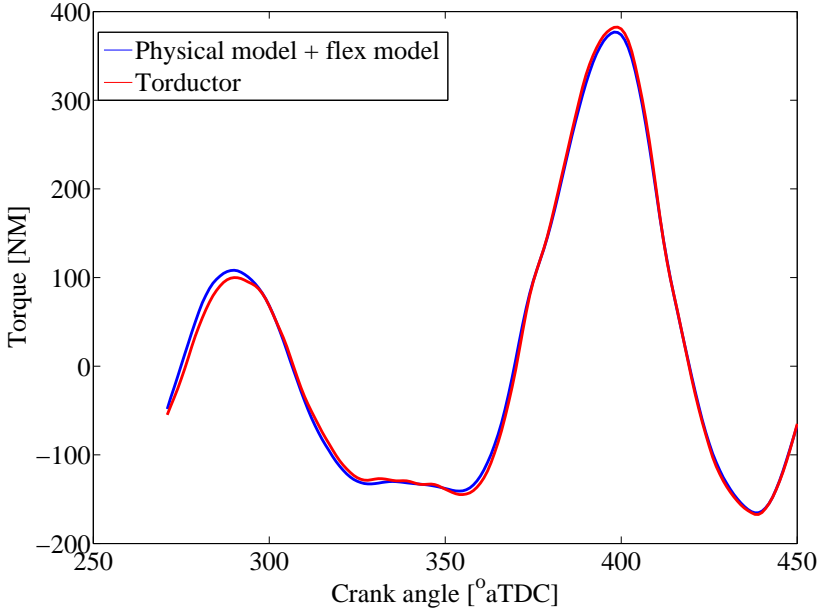
Figure 4.20 The physical torque models combined with the identified transfer functions yields a result very similar to the Torductor signal.

only the valve timings and the intake/exhaust pressures for them are known. Simulation of the non firing cylinders with closed valves are calculated using polytropic relations according to

$$P(\alpha) = P(\alpha_{vc}) \left(\frac{V(\alpha_{vc})}{V(\alpha)} \right)^{\gamma} \tag{4.29}$$

where $P(\alpha)$ and $V(\alpha)$ states the pressure and cylinder volume at a crank angle α and vc denotes timing for either an exhaust or intake valve closure event. γ is the specific heat ratio

The result of this torque conversion by using Eq. 4.28 for going from the Torductor signal to an individual cylinder torque can be seen in Fig. 4.21. The estimated torque signal is noisy but otherwise follows the real torque contribution well.

Inverting the Pressure to Torque Model It is straightforward to invert the pressure to torque functions (Eq. 4.17 to Eq. 4.23) described in the section
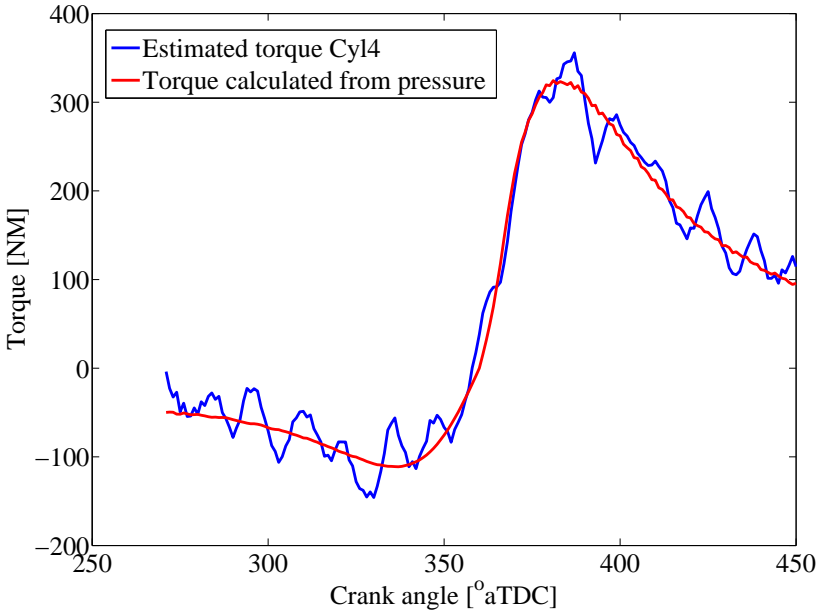
Figure 4.21 By making an inverse filtering the estimated torque contribution is given. It is noisy but otherwise matches the torque contribution from the pressure trace fairly well.

"Designing a Pressure to Torque model ". The results of the inversion is given by

$$P = (\frac{t}{L} - F_m)\frac{1}{A_p} \tag{4.30}$$

It is not difficult to see that the inverse is ill-conditioned at TDC and close to TDC where the torque lever L is zero or close to zero. This means that the errors in the estimation of the cylinder individual pressure are amplified. Unfortunately this region is very close to where the combustion occurs and thus important information can be lost. Fig. 4.22 illustrates an example of a reconstructed pressure trace by using Eq. 4.30. The resulting signal is noisy especially around TDC. An estimated pressure trace using the described approach is unfortunately too poor for performing any reliable heat release calculations. The noise originates from the estimation of cylinder individual torque (see Eq. 4.28 and Fig. 4.21) and this is where the problem should be eliminated.
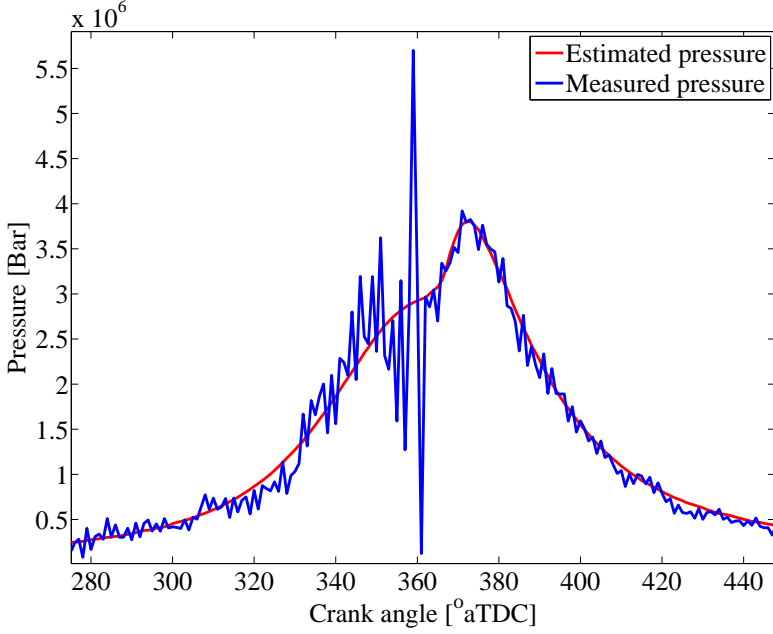
Figure 4.22 Estimated pressure trace versus measured pressure trace. At TDC and BDC the length of the torque lever is zero which makes the inversion impossible. Therefore an interpolation has been made between the points BDC/TDC +-1. The errors are amplified around TDC.

Parameter Tuning Against Estimated Torque

The noisy estimate of the cylinder individual torque as seen in Fig. 4.21 is improved by fitting a combustion to torque model to the measurements. The model is based on the physical torque model described by Eq. 4.23 where the cylinder pressure in Eq. 4.19 is taken from a combustion model based on the ideal gas law and isentropic relations. The equation for the pressure (which holds when the valves are closed) is defined as follows:

$$P_\alpha = P_{\alpha-1} \left(\frac{V_{\alpha-1}}{V_\alpha} \right)^\gamma q_{comb} \tag{4.31}$$

where P_α denotes the pressure and V_α the cylinder volume for a specific crank angle α. The parameter q_{comb} is the quotient of the temperature before and after a segment of fuel is burnt. q_{comb} is described by

$$q_{comb_\alpha} = \frac{T_2}{T_1} = \frac{m_{fuel_\alpha} Q_{LHV}}{m_{tot} C_v T_1} + 1 \tag{4.32}$$
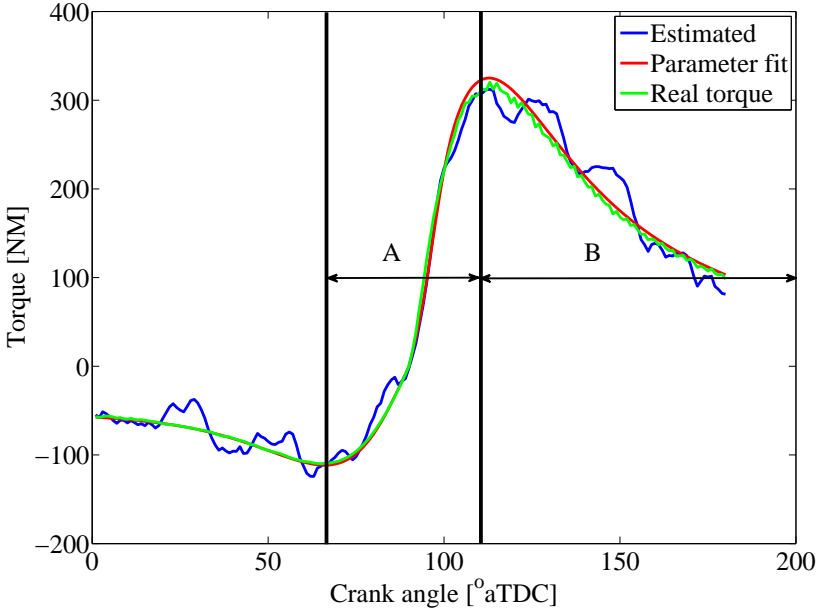
47

Figure 4.23 Example of estimated torque, torque calculated using parameter fit and the true torque calculated using cylinder pressure in the corresponding cylinder. A and B is the regions where $CA50$ and fuel are tuned respectively.

where Q_{LHV} is the lower heating value for the fuel and m_{fuel_α} is a segment describing the amount of fuel that is burnt at a specific α. By controlling how segments are defined at different α it is possible to build any desired pressure/torque trace. An numerical algorithm shapes these segments in such way that the mean square error between the estimated torque and the torque of the model is minimized. The algorithm works in two steps. First a minimization with respect to total fuel mass is made in the region B (see Fig.4.23), located after combustion. Secondly, a minimization with respect to CA50 is made in region A where the combustion occurs. The minimization tasks are made in this order since the torque in region B is unaffected by the optimization of region A but not the reverse. The mean square error of the two regions A and B for different fuel and CA50 can be seen in i Fig. 4.24. The resulting torque trace after the parameter fit for one cycle is seen in Fig. 4.23. The deviation between the true torque calculated from the pressure and the torque from the parameter fit is small.
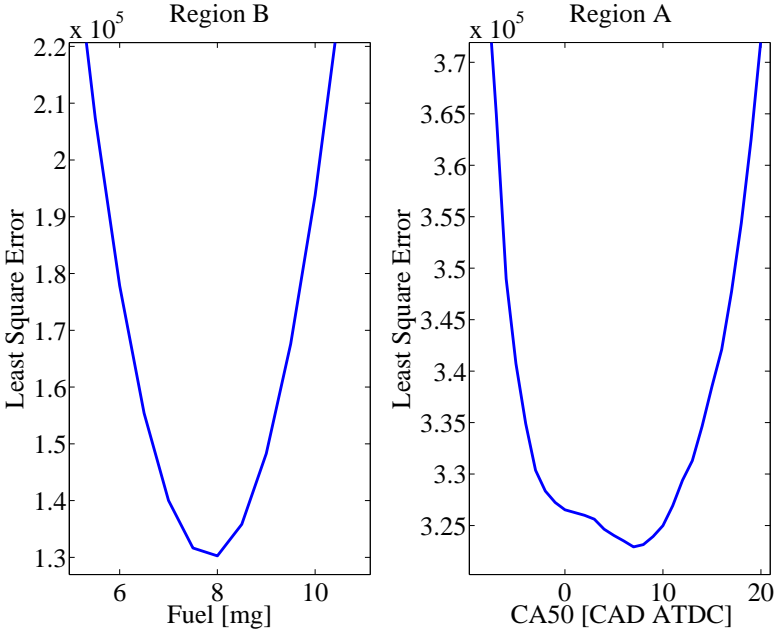
Figure 4.24   The mean square error of the two regions a and b for different fuel mass and CA50. The numerical algorithm locates the combustion parameters giving the minimum of these curves.

Estimated CA50 Versus True CA50   An example of how an estimated pressure trace can look compared to true pressure is seen in Fig. 4.25. CA50 is extracted from the parameter fit and compared against true CA50 (pressure based) and the relation between these two parameters is seen in the scatter plot in Fig. 4.26.

There is quite a large spread of the data and the correlation is not good enough for cycle to cycle control. To improve the estimates, ensemble averaging is implemented as a window sliding over the torque estimates while calculating the mean for the exposed samples. A scatter plot using these results from ensemble averaging with a length of ten cycles is seen in Fig 4.27.

The coefficient of determination between the two data sets is 0.948. Using the method of ensemble average will not allow true cycle to cycle control but it will provide useful feedback information and the accuracy of the estimates can clearly be improved.
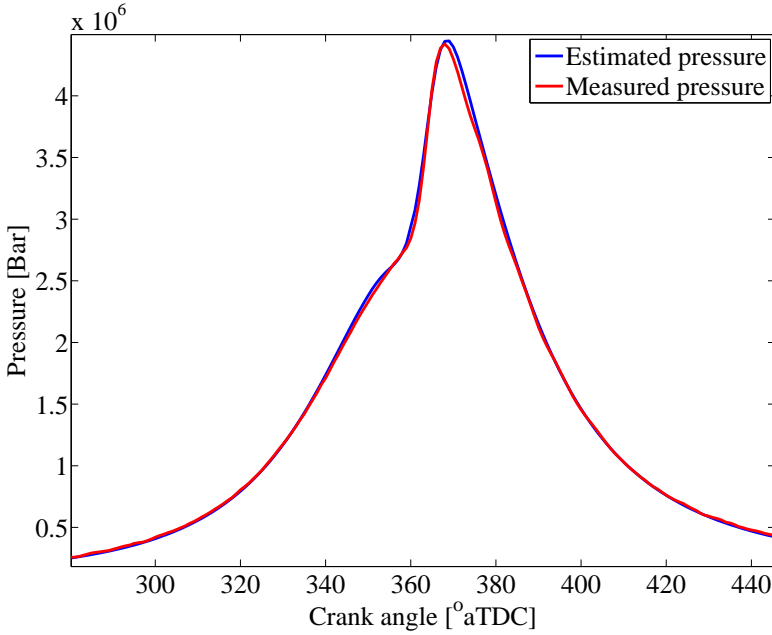
Figure 4.25   Example of a rebuilt pressure trace versus true pressure.

Discussion

The proposed algorithm was evaluated around one speed and load point with different CA50 swept from early to late combustion. The results of the CA50 estimations seem encouraging but the limited nature of the investigation makes it difficult to draw definite conclusions. The method must be evaluated at more operating points with different speeds and loads to really understand the performance and the robustness of the method.

HCCI has extremely fast combustion, it typically lasts for 4 to 7 crank angle degrees with its timing close to TDC. If the combustion is too close to TDC, the proposed method should still be able to handle the estimation but with decreased precision as a result. The decrease in precision around TDC is caused by the structure of the engine with a torque lever of zero or close to zero in length. Slower combustion, as with Diesel or SI combustion, should provide better results since much combustion related information is present further away from TDC.

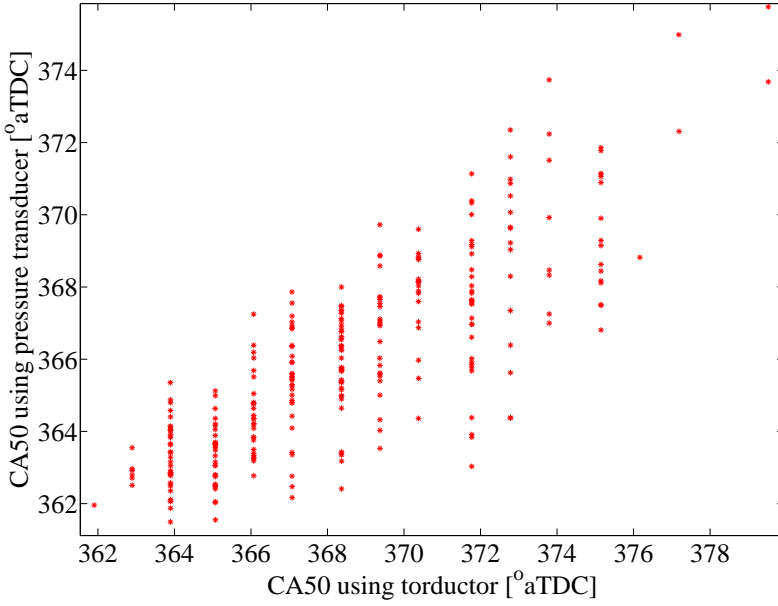Another factor working against the estimation for the type of engine used

Figure 4.26   Scatter plot demonstrating the correlation between estimated and true, pressure based CA50.

is the NVO which causes a recompression event simultaneously (in a four cylinder engine) while another is compressing. The recompression is modeled in order to allow data extraction from the cylinder with combustion. Errors in the modeling of the recompression may introduce errors in the data extraction.

Attempts were also made to improve the signal to noise ratio of the estimated torque in Fig. 4.21 by filtering the oscillations superimposed on the reconstructed signal. Unfortunately the frequency content of the oscillations is too close to the frequency content of the useful torque signal to allow effective filtering.

The probably most precise methods for extracting pressure related data is by using a parameter fit according to or similar to the described algorithms. A drawback with the proposed algorithm is the high computational demand which makes it less suitable for real time application. Optimizing the algorithm for real time implementation together with evaluation in more speed and load points are the tasks for future work on the proposed concept.
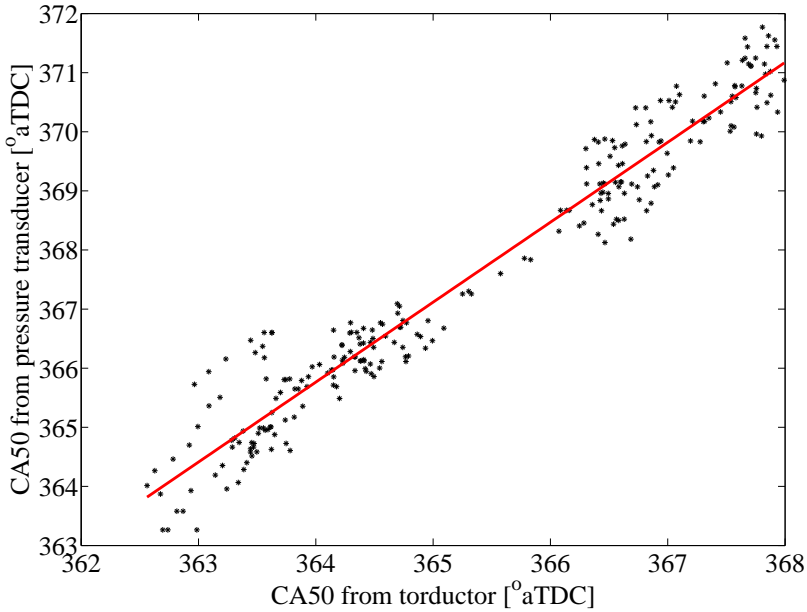
Figure 4.27 Example demonstrating how CA50 calculations based on Torductor measurements compare vs pressure based measurements when using ensemble averaging with a length of ten cycles.

Summary

A method for extracting CA50 using the signal from a high precision torque sensor has been proposed. The method utilizes a physics-based torque model combined with data driven crankshaft flex models derived using least squares methods in the frequency domain. The problem of estimating cylinder individual torque can be solved only if the torque contributions of the other cylinders are known (see Eq. 4.25). Since only one cylinder fires at a time, it is possible to simulate the others using polytropic relations (see Eq. 4.29). When the cylinder individual torque estimate is known it is improved by making a parameter fit between the estimates and a combustion to torque model. The resulting torque is then used to estimate the CA50 and reconstruct the cylinder pressure. The torque based CA50 estimations demonstrated good correlation with a coefficient of determination of 0.95 against "true" CA50 based on 10-cycle ensemble averages.

4.5 Cylinder Air Charge Estimation Using Cylinder Pressure Transducers

This section aims at introducing how instantaneous cylinder individual air charge estimation can be achieved by using cylinder pressure transducers. Sensors commonly used for estimating cylinder air charge suffer from measurement errors during transients. It is likely that the combustion engines of tomorrow will have in-cylinder pressure sensors installed in order to estimate load and combustion phasing of the engine.

Cylinder pressure sensors can also be used to estimate the airflow into the engine. Some research has been conducted in this area already [30]. However, the algorithms described to date work by pegging the pressure traces to the intake pressure and will therefore not provide reliable measures of the true cylinder-individual air charges. The algorithm presented here does not need an intake pressure sensor because the pressure offset is extracted using a least squares fit against a polytropic compression curve. It is therefore possible to make instant estimates about the conditions in each cylinder. The sensors that are required are an intake thermocouple sensor and the in-cylinder pressure transducers. The method is based on the ideal gas law and a residual gas model combined with an observer for improved estimates. The algorithms predictions were compared to data measured using a high-precision air mass flow meter and its sensitivity to measurement errors is considered. The algorithm generated promising cylinder air charge estimates, and should be used for improved transient control of the mass flow in any engine equipped with cylinder pressure transducers.

Measurement Setup

The A20DTH engine (see Chapter 3) equipped with individual pressure transducers was used. A hot-wire Bronkhorst F-106BI-AFD-02-V mass flow meter was used for reference measurements

Description of the algorithm

The algorithm is based on the ideal gas law (Eq. 4.33); calculations are performed using values appropriate for the conditions encountered just after the intake valve closure event. The cylinder is modeled as a closed boundary system, making it possible to solve for the mass of gas in the cylinder:

$$m_{ivc} = \frac{P_{ivc}V_{ivc}}{T_{ivc}R} \qquad (4.33)$$

The inputs required to estimate the cylinder charge mass using this equation are the temperature T_{ivc}, the cylinder volume V_{ivc}, and the pressure P_{ivc}.
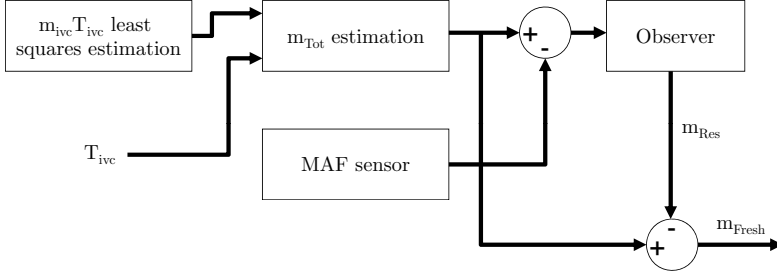
Figure 4.28   The complete cylinder air charge model including the observer used to determine the nature of the residual mass.

The first of these can be estimated by assuming it to be equal to the intake manifold temperature. The second is known from the geometry of the engine, and the third is obtained from the pressure transducer signal. However, current leakage, and thermal stress causes the pressure signal to drift over time, also noise is superimposed on the measured pressure signal, and this must be compensated for. This is done using a least squares fit between the measured, offset signal and a polytropic compression curve.

The described algorithm only estimates the total mass in the cylinder. It cannot be used to determine whether the cylinder contains air or residual gases. A complementary residual gas model was therefore developed that can, in conjunction with input from an observer, be used to distinguish between fresh and residual mass charge; this model was used to extend the algorithm. Fig. 4.28 illustrates the work flow for the complete cylinder air charge model including the observer used to determine the nature of the residual mass.

Improving the Pressure Measurement Data

The compression can be described using a polytropic compression curve at any instant, n after the closing of the intake valve. This can be combined with the ideal gas law to yield Eq. 4.34, which holds for any crank angle between IVC and the start of combustion

$$m_{ivc}T_{ivc}\left(\frac{V_{ivc}}{V_{ivc+n}}\right)^{\gamma-1} = \frac{P_{ivc+n}V_{ivc+n}}{R} \tag{4.34}$$

The long term drift, ΔP of the pressure trace is taken into account by rewriting this equation as follows:

$$m_{ivc}T_{ivc}\left(\frac{V_{ivc}}{V_{ivc+n}}\right)^{\gamma-1} = \frac{(P_{ivc+n} + \Delta P)V_{ivc+n}}{R} \tag{4.35}$$

This is rewritten as

$$m_{ivc}T_{ivc}\left(\frac{V_{ivc}}{V_{ivc+n}}\right)^{\gamma-1} - \frac{\Delta P V_{ivc+n}}{R} = \frac{P_{ivc+n}V_{ivc+n}}{R} \qquad (4.36)$$

and finally as

$$m_{ivc}T_{ivc}a_{n1} - \Delta P = y_n \qquad (4.37)$$

The equation can be restated in matrix form $(AX = Y)$, giving the following expression for a series of different pressure readings (1....n):

$$\begin{bmatrix} a_{11} & 1 \\ . & . \\ . & . \\ a_{n1} & 1 \end{bmatrix} \begin{bmatrix} m_{ivc}T_{ivc} \\ \Delta P \end{bmatrix} = \begin{bmatrix} y1 \\ . \\ . \\ y_n \end{bmatrix} \qquad (4.38)$$

A least squares estimate of $m_{ivc}T_{ivc}$ and ΔP using the pseudo inverse as in Eq. 4.39 can now be made:

$$\begin{bmatrix} m_{ivc}T_{ivc} \\ \Delta P \end{bmatrix} = \left(A^T A\right)^{-1} A^T Y \qquad (4.39)$$

The procedure is performed each cycle, yielding a precise estimate of the $m_{ivc}T_{ivc}$ term without needing to use a manifold sensor.

Cylinder Air Charge Estimates

The throttle position was adjusted in a stepwise fashion and the mass flow measured using the Bronkhorst Mass Air Flow (MAF) sensor was compared to the values estimated by the algorithm. The results are shown in Fig. 4.29. It is clear that the estimated CAC values respond instantly to changes while the MAF sensor responds more slowly.

Sensitivity to errors in temperature

The cylinder pressure sensors are instant but the temperature sensors that are used do have some lag. It is to be expected that the intake temperature will change somewhat due to the differences in pressure on either side of the valves and to heat transfer. This raises a question: how will these errors in the measured temperature affect the estimated cylinder air charge? The algorithm estimates the cylinder mass using Eq. 4.33. Looking at this expression, one might intuitively suggest that the error then will be affected according to the ratio $\frac{1}{x}$ where x is the ratio of the measured and the true temperatures. Fig. 4.30 demonstrates how the error of the temperature on the x-axis affects the estimation error on the y-axis. The estimation of T_{ivc} could be improved
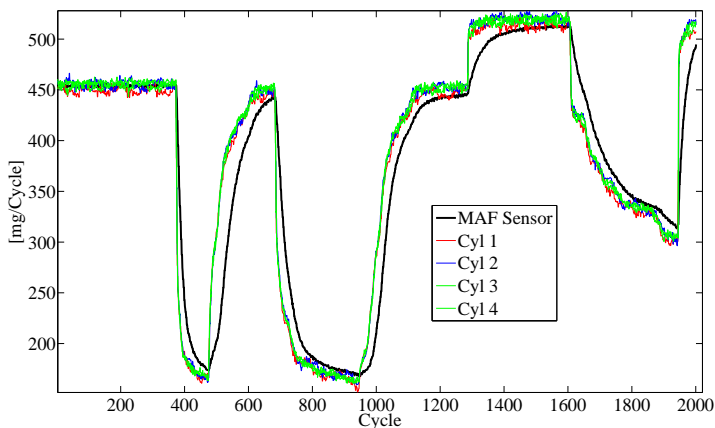
Figure 4.29   Data obtained using an MAF sensor compared to the estimated air charge values for each cylinder generated using the new algorithm without the observer.

Figure 4.30 T_{ivc} error (for a true intake temperature of 320 K) versus cylinder air charge estimation error.

in various ways, for example by using mean value models to handle transient conditions. With an error of 20 K at a real temperature of 320 K, the estimated cylinder air charge would be 6% greater than the true value.

Figure 4.31   Artificial white noise in the pressure traces has very little impact on the biasing (E(X)) of estimated cylinder air charge.

Sensitivity To Measurement Noise
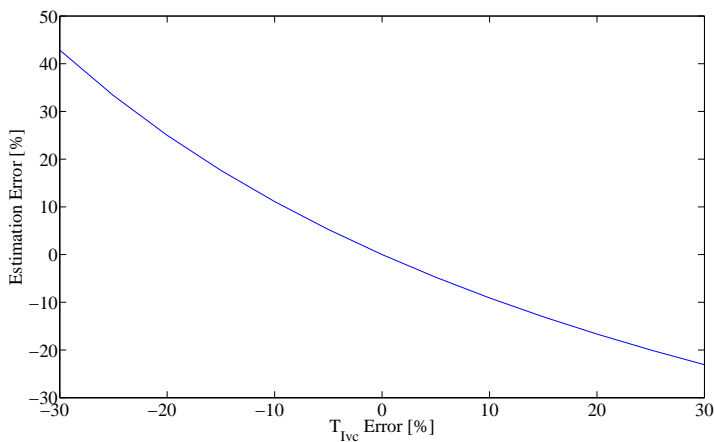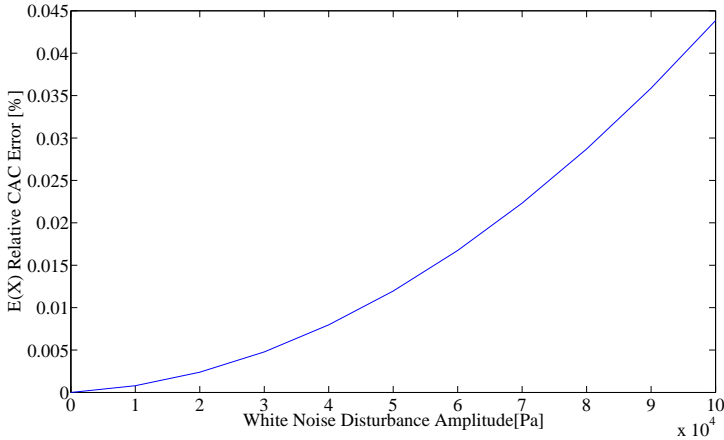
The influence on E(X) of the biasing error is less than 0.05% if the measured pressure trace is disturbed by white noise below 1 bar. Larger disturbances than this are not likely to ever occur. The relative biasing error as function of the amplitude disturbance is shown in Fig. 4.31. The standard deviation of the relative error is shown in Fig. 4.32. It is apparent that the least squares parameter fit against the polytropic compression model is highly effective at suppressing noise.

Compensating for Residuals and Short-Route EGR

It should also be possible to estimate the air charge when operating with internal EGR, whether short- or long-route. However, the algorithm discussed above only estimates the total mass inside the cylinder. One way to estimate the composition of the residual gas would be to use an observer that could generate estimates of the masses of the residuals (see Fig. 4.28). The residual model used here is defined in the most simple way possible, meaning that the mass of residuals, x from cycle $k + 1$ equals that in cycle k

$$x_{k+1} = x_k$$
$$y_k = x_k \tag{4.40}$$

The measured signal y_k from the sensor used to provide feedback to the observer corresponds to the difference between the total estimated mass (taken
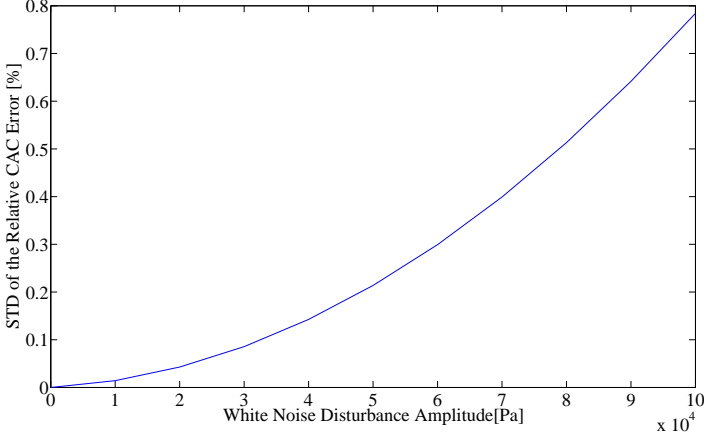
Figure 4.32 Artificial white noise in the pressure traces has relatively little impact on the standard deviation of the relative error.

from the proposed algorithm) less mass measured using the mass air flow meter. Alternatively, it should be possible to use data from the lambda sensor for this purpose, since the mass of injected fuel is known.

$$y_k = m_{tot} - m_{MAFSens} \tag{4.41}$$

The observer is described by

$$\hat{X}_k = (A - LC)X_k + LY_k \tag{4.42}$$

where A and C in this case are equal to 1 and the coefficient L must be below 1 to maintain the stability of the filter. The coefficient was manually tuned for stable correction and fast response. This observer can keep up with slow changes in EGR mass or intake temperature. The complete cylinder mass charge model combined with the residual air charge model is now described by

$$m_a = \frac{P_{ivc}V_{ivc}}{T_{ivc}R} - \hat{X}_k \tag{4.43}$$

Where m_a is the estimated cylinder air charge. An example of the results obtained using the observer can be seen in Fig. 4.33. The engine is operated with EGR and the intake throttle is adjusted in a stepwise fashion. The observer is initiated at cycle 500 to correct for the offset of the estimated mass flow.
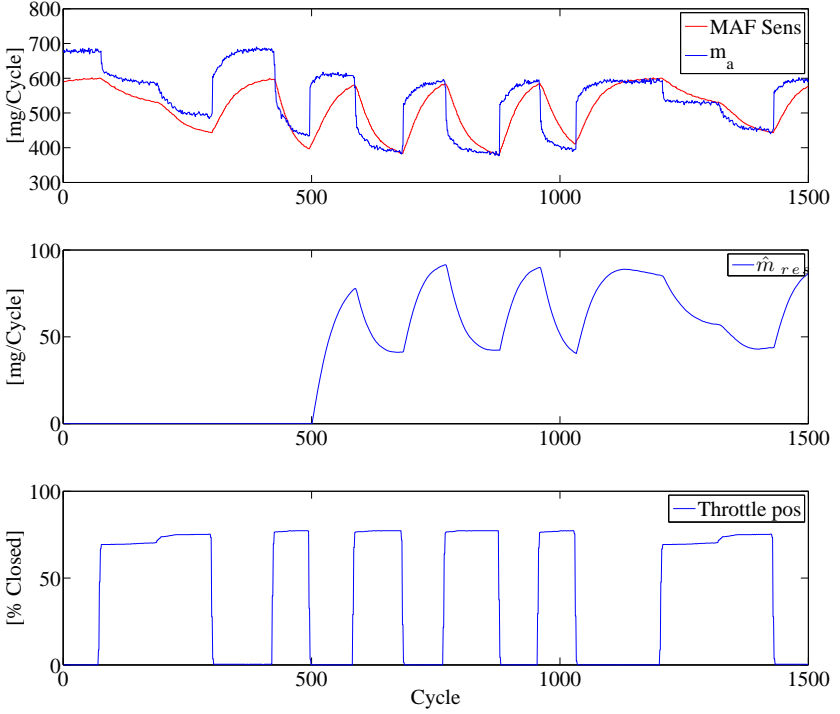
Figure 4.33   The observer is initiated at cycle 500. It estimates the mass of residuals which is used for correcting the mass flow.

Summary

A new algorithm has been proposed that estimates the air charge in each individual cylinder during the engine cycle. It uses the cylinder pressure and the intake manifold temperature sensor as inputs. The basic concept relies on the ideal gas law according to Eq. 4.33. The calculations are based on conditions present during the intake valve closure event, when the system can be described as a closed boundary system. It is very important to obtain an accurate and precise measurement of the pressure during the IVC event. This is achieved by fitting a polytropic compression model against data from measured pressure traces. The estimates generated by the new algorithm are promising for transient conditions but may be prone to bias under steady state conditions. This is caused by differences between the in-cylinder temperature and the manifold temperature, and to external and internal EGR. A simple EGR model was therefore defined stating that the residuals at cycle $k+1$ are equal to those in cycle k. This model was used to design an observer

that was capable of compensating for the estimation errors.

4.6 Conclusions

This chapter described investigations into the use of different combustion feedback sources. The piezo-electric pressure transducer is superior to the alternatives; it generates precise pressure readings that can be used to reliably determine how much energy was released and how it was released. This cannot be done with anything like the same precision using any of the other methods considered. However, the cost of these sensors is high.

If the objective is simply to estimate the combustion phasing, and if the signal-to-noise ratio is sufficiently high, the in-cylinder ion current could serve as a useful alternative sensor. This will not be viable at low loads (below about 2.4 bar NMEP). The control system was changed to use the position of the ion current peak as feedback instead of CA50. The engine was operated in this fashion; it was found that using this input, the system was able to exert adequate control over combustion phasing.

The experiments with the Torductor torque sensor demonstrated that the pressure traces in each cylinder could be reconstructed using a combination of physical torque, combustion and black box models and that these reconstructed traces could be used to estimate the CA50. While the estimated CA50 values seem to be encouragingly accurate, the limited nature of the investigation makes it difficult to draw strong conclusions. The method must be evaluated at more operating points with different speeds and loads to fully understand the performance and the robustness of the method. The proposed algorithm also needs to be refined so as to be suitable for realtime implementation.

A new algorithm was proposed that uses the in-cylinder pressure and data from the intake manifold sensor to estimate in-cycle cylinder-individual air charges. It is recommended that this algorithm is used for improved transient control of mass flow in any engine equipped with cylinder pressure transducers.

5

Turbo NVO HCCI

This chapter focuses on the behavior of Turbo NVO HCCI engines and discusses their modeling and control, with particular emphasis on actuator-based methods and various alternative approaches.

HCCI engines do not have any direct ignition trigger such as the spark in SI or the time of injection in the diesel engine. Instead, self-ignition occurs at a point dictated by the internal conditions in the cylinder - the temperature, pressure, mass of fuel, and residual gas fraction [31]. It is not easy to reliably predict or measure these variables and it is therefore extremely difficult to reliably control combustion in a HCCI engine without feedback control. Several approaches for the control of HCCI have been proposed, including the use of dual fuels [32], variable compression ratios [33], and variable effective compression ratios through Intake Valve Closure (IVC) timing [34]. The approach developed in this thesis is based on controlling the ratio of hot residuals [10]. This is achieved through the usage of Negative Valve Overlap (NVO) i.e. early Exhaust Valve Closing (EVC). Hot residuals are captured by manipulating the timing of EVC. These residuals are then used in the next cycle to heat up the mixture so as to ensure that conditions suitable for auto-ignition are achieved at the desired moment in time.

Typical Naturally Aspirated (NA) NVO HCCI engines have restricted operating ranges due to the limitations imposed by rapid increases in the in-cylinder pressure and the ringing intensity at high loads. A turbocharger can be used to suppress the ringing by diluting the mixture with more oxygen [35], thereby increasing the load range tolerated by the engine. Fig. 5.1 illustrates how the load is increased for a given set of limitations in ringing index, emissions, combustion stability etc for the engine used in this study. The early closing of the exhaust valves makes the engine sensitive to pressure changes over the intake and exhaust manifolds. Since the operation of the turbocharger greatly affects both the exhaust and intake pressure, the turbo
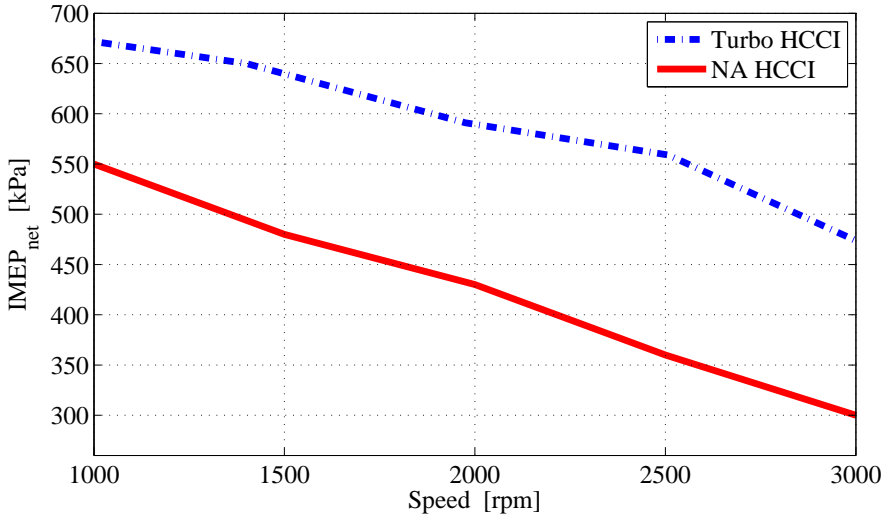
Figure 5.1 Load increases achieved using a turbocharger with a NVO HCCI engine subject to a given set of limitations on the ringing index, emission profile, and stability of combustion.

dramatically increases the difficulties associated with controlling the engine.

The turbo fundamentally changes the way that EVC works as an actuator. From a short-term perspective, turbo lag means the EVC affects the residuals in the same way as would be expected for a NA engine. EVC also affects the volumetric efficiency and hence the mass flow through the turbo. This means that EVC also indirectly affects the mass of the fresh cylinder air charge.

In recent years, model-based controllers have been favoured for the control of HCCI combustion. The main steps involved in the development of a model-based control system are: the design of a plant, controller design, simulation, and real experiments. It is likely that the experimental results will be less satisfactory than the simulated data in the first instance. Consequently, an iterative process of simulation and experiment is generally required to achieve optimal performance. The advantage of model-based controllers is that errors can be detected at an early stage in the design process. The plant model is used to identify the dynamics and the characteristics of the plant, which are then used to synthesize a controller. The simulations quickly provide detailed insights into what actually happens in the plant. The primary drawback of using model-based control is that accurate models can be difficult to obtain.

In addition, non-model-based controllers are often more intuitive to tune and can be used and maintained by less-skilled engineers.

[36] developed an LQG controller using a model that had been derived using system identification methods. [37] developed physical models working in the crank angle domain. A viable HCCI engine model must be able to accurately predict the start of combustion. Some authors have tried to achieve this by incorporating derivatives of the Arrhenius knock integral model [37, 38, 39]. To further capture the dynamics of the engine's behavior, [40] also incorporated a wall temperature model to capture the slow dynamics of a drifting CA50. The author developed a physical model which describes the temperature in the cylinder by using three states with physical meanings. The model temperature is correlated against experimental data for providing an expression describing how the combustion phasing behaves on a cycle to cycle basis. The model which is presented in Chapter 5.5 was used for the design of a LQG controller presented in Chapter 5.6.

5.1 NVO HCCI Control Means

This section discusses the two processes that are most commonly used when trying to exert actuator-based control over combustion phasing. These are the valve timing and the injection timing events.

Valve Timing

The valve lift curves for the intake and exhaust valves are shown in Fig. 5.2. The effects of NVO are visible in the recompression (in the lower subplot) over the gas exchange TDC (@180 CAD). Adjustment of the EVC timing is the most effective "tuning knob" for exerting control over the timing of combustion in HCCI engines. However, when it comes to the timing of Intake Valve Opening (IVO), it is not as obvious how to set the timing since it has little effect on the combustion phasing . It should therefore be set to maximise efficiency. This is done by avoiding a blowdown into the intake manifold. Consequently, the volume at IVO (V_{ivo}) should always be equal to the volume that would be occupied by the mixture if it were allowed to expand isentropically to the intake manifold pressure, P_{im}. This is given by:

$$V_{ivo} = V_{evc} \frac{P_{im}}{P_{em}}^{-\frac{1}{\gamma}} \tag{5.1}$$

Where V_{evc} and P_{em} are the cylinder volume at exhaust valve closing and exhaust manifold pressure, respectively. At high load, some efficiency must be sacrificed and IVO should be retarded further to increase the mass flow into the cylinder, which is required to maintain low noise levels.
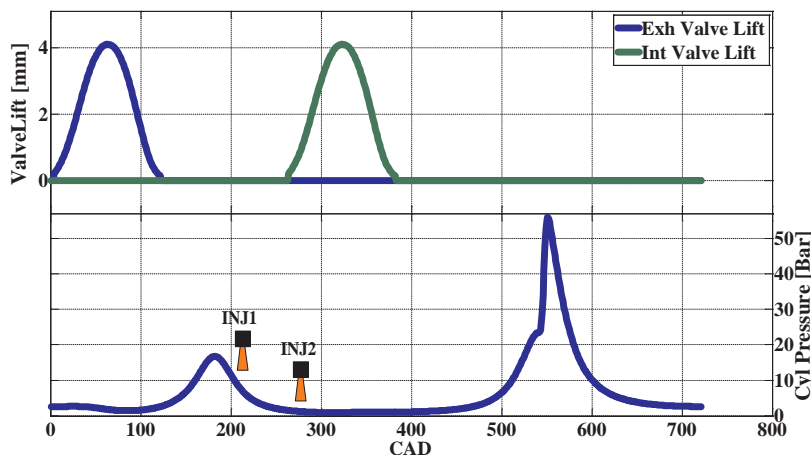
Figure 5.2   Valve lift curves and the corresponding pressure trace for a load point. The injection strategy is also shown. Inj1 is used for CA50 balancing and Inj2 (the main injection) for NMEP balancing.

Injection Timing

Two injections are required during each engine cycle, one small injection (INJ1) during the negative valve overlap, and one main injection (INJ2) during the intake stroke (see Fig. 5.2). Since INJ1 occurs during the period of negative valve overlap when the pressure is high, some of the fuel will reform releasing heat. The further the timing of INJ1 is advanced, the greater the degree of reformation. In this way, the temperature at IVC can be adjusted and so the phasing of the combustion process can be adjusted as required on a per-cylinder basis. When the load increases, the EVC must be retarded to make it possible to maintain the desired combustion phasing. The pressure during recompression will then change, which will affect the reformation of the fuel. Therefore, the actuation response used to control the temperature of the mixture at IVC is strongly affected by the load.

5.2 Cylinder Balancing Control

This section discusses ways in which NMEP and CA50 can be balanced on a per-cylinder basis.

If all the cylinders' injection actuator settings are the same, it is possible

to obtain a situation in which a high Ringing Intensity (See Eq. 4.3) occurs in some cylinders while others may be close to misfiring. Such imbalances can have a variety of causes, including differences in wall temperature, volumetric efficiency, and compression ratios. The stability of the engine can thus be improved by balancing these differences using active controllers for both load and combustion phasing.

The first injection is used to balance the combustion phasing. Four cylinder individual integral-controllers continuously manipulate the degree of reformation during the negative valve overlap period and INJ1 so as to achieve equal combustion phasing in all cylinders. Typically, around 3 mg of fuel was injected in this first injection (corresponding to a FuelMEP of 2.7 bar). To avoid having the injection timings drift out of synchronisation, the controller maintains the injection timing for the earliest cylinder at a reference value specified by the main controller. The start of injection for the other cylinders is allowed to vary within a predefined distance of this reference value to maintain equal phasing. The SOI for each cylinder, x is denoted by $SOI_x(n)$ which is mathematically given by:

$$SOI_x(n) = SOI_{ff}(n) + u_x(n) \tag{5.2}$$

$$u_x(n) = K_{i\alpha} \sum_{k=0}^{n} (e_x(k) - \frac{\phi(k)}{K_{i\alpha}}) \tag{5.3}$$

$$e_x(n) = min(\alpha_1, \alpha_2, \alpha_3, \alpha_4) - \alpha_x, \ \phi(n) = min(u_1, u_2, u_3, u_4) \tag{5.4}$$

where n denotes a specific cycle, α_x equals CA50 for cylinder x, $SOI_{ff}(n)$ is the feedforward from the main controller, $K_{i\alpha}$ is the integral gain for the balancing control, and u_x is the injection offset for each cylinder x. The $\frac{\phi(k)}{K_{i\alpha}}$) term is used to ensure that the injection offset for the earliest cylinder remains equal to zero. It is important that SOI_{ff} be set as late as possible just before IVO to allow for a large offset between the cylinders while making sure that that the injection occurs during the negative valve overlap when reformation occurs.

NMEP balancing proceeds in a similar way but is done during the main injection. In this case, the reference value used by the controller is the maximum load of the four cylinders. The controller distributes the appropriate quantity of fuel to each of the four cylinders while ensuring that the total amount of fuel delivered is equal to the reference amount specified by the main controller. The amount of fuel injected into a specific cylinder, x is given by $Fuel_x(n)$ which is calculated as follows:

$$Fuel_x(n) = Fuel_{ff}(n) + u_x(n) \tag{5.5}$$

$$u_x(n) = K_{i\sigma} \sum_{k=0}^{n} (e_x(k) - \frac{\phi(k)}{K_{i\sigma}}) \tag{5.6}$$

$$e_x(n) = max(\sigma_1, \sigma_2, \sigma_3, \sigma_4) - \sigma_x, \ \phi(n) = mean(u_1, u_2, u_3, u_4) \tag{5.7}$$

Here, n denotes a specific cycle, σ_x is the load for cylinder x, $Fuel_{ff}(n)$ is the feedforward from the main controller, and $K_{i\sigma}$ is the integral gain for the balancing control. The $\frac{\phi(k)}{K_{i\sigma}}$ term is included to ensure that the mean offset is equal to zero.

The controller is adaptive and stores the value of the integral term in an adaptive speed and load map. These maps should only be adapted during fairly stationary conditions. This is realized by changing the integral gain, $K_{i\sigma}$ according to

$$K_{i\sigma} = \frac{K_{i\sigma T}}{CoV_{NMEP}} \tag{5.8}$$

Where $K_{i\sigma T}$ is a tuning parameter. The difference between deactivated and activated cylinder balancing is shown in Fig. 5.3 where the load and phasing controller is activated at Cycle 210. It should be noted that the cylinder balancing controllers is tuned for maximum stability rather than speed. Still, the controller is able to settle rapidly and improve the overall combustion stability. The improvement in the cyclical variation in NMEP in cylinder 1 is especially striking in this instance. Cylinder balancing becomes especially important at higher loads because as the load increases, the margins between stable and unstable combustion decrease.

Another illustrative example of the effect of the phasing balancing controller is shown in Fig. 5.4 where the start of injection is shown together with the combustion phasing in the two upper sub plots. Note that initially, SOI_1 for cylinder 4 is maintained at the reference value and that of all the other cylinders is allowed to vary. The SOI_1 of cylinder 1 declines steadily from Cycle 0 to 570, at which point it would fall below the reference value if allowed to decrease further. To avoid this, the SOI_1 of cylinder 4 is allowed to vary. Cylinder 1 takes over as the one which is maintained at the reference value. In this case, the reference value for SOI_{ff} was locked at 320 Deg BTDC. The lower subplots also show how the fuel is individually distributed to equalize the NMEP.
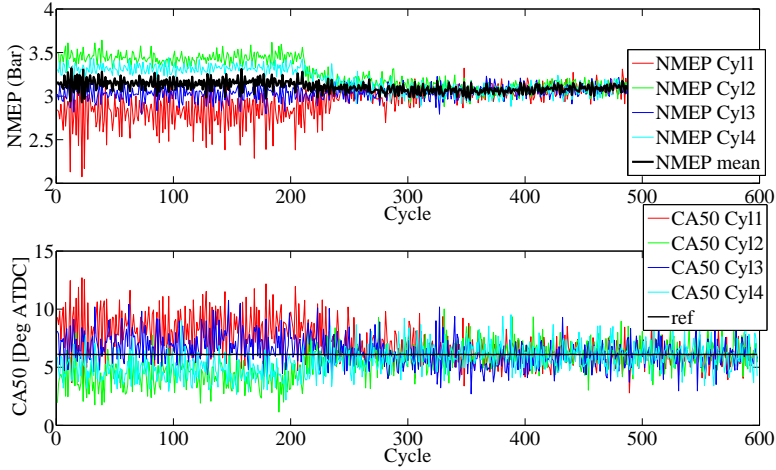
Figure 5.3   Activation of cylinder balancing at cycle 210. The controller settles quickly, minimizing the probability of misfires.

Summary

Cylinder individual integral-controllers can be used to manipulate the degree of reformation over the negative valve overlap through INJ1. In this way equal phasing can be achieved on all of the cylinders. Load balancing can be aciheved using similar controllers acting on the fuel amount in the second injection. The usage of cylinder balancing is important for keeping stable combustion and to avoid high cylinder pressure derivative.
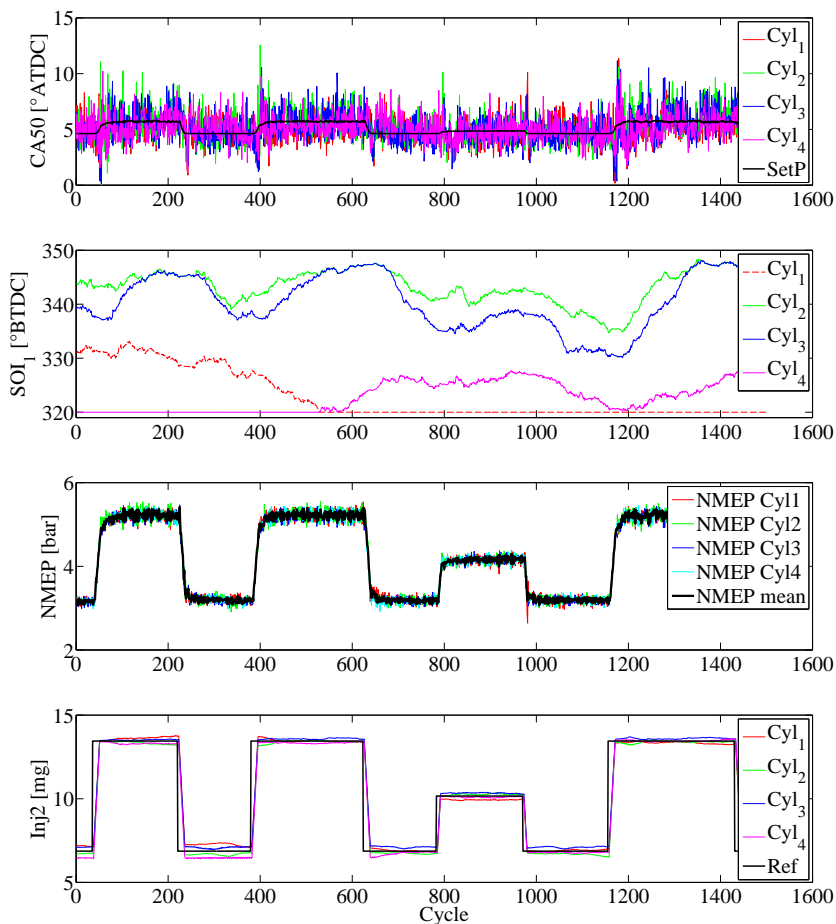
Figure 5.4   Balancing of CA50 and NMEP by changing the start of injection and fuel balance respectively. Note how SOI_1 for cylinder four is maintained at the reference value from Cycle 0 to 570. As SOI_1 of cylinder 1 falls towards this value, the start of injection for cylinder 4 is allowed to vary freely and it is the SOI_1 of cylinder 1 that is maintained at the reference value instead. The reference value in this case is 320 ° BTDC. NMEP is equal for all cylinders. The fuel offset for each injector is stored in adaptive maps. This result of this is seen in the lowest plot.

5.3 Main Combustion Control

This section discusses different non-model based combustion controller strategies that can be used for control of EVC and to generate feed-forward for the cylinder balancing control system.

PID Control and Map Based Feed Forward

The initial feedback experiments were done using PID controllers to control the EVC. The discrete representation of the PID controller is given by:

$$u_x(n) = K_p e(n) + K_i \sum_{k=0}^{n} e(k) + K_d(e(n) - e(n-1)) \qquad (5.9)$$

where u_x acts on EVC and e is the controller error, which was defined as the difference between the setpoint and the real CA50 . K_p, K_i, K_d is the proportional gain, integral gain and derivative gain, respectively. n is a specific cycle. This main controller sees the the engine as a single cylinder engine and acts on measurements from the mean of the four cylinders. Any differences between the cylinders are taken care of by the cylinder balancing controllers.

Also map-based feed forward is used for valve timing, injection pulse timing, and CA50 reference mapping. However, mapping of a HCCI engine is difficult because its behavior is highly dependent on many states, not all of which are easily measured. This will inevitably lead to errors in the final result. Moreover, the mapping will not take dynamic effects into account.

The maps will have an offset if the conditions under which the engine operates are not identical to those under which the mapping was conducted. However, the trends in the maps will be fairly equal meaning that the offset can be compensated for by the feedback controller.

Fig. 5.5 shows a series of load steps using PID control of EVC and feed-forward for the Start Of Injection (SOI) of the two injections and EVC. The increase in fuel rate was limited by using a low pass filter to avoid the occurrence of faster transients than the system could handle. The engine follows the CA50 set point, which is mapped so as to allow stable combustion and to span a large load range. Note the instability that occurs between cycles 320-350, which is caused by the timing of Inj1 being too early. In general, Inj1 should instead occur at the latest possible point during the period of negative valve overlap. Fig. 5.6 illustrates a part of the NEDC test cycle using the same controller structure. It should be noted that the data in this scheme is temporally compressed by a factor of ten and that only loads between 1.8 and 4.5 bar NMEP were examined. Misfiring occurs when the load
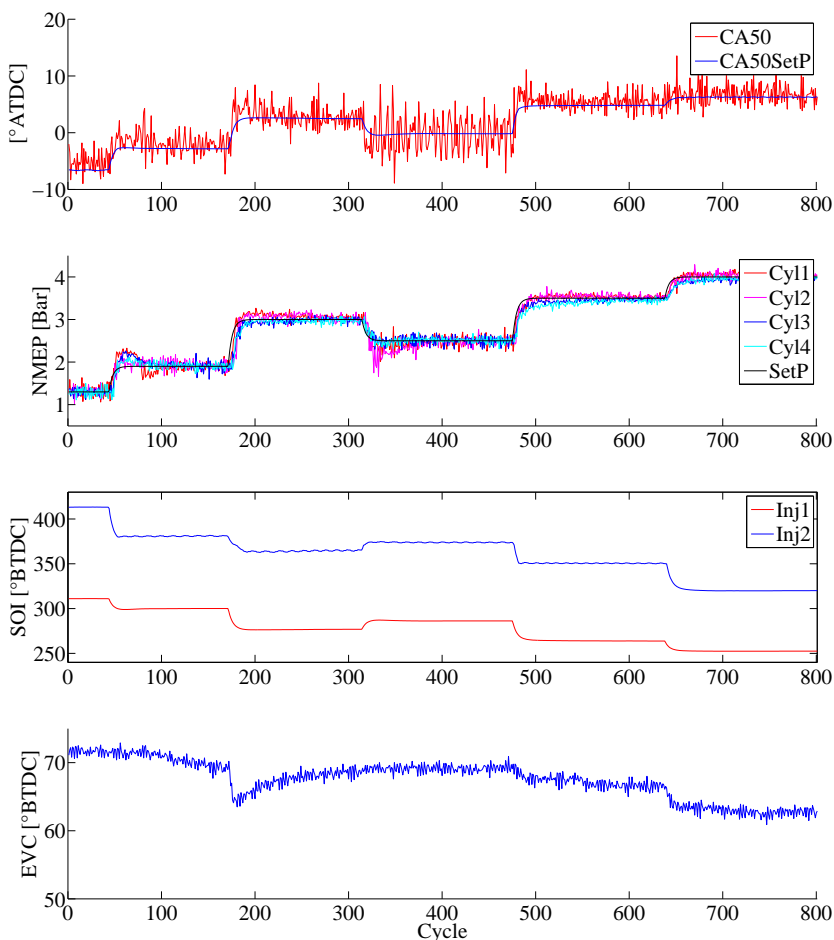
Figure 5.5 Load steps using the PID controller with feedforward and CA50 set point maps. Note the unstable conditions between cycles 320 and 350.

is decreased; this is generally attributable to the fact that the controller does not have sufficient knowledge of the system to properly compensate for the dynamics.

Multiple Inputs, Single Output Control of CA50 using Nonlinear Compensation

The previous subsection demonstrates how the feed-forward for start of the injections and EVC was mapped against speed and the quantity of fuel injected. It was later discovered that EVC should be the primary actuator
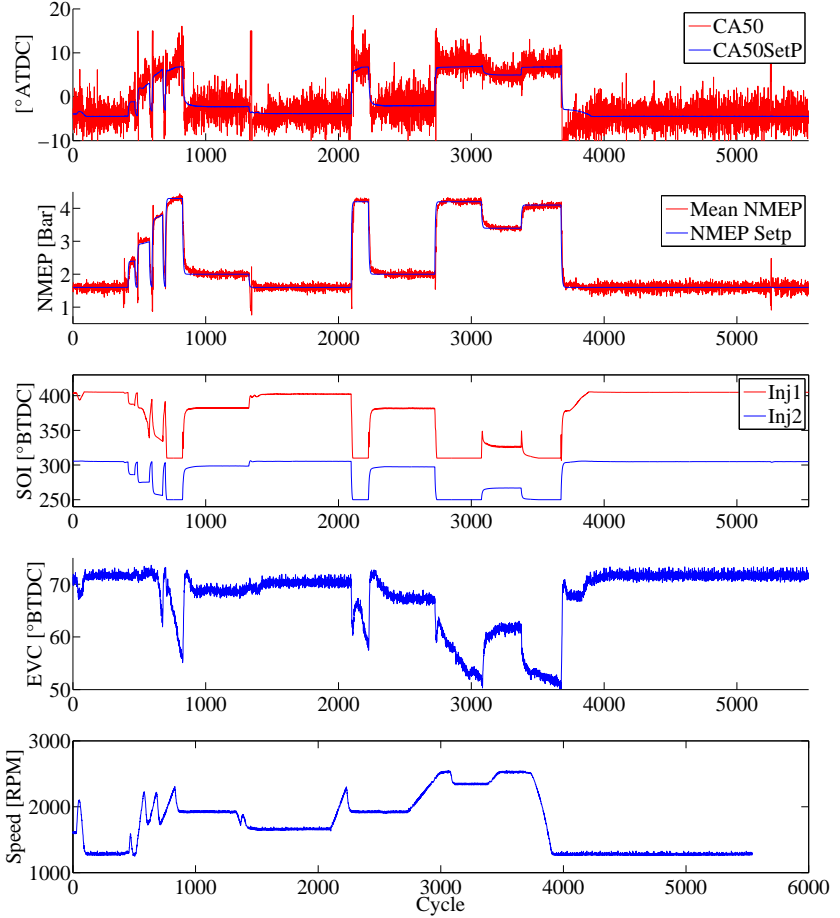
Figure 5.6   Parts of the NEDC test cycle. Note that it is ten times faster than the original and that the load is limited between 1.8 to 4.5 bar NMEP. Misfires occur when the load is reduced; these are generally due to the fact that the controller has insufficient knowledge of the system to adequately compensate for its dynamics.

during normal operation, the timing of the injections would have to be given greater weight under certain load conditions. That is to say, the engine should be operated in different actuator modes depending on the load. The different modes considered are *EVC mode*, *Injection Timing Mode,* and *Fuel Balance mode.*

- **EVC Mode** uses EVC as the main actuator for combustion control. The first injection should occur during the negative valve overlap. The

second, main injection should occur during the induction period. This injection strategy provides for the best emissions and highest stability without saturating EVC and can (while not being saturated) be used to position CA50 at the desired point on the basis of feedback and map-based feedforward.

- **Injection Timing Mode** must be implemented when EVC becomes saturated at low load. In this mode of operation, the timing of the first injection is the key parameter in combustion control. The second, main injection should still occur during induction. This mode is not preferred because it restricts the authority of the cylinder balancing controller, which becomes less able to independently adjust the timing of Inj1 in the different cylinders. Another drawback is the decreased stability of combustion and increased soot formation when the first injection is too early (see the trace in Fig. 5.5 between cycles 320 and 350).

- **Fuel Balance Mode** should be implemented if the timing of the first injection becomes saturated when operating under injection timing mode. In this mode of operation, the fuel distribution between the two injections is regarded as the key parameter in combustion control. The injection of larger quantities of fuel during the negative valve overlap moves CA50 to an earlier point in the cycle. The second, main injection should still occur during the induction period. This mode should also be avoided due to its high soot production.

EVC mode is the preferred mode of operation because it allows the injection timing and fuel balance to be set so as to achieve the highest efficiency and lowest emissions. Use of the other two modes could be avoided by phasing the EVC over a larger interval (this is not possible with the used hardware). One way to build a controller that can handle all three different modes is to map the actuator outputs against a single input signal, CtrlV. This is described by Fig. 5.7. It demonstrates how the different actuator means are affected by the input at a fueling level corresponding to 3 bar NMEP. The mapping was defined in such a way that a low value of CtrlV gave early combustion timing and a high value corresponded to late combustion. Fig. 5.8 illustrates how CtrlV affected the combustion phasing for a load of 3 bar NMEP.

A PID controller was used to adjust CtrlV so as to achieve the desired combustion phasing. In this way, it was possible possible to implement a Multiple Input Single Output, MISO control using a Single Input, Single Outpu (SISO) controller over the entire load range.

Nonlinear Compensation and Feed Forward   The usage of the "mode mapping" through CtrlV introduces nonlinearities. A series of sweeps similar
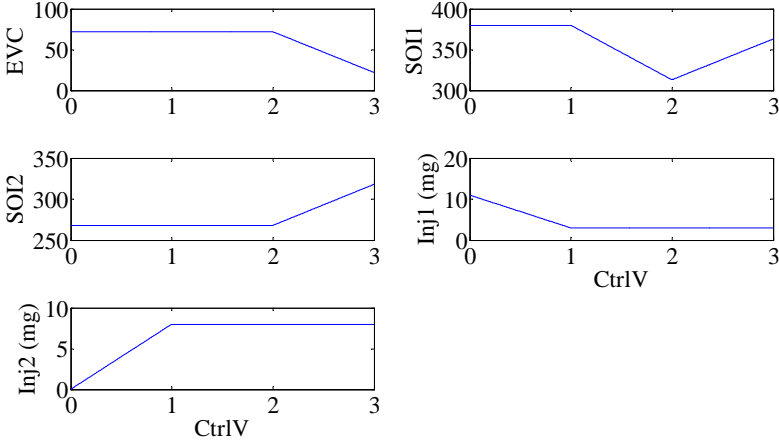
Figure 5.7 CtrlV was mapped against the different actuators. Mode 0-1 acts on the fuel ratio between the second and first injection. Mode 1-2 locks the fuel quantity and acts on the start of injection of the first injection. Mode 2-3 acts on EVC. Additionally, SOI1 is changed to make sure that the injection occurs during the negative valve overlap.

to Fig. 5.8 were performed at different fueling levels to be able to span maps describing the nonlinearities for different fueling levels and speed. The map describing the behavior at 2000 RPM is given by Fig. 5.9.

A static compensation of the nonlinearities can be made if it is assumed that the system can be modeled as a Hammerstein system. This means that that it consists of a static nonlinearity connected in series with a linear dynamic system. This would then give a linear closed loop system.

Nonlinear compensation is achieved by inverting the surface described in Fig. 5.9. The structure of the controller together with the compensation is shown in Fig. 5.10 . The nonlinearity and the compensation are represented by the two middle blocks. The compensation should provide for a linear 1 to 1 relationship between input and output. The inverted nonlinear maps were also used for the feedforward.

Fig. 5.11 depicts a load step using the new approach. It can be seen that there is only a small deviation in CA50. It is also apparent that RI becomes rather large during the transient. This is difficult to avoid without limiting the fuel rate since the noise is caused by the lack of boost pressure [13].
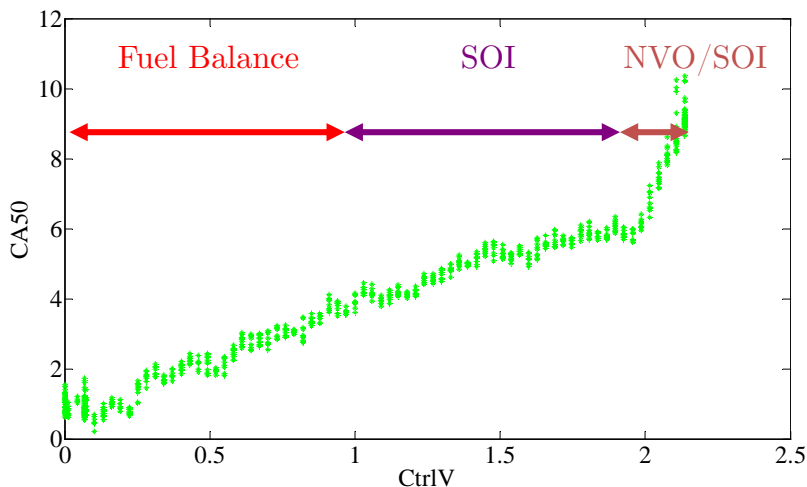
Figure 5.8   The nonlinear dynamics of CA50 vs. CtrlV for a load point of 3 bar NMEP at 2000RPM. The combustion can go into three different HCCI combustion control modes which affect different actuator means. The mode the engine should be working at depend on engine load, temperature etc. Mode 2-3 correspond to EVC mode, 1-2 correspond to Injection timing mode and mode 0-1 correspond to fuel balance mode.
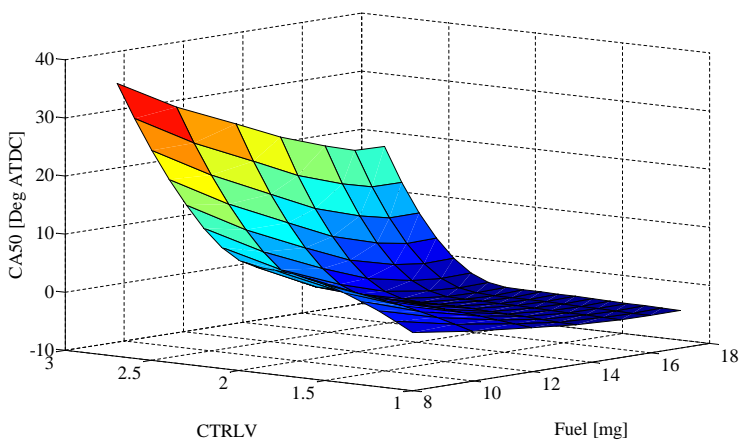

Figure 5.9   The nonlinear dynamics for different loads at 2000 RPM. The surface is a result of curve fitting against experimental data from experiments similar to Fig. 5.8.
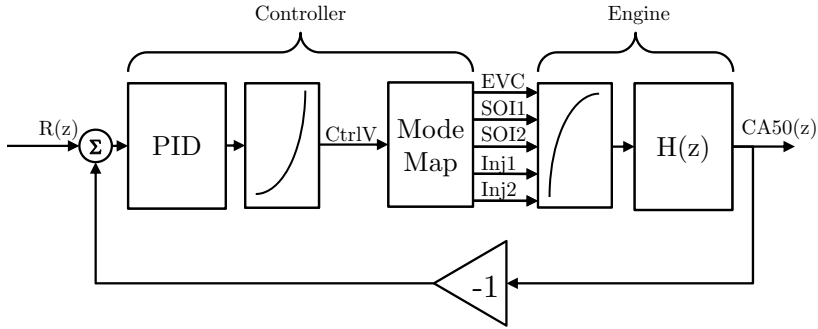
Figure 5.10 Example of the controller using the nonlinear compensation that should give a linear closed loop system.

Summary

Manually tuned PID controllers can be used to control load and combustion phasing of a turbocharged HCCI engine. The engine should be operated in EVC mode. It uses EVC as the main actuator while keeping beneficial injections for providing the best emissions and highest stability. The other modes, "injection timing mode" and "fuel balance" mode should only be used if EVC saturates. These different modes are mapped against a single controller signal which is manipulated through a PID controller. In this way a SIMO controller is achieved which provides for control over a wider load range. The mode mapping introduces static nonlinearities which are taken into account through a static non linear compensation map. This map is also used for feed-forward to the system.
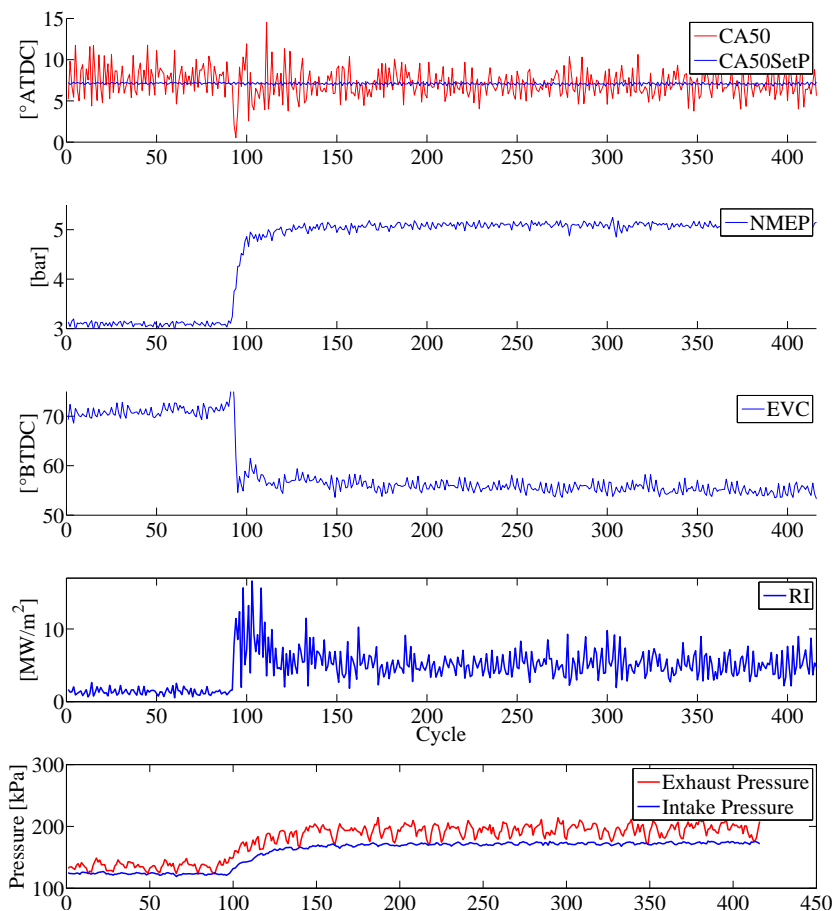
Figure 5.11   Load step using the the CtrlV mapping for feedforward and non-linear compensation. The CA50 is hardly disturbed. Note how RI increases over the transient. This is difficult to avoid without limiting the fuel rate. The noise is caused by the lack of boost pressure
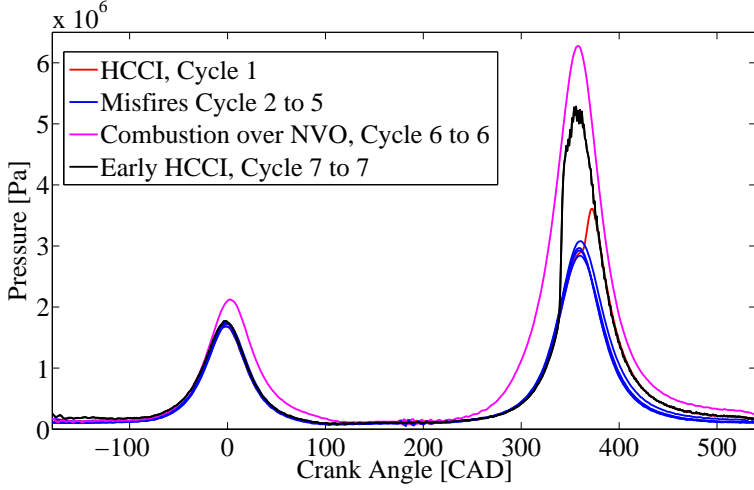
Figure 5.12   An unstable HCCI load point of 3 bar NMEP and a mean CA50 of 9 °ATDC. Misfires occur during cycles 2 through 5, resulting in the accumulation of fuel during the negative valve overlap. This fuel is later ignited by compression at cycle 6 during the negative valve overlap. This in turn gives rise to a high mixture temperature during IVC and so combustion begins at an extremely early stage during the compression stroke. This early combustion gives rise to very hot residual gases, which in turn trigger the 7th cycle prematurely . This kind of behavior must be avoided.

5.4 Turbo NVO HCCI Dynamics

This section provides an introductory discussion of the parameters that affect combustion. The results form the basis for the design of the HCCI model discussed in Chapter 5.5.

Because residual gases are used to heat up the fuel-air mixture, the combustion process in any given cycle is highly dependent on that of the preceding cycle. Fig. 5.12 demonstrates how misfires occur over cycles 2 through 5, resulting in the accumulation of fuel during the negative valve overlap. The mixture reaches near-stoichiometric conditions and is thus ignited prematurely in cycle 6, during the negative valve overlap. Consequently, the temperature of the mixture is very high during IVC, and so combustion begins immediately after the main injection. As a result, the temperature of the residual exhaust gases is extremely high; this causes the 7th cycle to also be triggered prematurely. The likelihood of unstable combustion of this kind is highly dependent on the operating conditions.
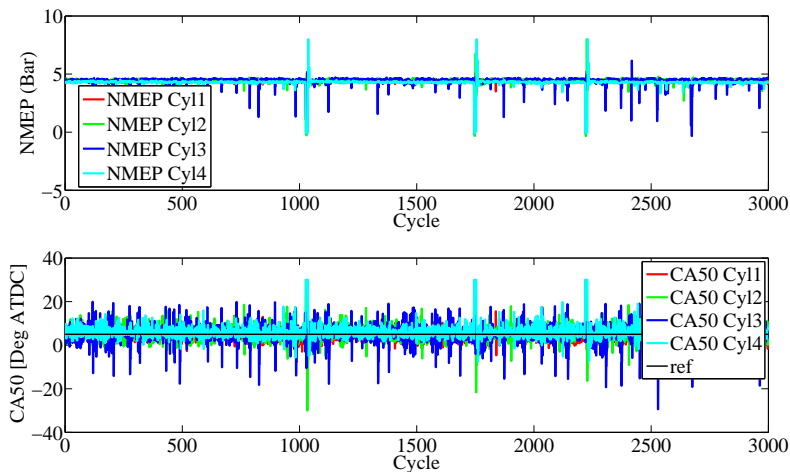
Figure 5.13 Engine behavior when T_{in} is too low or the engine is too cold; note the significant fluctuations in CA50 and NMEP.

Fig. 5.13 depicts the typical behavior of the engine when the intake temperature is too low. Fig. 5.14 depicts the situation observed under similar operating conditions, albeit with a higher intake temperature and retarded EVC timing to achieve the same mean CA50 timing. A series of experiments were performed to better understand the cause of this behavior in engines of this type.

The Influence of Fueling level on Combustion Phasing

The results described in Fig. 5.12 clearly show that combustion is strongly influenced by previous cycles, but the magnitude of this influence was unknown. To eliminate this uncertainty, a series of experiments was undertaken in which the engine was operated at 2.5 bar NMEP. The amount of fuel injected was randomly increased every 17th cycle for one of the cylinders (see Fig. 5.15). The large gap between the perturbations was chosen so as to minimize the influence of the turbo charger and maintain a constant intake and exhaust pressure. Fig. 5.16 shows the NMEP(k) for disturbances at cycles, k plotted against CA50(k) for the same cycle. It is apparent that there is no correlation between CA50 and NMEP attributable to the perturbation. An advance in combustion phasing was expected since the fuel to air ratio was drastically increased. However the increase in fuel also leads to increase in vaporization, which should retard combustion. These two factors seem to counterbalance one-another, but they both seem to be very weak. The orig-
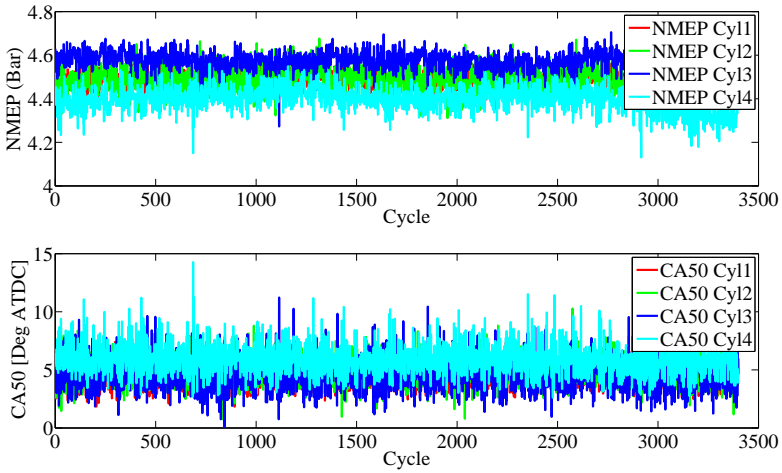
Figure 5.14   This data was collected directly after that shown in Fig. 5.13, and so the engine operating conditions were basically the same as those described previously. The only difference is that T_{in} was 20 °C higher and the exhaust camshaft was retarded to maintain a constant CA50. The variation is now drastically reduced.
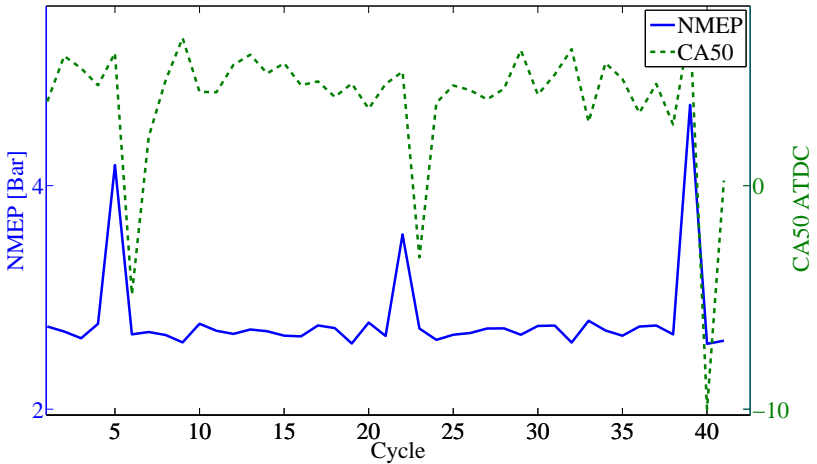

Figure 5.15   The amount of fuel injected was perturbed by a random amount every 17th cycle @ 2.5 bar.
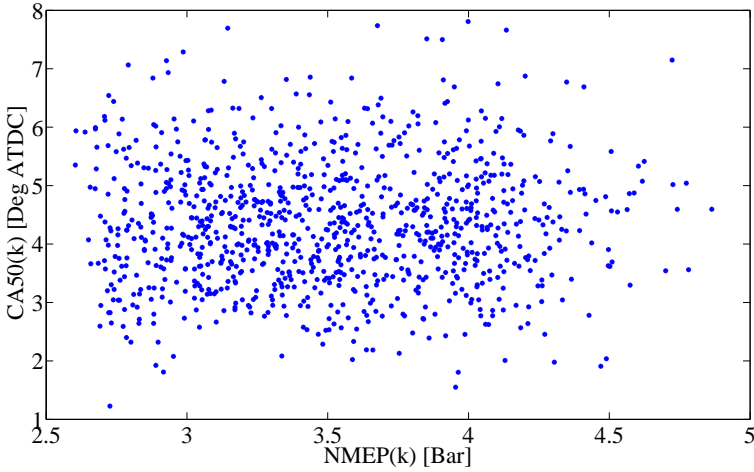
Figure 5.16 CA50(k) vs NMEP(k) demonstrating the non existing correlation between NMEP and CA50 for the same cycle.

inal hypothesis was that the large increase in air to fuel ratio would have a significant influence on the timing of the start of combustion for the current cycle, these data suggest that this hypothesis can be rejected.

Fig. 5.17 shows a plot of NMEP(k) against CA50(k+1) for the same experimental data; it is readily seen that these variables are strongly correlated [41]. In cycle k+1, the total mass of injected fuel is reduced so as to restore an NMEP of 2.5 bar. However, the high exhaust temperature from cycle k will decrease the amount of captured residuals due to its lower density. The air to fuel ratio for the residuals is thus richer, yielding a richer mixture than would be obtained during the steady state. The influence of these factors is low. The main factor responsible for this high correlation is the temperature of the residuals from the previous cycle, which gives rise to a high mixture temperature in the current cycle.

The large amount of fuel injected during cycle k also results in an elevated wall temperature during cycle k+1. The impact of this may be quite low but should not be neglected. Those cycles(k) with high load and ringing likely cause boundary layer breakdowns near the cylinder walls in the subsequent cycles, which in turn will affect the wall temperature in subsequent cycles. This is difficult to see in Fig. 5.17 because it is dwarfed by the influence of the residual temperature. However, Fig. 5.18 , which shows a plot of NMEP(k)

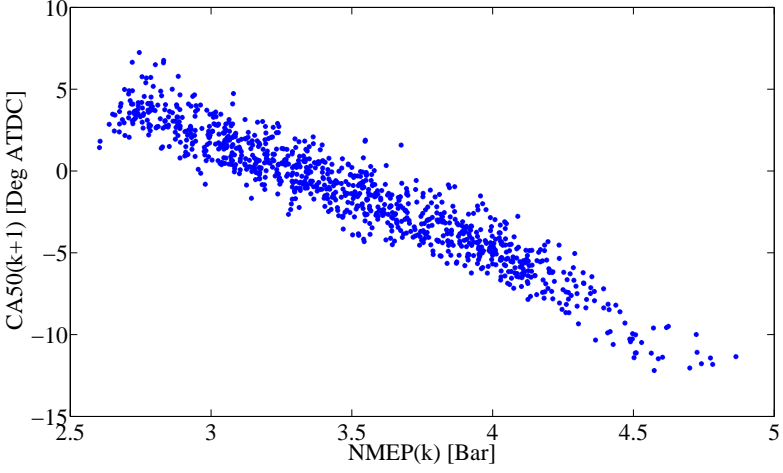**Figure 5.17**   CA50(k+1) plotted against NMEP(k). The high correlation indicates that CA50 is strongly coupled to the temperature of the previous cycle's exhaust (and thus to its NMEP).
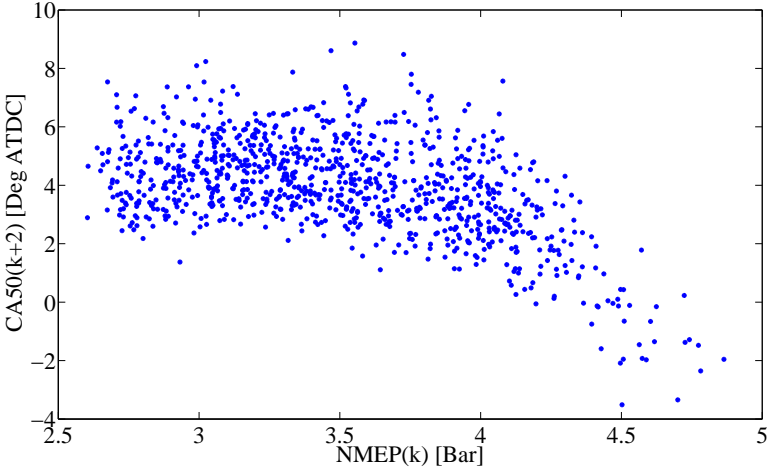

Figure 5.18   CA50(k+2) vs NMEP(k) the combustion phasing is observed to be advanced when NMEP(k) gets above 3.5 bar . This could be due to wall heat transfer from previous cycles.

against CA50(k+2) show this effect quite well.

During cycle $k+2$, the composition, temperature, and pressure of the mixture closely resemble those in cycle $k - 1$; if anything, the mixture may be a little colder because of the early combustion in the preceding cycle. These two factors largely seem to balance each other out, but the combustion phasing is observed to be advanced when NMEP(k) gets above 3.5 bar . This could be due to wall heat transfer as described above.

These experiments were conducted at several different loads, but in all cases the results were similar to those described above. Some conclusions can be drawn from these findings. First, the equivalence ratio has little or no impact on combustion phasing. The wall temperature has some impact and its dynamics seem to be faster than was initially thought. The mixture temperature has the largest impact on the combustion phasing, at least when the intake pressure is constant. It would therefore be desirable to examine the effect of varying the intake pressure on the temperature.

The Relations Between T_{ivc} and Combustion Phasing

It is difficult to estimate the mixture temperature in the cylinders precisely. An approach for estimating the temperature at IVC (T_{ivc}) using the cylinder pressure traces is suggested in Appendix A; this method was used to generate the T_{ivc} results discussed in this section.

The engine was operated at 5 bar NMEP. An EVC controller was used to maintain constant combustion phasing. The intake temperature (T_{in}) was slowly decreased from 110 to 30 °C . The temperature of the residuals (T_r) and the fresh air charge (T_{in}) prior to mixing and the resulting mixture temperature of these (T_{ivc}) are shown in Fig. 5.19. The results indicates that for a given combustion phasing, T_{ivc} remains constant. This is in accordance with the hypothesis that the start of combustion is mainly controlled by the mixture temperature. Note that the wall temperature also should be unchanged since the load and phasing remain constant.

Fig. 5.19 also demonstrates that the stability of the combustion decreases as the intake temperature falls. This is seen in as larger variations of NMEP and CA50 for the same sweep. It is possible that the change in stability is due to the controller's advance in EVC yielding larger fraction of internal residuals. The temperature fluctuations of the residuals are larger than those of the intake manifold air and T_{ivc} will therefore fluctuate to a larger extent, resulting in increased variations of CA50. The decreased oxygen concentration caused by the increased amount of residuals may also influence the results.
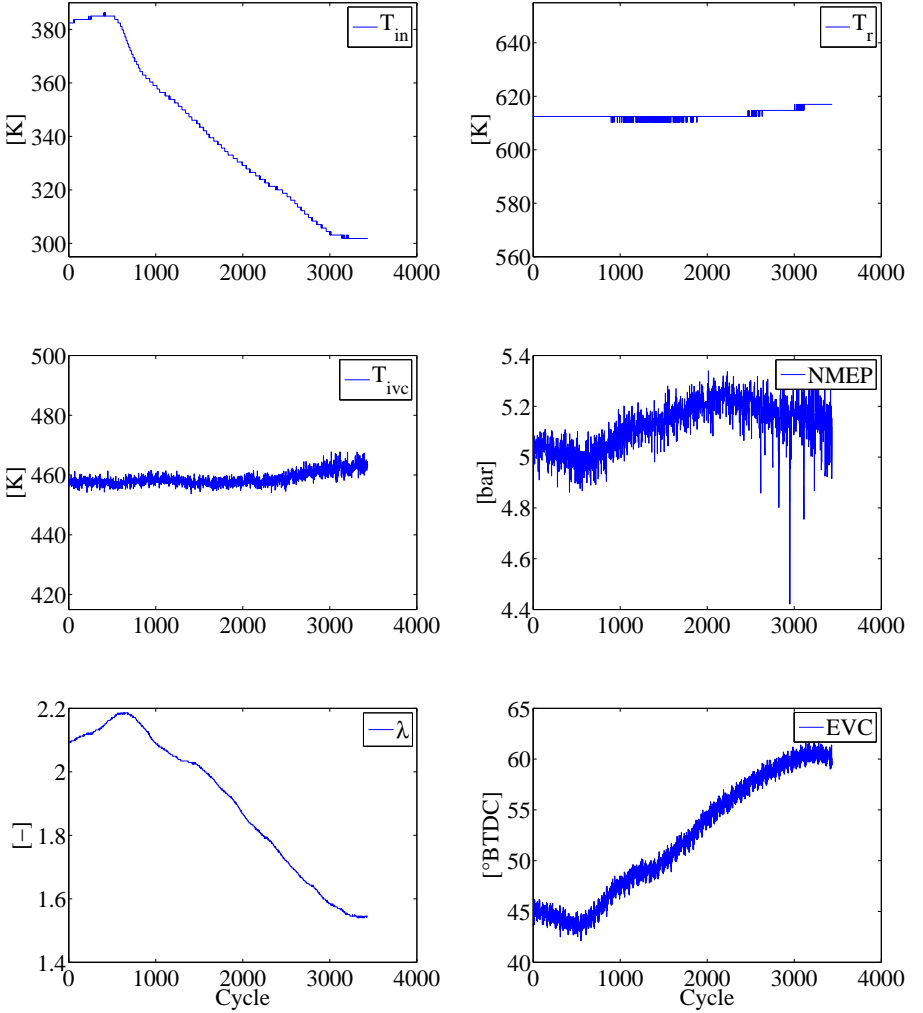
Figure 5.19   The behavior of the engine in response to an 80 degree decrease in the intake temperature. Note how the mixture temperature at T_{ivc} remains constant and how combustion stability decreases with advanced EVC.

The next question is how T_{ivc} is affected by load? A load sweep was performed while operating under EVC control to maintain constant phasing (Fig. 5.20) . The load was slowly changed from 2.5 to above 5 bar $NMEP$. This caused a decrease in the mixture temperature at IVC as the load increased. The decrease might be a consequence of the higher wall temperatures given by

the higher load. This could potentially give the same temperature just before combustion for all the load points.

Cylinder Air Charge and Mass of Residuals Dependence of EVC

The exhaust valve timing directly affects the mixture temperature for the next cycle in a NA NVO HCCI engine. This is also the case when running the same engine with a turbo, but EVC also has a great impact on the volumetric efficiency of the engine. This controls the mass flow through the engine which affects flow through turbine, turbo speed, flow through compressor and finally pressure/temp after compressor. Since the pressure and temperature of the residuals have such a large influence on combustion timing, the turbo will significantly increase the complexity of the engine dynamics. Fig. 5.21 shows a slow load sweep from 3 to 6 bar NMEP at a CA50 of 5. It is interesting to note that the mass of residuals basically remains constant. It is instead the mass of air charge that changes, due to the increase in boost pressure. On the exhaust side the pressure increases but since EVC is continuously retarded, the amount of residual gas is more or less constant. This is a large fundamental difference compared to a NA HCCI engine. An interesting observation of this behavior is that it can give rise to a non minimum phase behavior meaning that a change in actuator position might in the beginning give response in one direction and after a while go in the other direction. An example of the non minimum phase behavior described is seen in Fig. 5.22. The example demonstrate how EVC in the short time perspective reduces the residual mass and in a longer time perspective increases residual mass.

Summary

The combustion in a NVO HCCI engine is highly dependent on the combustion from previous cycles. This is due to the NVO, which captures a significant amount of residuals that affect T_{ivc}. The engine has operating points at which misfires are common. These are often connected to low engine and intake temperatures, and result in early EVC. The causes of these instabilities are believed to relate to significant temperature excursions in the residuals, which cause large fluctuations in T_{ivc} with early EVC. The start of combustion is primarily dependent on T_{ivc}.

Ensuring reliable combustion on a cold winter's day could be problematic. It is likely that the engine would exhibit unstable behavior and be difficult to control under such circumstances, as shown in Fig. 5.12 and Fig. 5.13

The presence of a turbo fundamentally changes how EVC works as an actuator. In a NA NVO HCCI engine, EVC primarily affects the amount of residuals. In a Turbo NVO HCCI engine, EVC primarily affects the mass of the fresh cylinder air charge. However, on a short time scale, EVC primarily

affects the residuals (as in an NA engine) because of turbo lag.

On the basis of these results, it can be concluded that the primary task of the engine controller should be to maintain a constant T_{ivc} so as to facilitate stable combustion.
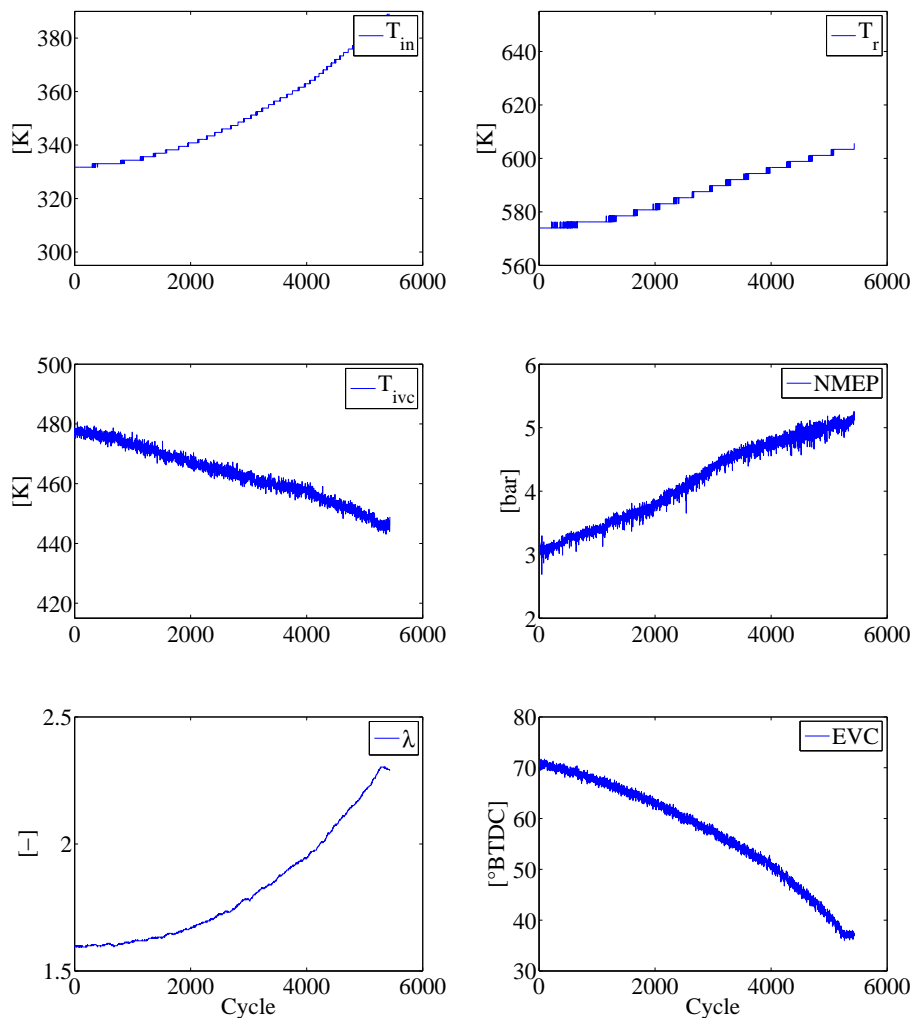
Figure 5.20   Slow increase in load from 3 to 6 bar NMEP with a mean CA50 of 5 gives a decrease in mixture temperature with increased load. The decrease could be caused by higher wall temperatures as a result of the increased fueling level. Possibly, this could give the same temperature just after compression for all the load points. This would then support the hypothesis that the mixture temperature is the main ignition trigger.
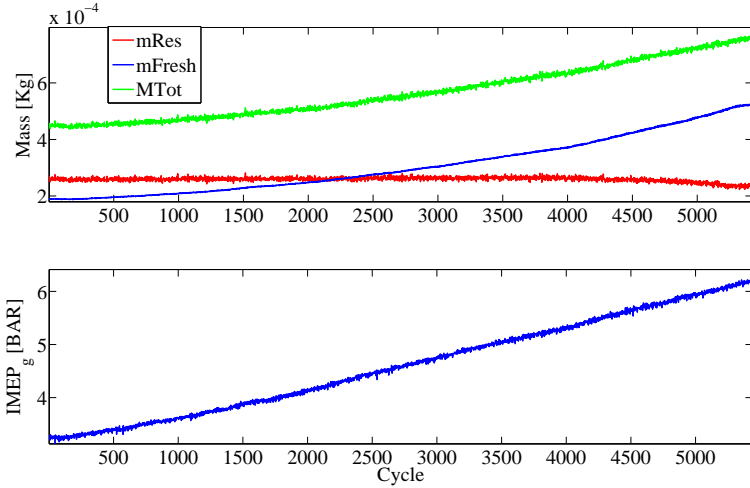
Figure 5.21   For a given CA50, the mass residuals basically remain constant. The turbo and the air charge are controlled by EVC rather than the mass residuals; this is a fundamental difference compared to a NA NVO HCCI engine.
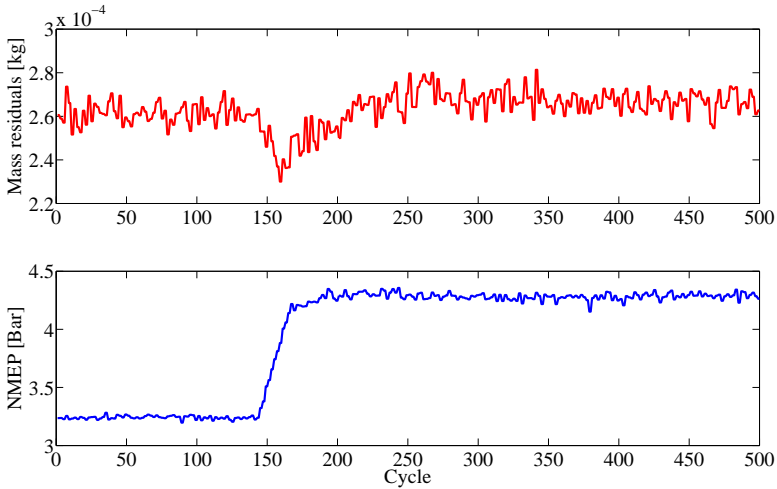
Figure 5.22   The mass of residuals can have a non minimum phase behavior. A normal NA NVO HCCI Engine would decrease the mass of residuals when going up in load. This is also the case here in the short time perspective. The residuals increases in the longer time perspective.

5.5 A HCCI Combustion Model for Controller Design

This section describes the development of a physics-based control-oriented HCCI model. This model is later used in Chapter 5.6 for controller design.

The overlap strategy with early closing of EVC makes the engine sensitive to pressure changes over the exhaust manifold because these conditions are directly coupled to the mass of captured residuals and the fresh charge. This affects the combustion phasing. The turbocharger therefore necessitates the use of more sophisticated control methods than does conventional HCCI.

The HCCI model is similar to models described by [42] and [43]. They basically use the same thermodynamic relations which are used to describe each cycle. The aim of the model by [42] was to describe the cylinder pressure while the model of [43] describes the behavior of both cylinder pressure and combustion phasing. The latter uses two states which describe the total number of moles of oxygen and the temperature in the cylinders. The model by the author describes the temperature in the cylinder by using three states, describing the mass of residuals, mass of unburnt gas and temperature at TDC. The approach of modeling the mixture temperature is taken based on the fact that the mixture temperature is the main ignition trigger. The model temperature is therefore correlated against experimental data for providing a complete expression describing how the combustion phasing behaves on a cycle to cycle basis.

The objective when developing the model was not to build the perfect HCCI model but to make one that was capable of reproducing the basic dynamics of the engine while also being simple enough to be used in controller design. The model gives an intuitive understanding of the initiation of the combustion from one cycle to another. It is in Chapter 5.6 linearized to yield a three state linear model. The model was subsequently inverted for use in feed-forward control, and the linear model was used in the design of Kalman filters and a feedback controller. The following sections describe the methodology used when developing the model.

Model Structure

The engine model is based on ideal cycle calculations. It works in iterative steps or cycles, k, for which calculations are made to update three states describing the conditions in the cylinders at TDC_f. The calculations are based on the states from the previous cycle, $(k-1)$, and environmental inputs, $u(k)$, such as the fuel mass, intake and exhaust pressure etc. The states are updated according to the following expressions:

$$m_a(k) = f_1(u(k), m_a(k-1), m_e(k-1), T(k-1)) \tag{5.10}$$

$$m_e(k) = f_2(u(k), m_a(k-1), m_e(k-1), T(k-1)) \tag{5.11}$$

$$T(k) = f_3(u(k), m_a(k-1), m_e(k-1), T(k-1)) \tag{5.12}$$

The first state, m_a, is the mass of the unburned air. The second state, m_e, describes the mass of the residual gas, which is considered to be inert. The last state, T, describes the temperature of the mixture. This is related to CA50 for different fueling and speed levels.

$$CA50(k) = f(\omega, m_{fuel}, T(k)) \tag{5.13}$$

The functions Eq. 5.10 to 5.13 can be combined to generate a complete expression describing the phasing behaviour of the combustion process from one cycle to the next. The different equations describing these functions will now be presented.

Combustion

The model assumes instantaneous combustion at top dead center and constant specific heat. The temperature increase depends on the amount of energy released during combustion and the total mass in the cylinder. The temperature $T_2(k)$ after combustion is then given by

$$T_2(k) = \frac{m_{fuel}Q_{LHV}}{(m_a(k-1) + m_e(k-1))C_v} + T(k-1) \tag{5.14}$$

where m_{fuel} and Q_{LHV} represent the mass of injected fuel and the fuel's lower heating value, respectively. If the temperature is known and the volume remains constant during combustion, the cylinder pressure, $P_2(k)$, can be calculated using the ideal gas law

$$P_2(k) = \frac{P_{in}(k)T_2(k)}{T(k-1)} \tag{5.15}$$

where P_{in} is the intake pressure. If it is assumed that sufficient oxygen is present for complete combustion. The amount of unused air that remains is given by

$$m_{a2}(k) = m_a(k-1) - m_{fuel}\left(\frac{A}{F}\right)_s \tag{5.16}$$

where $\left(\frac{A}{F}\right)_s$ is the stoichiometric air to fuel mass ratio. Since the valves are closed, the total mass in the cylinder is constant. The mass of the burned gas therefore increases according to:

$$m_{e2}(k) = m_e(k-1) + m_{fuel} \left(\frac{A}{F} \right)_s \qquad (5.17)$$

Expansion

If the heat losses during expansion are ignored, isentropic equations can be used to describe the relationships between the final temperature T_3 and pressure P_3 on the one hand and the initial temperature T_2 and pressure P_2 on the other. That is to say, the temperature and pressure after the expansion of the cylinder volume induced by exhaust valve opening are given by

$$T_3(k) = T_2(k) \left(\frac{V_{tdc}}{V_{evo}} \right)^{\gamma - 1} \qquad (5.18)$$

and

$$P_3(k) = P_2(k) \left(\frac{V_{tdc}}{V_{evo}} \right)^{\gamma} \qquad (5.19)$$

where V_{tdc} and V_{evo} represent the cylinder volume directly after combustion and at exhaust valve opening, respectively. γ is the polytropic exponent and is assumed to be constant. The other parameters are left unmodified

$$m_{a3}(k) = m_{a2}(k), \, m_{e3}(k) = m_{e2}(k) \qquad (5.20)$$

Blow Down

After the opening of the exhaust valve, the burned gas expands until its pressure is equal to that of the manifold pressure. The temperature after expansion can be calculated as follows

$$T_4(k) = T_3(k) \left(\frac{P_{exh}}{P_3} \right)^{\frac{\gamma - 1}{\gamma}} \qquad (5.21)$$

Here, P_{exh} is the exhaust manifold pressure. The other parameters are left unmodified

$$m_{a4}(k) = m_{a3}(k), m_{e4}(k) = m_{e3}(k), P_4(k) = P_{exh}(k) \qquad (5.22)$$

Exhaust Valve Closing

The early closing of the exhaust valves will cause the cylinders to trap some of the hot residuals. These residuals will later mix with the fresh charge during the intake stroke. The temperatures and the amount of the residuals will therefore affect the equivalence ratio and combustion phasing in the following cycle. The ideal gas law can be used to describe the situations just before

EVO and during EVC; by combining the two expressions, it is possible to calculate the amount of residual gas and the fresh charge at EVC.

$$m_{a5}(k) = \frac{m_{a4}(k)V_{evc}P_{exh}T_3(k)}{(\eta V_{evo}P_4(k)T_4(k))} \tag{5.23}$$

$$m_{e5}(k) = \frac{m_{e4}(k)V_{evc}P_{exh}T_3(k)}{(\eta V_{evo}P_4(k)T_4(k))} \tag{5.24}$$

The tuning parameter, η, is statically mapped in the model and depends on the engine speed and cam phasing; it is used to compensate for the higher pressure in the cylinder compared to the manifold due to the throttling over the low lift valves. Under high boost/load conditions, η is quite small (the lowest value it takes is approximately 0.5). This indicates that the low lift valves introduce throttling losses and remove part of the efficiency advantage that HCCI is otherwise so well known for. The other parameters are left unmodified

$$P_5 = P_{exh},\, T_5 = T_4 \tag{5.25}$$

Expansion to Intake Manifold Pressure

The residual mixture captured in the negative valve overlap will first be recompressed and will then expand to match the manifold pressure. The temperature, T_6, of the residuals at intake pressure is given by

$$T_6(k) = T_5(k)\left(\frac{P_{in}}{P_{exh}}\right)^{\frac{\gamma-1}{\gamma}} \tag{5.26}$$

Where P_{in} is the intake manifold pressure. The other parameters are left unmodified

$$m_{a6} = m_{a5},\, m_{e6} = m_{e5},\, P_6 = P_{in} \tag{5.27}$$

Mixing of Residuals at Intake Valve Closure

The hot residuals are mixed with the intake manifold air. The temperature of the resulting mixture at IVC is denoted by T_7 and can be calculated by combining

$$T_7(k) = \frac{P_{in}V_{ivc}\eta}{(m_{a7}(k) + m_{a6}(k) + m_{e6}(k))R} \tag{5.28}$$

and

$$T_7(k) = \frac{(m_{a6} + m_{e6})T_6 + m_{a7}T_{in}}{m_{a6} + m_{e6} + m_{a7}} \tag{5.29}$$

(where specific heat is assumed to be equal for the residuals and the fresh air) and solving for m_{a7}. With these results in hand, the mass of inducted air can be calculated using the following expression

$$m_{a7}(k) = \frac{P_{in}V_{ivc}\eta - RT_6 m_{e5} - RT_6 m_{a5}}{RT_{in}} \tag{5.30}$$

Throttling over the valves is assumed to be similar during exhaust and intake, and so the same value of η is used to compensate for the associated losses. The other parameters are left unmodified

$$m_{e7} = m_{e6}, \ P_7 = P_6 \tag{5.31}$$

Compression to TDC

Heat losses during compression are ignored, so the following isentropic relations can be used:

$$T_8(k) = T_7(k) \left(\frac{V_{ivc}}{V_{tdc}}\right)^{\gamma-1} \tag{5.32}$$

$$P_8(k) = P_7(k) \left(\frac{V_{ivc}}{V_{tdc}}\right)^{\gamma} \tag{5.33}$$

The other parameters are left unmodified

$$m_{a8} = m_{a7}, \ m_{e8} = m_{e7} \tag{5.34}$$

Heat Transfer

The heat transfer to the cylinder walls is estimated using Newton's law of cooling. The resulting equation for the temperatures is then

$$T_9(k) = \frac{-h_c A_c (T_8 - T_w)\Delta t}{mC_v} + T_8(k) \tag{5.35}$$

The heat transfer coefficient, h_c, is given by Woschni's correcation (see [18])

$$h_c = \frac{3.26 P_8(k)^{0.8} w^{0.8}}{B^{0.2} T_8(k)^{0.55}} \tag{5.36}$$

m is the total mass of the gas mixture ($m_{e8} + m_{a8}$), A_c is the surface area of the cylinder wall, T_w is the wall temperature, B is the cylinder bore, and w is the engine speed.

The Complete Model

Combining the equations discussed above (Eq. 5.14-5.36) and setting

$$m_a(k) = m_{a8}(k) \tag{5.37}$$

$$m_e(k) = m_{e8}(k) \tag{5.38}$$

$$T(k) = T_9(k) \tag{5.39}$$

completes the final step in the functions Eq. 5.10 to 5.12 which describes a complete cycle. The input, $u(k)$, to this system is defined by

$$u(k) = [\eta, m_{fuel}, V_{evo}, V_{evc}, V_{ivc}, T_{in}, P_{in}, P_{exh}, w]^T$$

and $m_a(k), m_e(k), T(k)$ are states that are updated from cycle to cycle. A number of simplifications have been made in the development of this model but it is sufficiently precise to capture the general trends and the dynamics of the engine's behavior.

Linearization

By making a Taylor approximation of the nonlinear equations Eq. 5.10-Eq. 5.12 for a given set of operating conditions, preferably in the middle of the speed load range, one obtains a linear discrete state space model of the form $x(k) = Ax(k-1) + Bu(k-1)$, $y(k) = Cx(k)$:

$$\begin{bmatrix} m_a(k) \\ m_e(k) \\ T(k) \end{bmatrix} = A \begin{bmatrix} m_a(k-1) \\ m_e(k-1) \\ T(k-1) \end{bmatrix} + B \begin{bmatrix} \eta \\ m_{fuel} \\ V_{evo} \\ V_{evc} \\ V_{ivc} \\ T_{in} \\ P_{in} \\ P_{exh} \\ w \end{bmatrix} \tag{5.40}$$

$$y_T = \begin{bmatrix} 0 & 0 & 1 \end{bmatrix} \begin{bmatrix} m_a(k) \\ m_e(k) \\ T(k) \end{bmatrix}$$

Here, the terms in $x(k)$ denote the mass of air, the mass of the residuals, and the mean temperature in the cylinder at TDC just before combustion. The inputs used are the charging efficiency, mass of fuel, cylinder volume at EVO,

EVC and IVC, the manifold intake/exhaust pressures and finally the engine speed.

Predicting CA50

The model presented so far does not estimate the combustion phasing directly. The common belief is that the main parameters that affect the combustion phasing are the mixture temperature, the oxygen concentration, and the pressure/temperature history. In previous studies, the Arrhenius knock integral model has been used in various ways to take these factors into account ([38],[39]). The Arrhenius expression is based on an exponential correlation between reaction rate, temperature and pressure in the cylinder.

It was previously shown that the mixture temperature was the main factor influencing the combustion phasing. Since any desired experimental data could be measured using the test cell, a series of experiments was performed to generate a map which takes the engine speed and injected fuel mass as inputs and produces the model temperature as output for a constant CA50 of 5 CAD aTDC. The difference between the map temperature and the model temperature is then used as input to a linear model for CA50. The gain, ζ, of the CA50 model was found through least squares fitting to experimental test data.

$$CA50_m(k) = (TempMap(\omega, m_{fuel}) - y_T(k))\zeta \qquad (5.41)$$

Fig. 5.23 depicts the map used for this function which shows how the estimated start of combustion temperature relates to speed (ω) and fuel mass (m_{fuel}) .

Model Verification

The models were implemented in Simulink and their predictions were compared to a set of experimental data points. Fig. 5.24 illustrates a load sweep at 2000 RPM with an oscillating exhaust cam. The model shows good agreement with experimental data. Similar performance was achieved at 1500 and 2500 rpm. Fig. 5.25 shows the result of stepping the load up from 3 to 5 bar NMEP and then back down to 3 bar again. Once again, good agreement was obtained between experimental and simulated data.

It is likely that similar model accuracy could be achieved using a black box system identification approach such as that described by [44]. Such an approach would require less tuning but the advantage of using the method described here is that it generates valuable insight into the combustion process during the engine cycle because the equations used in the model are physically meaningful.
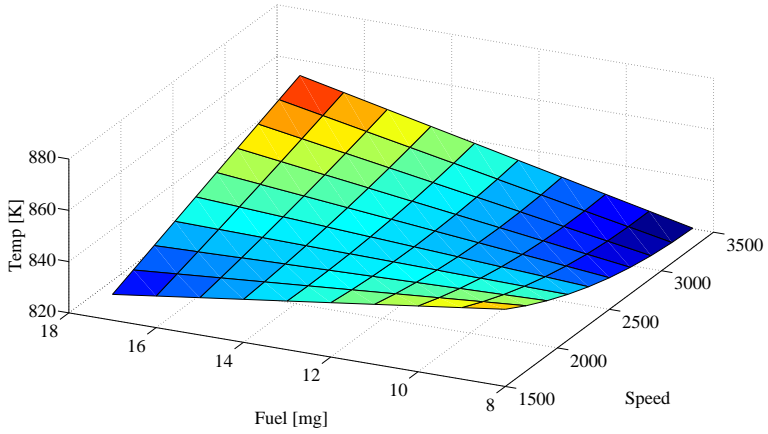
Figure 5.23 Data obtained using the model for the temperature at the start of combustion for a CA50 of 5 degrees after calibration for different loads and speeds.
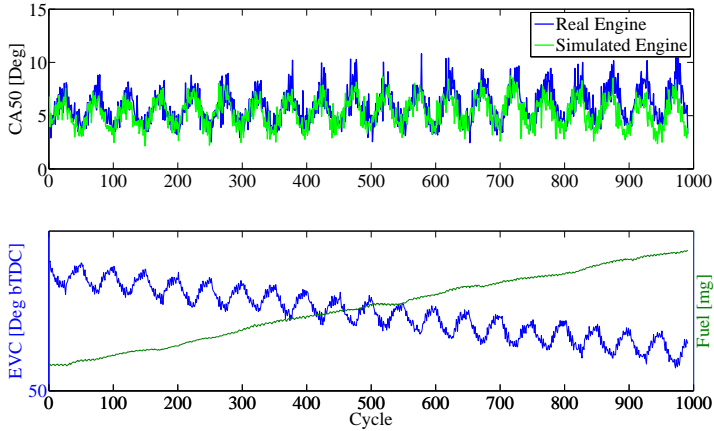

Figure 5.24 Validation of the model using a sweep from low to high load at 2000 RPM.

Conclusions

An HCCI model has been developed and linearized to give a state space model of the engine. A number of generalizations have been made but despite this the model manages to reproduce the general trends and dynamics of the
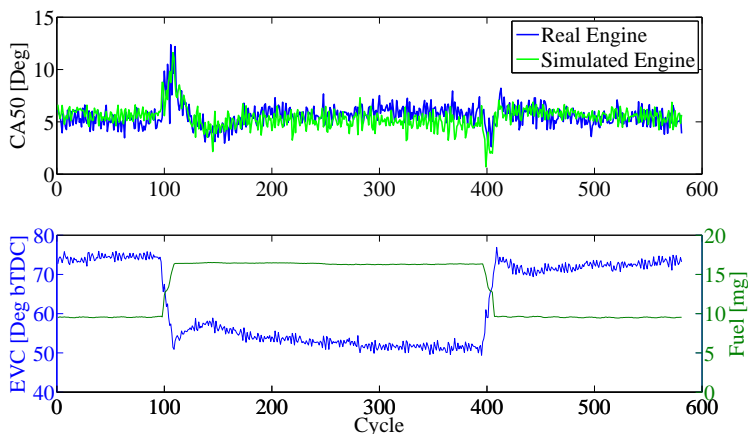
Figure 5.25   A comparison of the model's predictions to experimental data for a load step from 3 to 5 to 3 bar NMEP.

engine. The model takes the intake and exhaust pressures into account. That is particularly important since these parameters are greatly affected by the use of a turbo charger. The models were created for use in the design of feedback and feedforward controllers and in the development of a Kalman filter for state estimation.
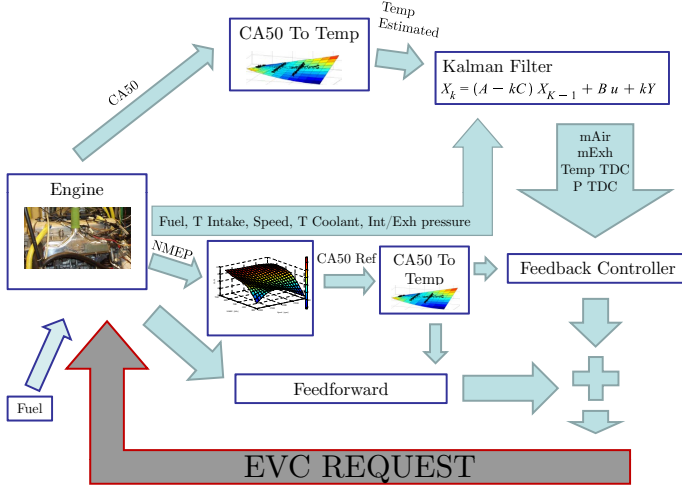
Figure 5.26   Control scheme describing the flow of control signals for handling EVC timing

5.6 The Model Based Controller - Design and Results

This section describes the design of a controller using the engine model presented in the previous section

Fig. 5.26 describes the flow of the main signals used in a model-based EVC controller structure. The controller has a number of components - the "CA50 to temperature converter", "the Kalman filter" , "feedforward", and "feedback". The structure is sampled after each combustion event inside the ECM

The EVC feedforward component consists of an inverted version of the non-linear temperature model. It uses the reference temperature as input. This reference temperature is determined on the basis of the speed and the load using a lookup table and the CA50-to-temperature equation obtained by inverting Eq. 5.41. The latter is given by

$$y_T(k) = TempMap(\omega, m_{fuel}) - \frac{CA50_m(k)}{\zeta} \qquad (5.42)$$

Similarly, the CA50 measured in the last engine cycle is used to estimate the corresponding model temperature. Together with the other model/engine in-

puts, this temperature is then fed into a Kalman filter to obtain an estimate of the states in the plant model.

The feedback controller acts on the state estimates and the temperature reference. It is used to compensate for errors in the feed-forward compensation.

The plant model described by Eq. 5.40 in the previous section was used in the design of the Kalman filter and the feedback controller. Interestingly, the structure of the system indicates that it actually controls the mixture temperature rather than the CA50. The reliance on temperature control is consistent with the results reported in the Chapter 5.4, indicating a static relationship between mixture temperature and combustion phasing.

The following sections contain descriptions of the individual components of the controller.

The Properties of the Engine Model

The A matrix in the state space model described in Eq. 5.40 is given by

$$A = \begin{bmatrix} -0.318 & -0.7814 & -4.834e-007 \\ 0.07305 & 0.5365 & 8.581e-008 \\ 2.191e+005 & 2.191e+005 & 0.3557 \end{bmatrix} \tag{5.43}$$

The pole map of the model is given by Fig. 5.27 . All of the poles are located within the unit circle, meaning that the system is stable. One of the poles is situated at the origin and corresponds to a time delay. This was expected and reflects the 1-cycle delay associated with perturbations in the amount of fuel injected that were discussed in Chapter 5.4 (see Fig. 5.17).

The use of a Kalman Filter for Predicting States

It is not possible to measure any of the states used in the model, and so they must be estimated. This is achieved by using an observer. Basically, an observer consists of a copy of the plant model; it uses the same equations save that it has an extra term that compares the output signal, y_T, of the plant to the estimated output, $\hat{y}_T$. The difference between them is connected in a feedback loop with the gain K which causes the estimated states, $\hat{X}$, to approach the states, X. The equation for the Kalman filter is given by Eq. 5.44. Note that an additional integrator state has been added to allow offset-free tracking of the output
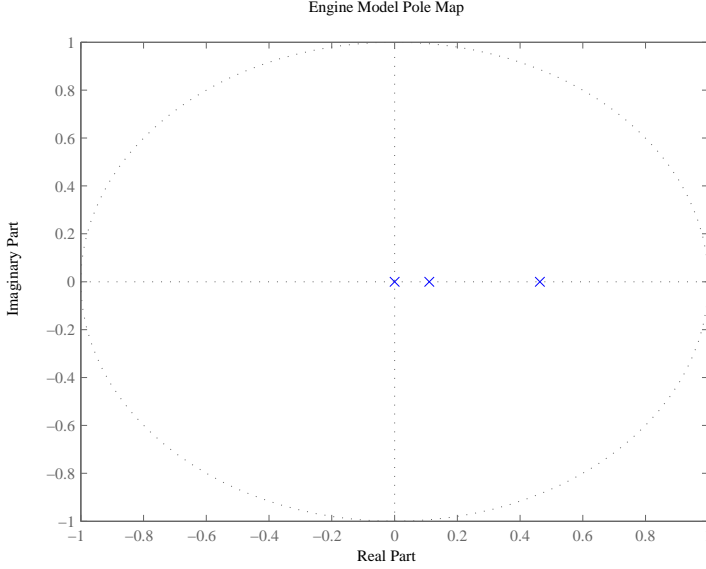
Engine Model Pole Map

Figure 5.27   Polemap of the linear model. One of the poles is located at the origin and corresponds to a time delay in the system. This is expected and is consistent with the results of the fuel disturbance experiments shown in Fig. 5.17.

$$
\begin{bmatrix}
\hat{m}_a(k) \\
\hat{m}_e(k) \\
\hat{T}_c(k) \\
x_i(k-1)
\end{bmatrix}
=
\left[
\begin{bmatrix}
A & 0 \\
0 & I
\end{bmatrix}
- K [\, C \quad 1 \,]
\right]
\begin{bmatrix}
\hat{m}_a(k-1) \\
\hat{m}_e(k-1) \\
\hat{T}_c(k-1) \\
x_i(k-1)
\end{bmatrix}
\tag{5.44}
$$

$$
+ Bu(k) + Ky(k-1);
$$

$$
u(k) = [\, \eta \quad m_{fuel} \quad V_{evo} \quad V_{evc} \quad V_{ivc} \quad T_{in} \quad P_{in} \quad P_{exh} \quad \omega \quad ...
$$
$$
T_{coolant} \quad y \,]^T
$$

The poles of $\left[\begin{bmatrix} A & 0 \\ 0 & I \end{bmatrix} - K [\, C \quad 1 \,] \right]$ describe the error dynamics of the filter. The Matlab function `Kalman` has been used for pole placement, which generates the optimal filter gain, K, by solving an algebraic Ricatti equation [45]. The Kalman function requires the noise covariance data for the process. These parameters were manually tuned with experiments. The resulting pole
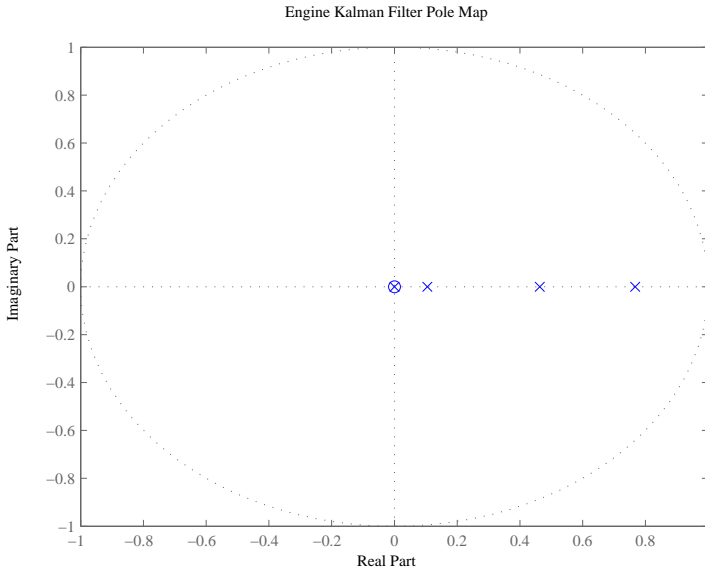
Figure 5.28   Polemap of the Kalman filter error dynamics. The system contains one extra pole compared to the engine model. This pole can be derived from the integrator used to augment the model for allowing error free tracking.

map is shown in 5.28 . Note that there are four poles instead of three. This is caused by the use of an additional integrator state. While this state is not necessary for the state feedback controller, it was included so as to facilitate the use of a simpler PID controller acting only on the output $\hat{T}_c(k)$.

Fig. 5.29 illustrates how the four observer states behave for real engine operation with EVC positional disturbances (the four lower subplots). The absolute values of the states are reasonable but should not be taken too seriously because we are talking about a linearized model. However, the trends of the states are more interesting. When EVC increases, a larger percentage of residual gases can be expected. At the same time, there should be a reduction in the amount of fresh gas. This is reflected in the states $\hat{m}_e$ and $\hat{m}_a$, respectively. The change in valve timing affects the mass flow through the engine and hence also the energy supplied to the compressor. This means that the turbo tends towards a new equilibrium point. This "turbo lag" explains the dynamic behavior of $\hat{m}_e$ and $\hat{m}_a$ after each disturbance step.

It should be clarified again that the "measured output", y_T, is the tempera-
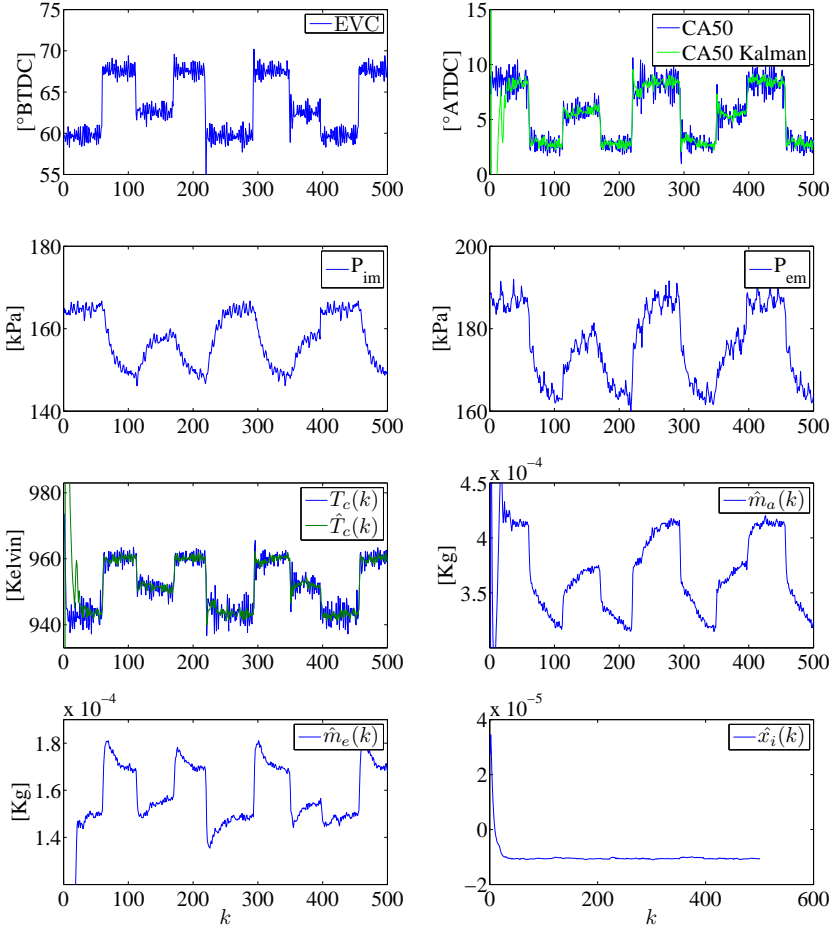
Figure 5.29   The observer state behavior for engine operation with *evc* position disturbances. The changes in EVC introduce pressure changes over the intake and exhaust manifold due to their impact on the volumetric efficiency of the engine.

ture of the mixture at TDC. It is calculated from the CA50 measurements using the inverse of Eq. 5.13.

Feedback

An LQG controller acting on the estimated states from the Kalman filter was used for feedback. The optimal feedback gain, K, is calculated using the Matlab command `LQRY`, which finds the optimal control law $u = Kx$ that minimizes the cost function

$$J = \sum(y'Qy + u'Ru) \tag{5.45}$$

Where Q and R are weighting matrices [46]. To handle modeling errors and achieve error-free tracking, an integrator state was used to augment the state space model according to:

$$\begin{bmatrix} X(k) \\ x_i(k) \end{bmatrix} = \begin{bmatrix} A & 0 \\ -C & I \end{bmatrix} X_a(k-1) + \begin{bmatrix} B \\ 0 \end{bmatrix} u(k-1) + \begin{bmatrix} 0 \\ 1 \end{bmatrix} r(k-1)$$

$$y(k) = \begin{bmatrix} C & 0 \\ 0 & 1 \end{bmatrix} X_a(k)$$

$$\tag{5.46}$$

Where $X = \begin{bmatrix} m_a(k) & m_e(k) & T_c(k) \end{bmatrix}^T$ are the original states, x_i the integrator state, X_a the augumented state vektor, r the reference temperature and u the model inputs. The weighting matrix for the outputs, Q, was set to $\begin{bmatrix} 1 & 0 \\ 0 & 1 \end{bmatrix}$ and the R matrix was manually tuned by decreasing its value until instability was reached. Its value was then slightly increased again to assure stable feedback. The resulting pole map is shown in Fig. 5.30. An example of the output generated by simulations using the controller is shown in Fig. 5.31 . This figure shows disturbances in the amount of fuel injected and corresponding changes in EVC to allow CA50 to be maintained at the reference value. The four lower subplots depict the estimated states of the model. There is however a deviation of the combustion phasing over the transient. This can be reduced by the usage of feed-forward.

Feedforward

The model's ability to predict engine behavior is used for feedforward. This is done by letting the nonlinear model run in paralell with the process. In this way the nonlinear states are estimated. Using these states together with an inverted version of Eq. 5.12 yields a mathematical expression relating the CA50 reference to feed-forward action for exhaust valve closure. It is likely that similar results would be achieved by inverting the linear transfer function for EVC to temperature and combine it with transfer functions for intake, exhaust pressure and fuel to temperature such as previously described in [47]. The results of a simulation using the nonlinear feed-forward together with the LQG controller can be seen in Fig. 5.32 . The figure should be compared to the feedback experiments demonstrated in Fig. 5.31. The use of feed-forward reduces the CA50 spikes during the transient compared to the pure feedback experiment. It is also seen that the feed forward introduces noise that propagates from the measured input signals to the feed-forward
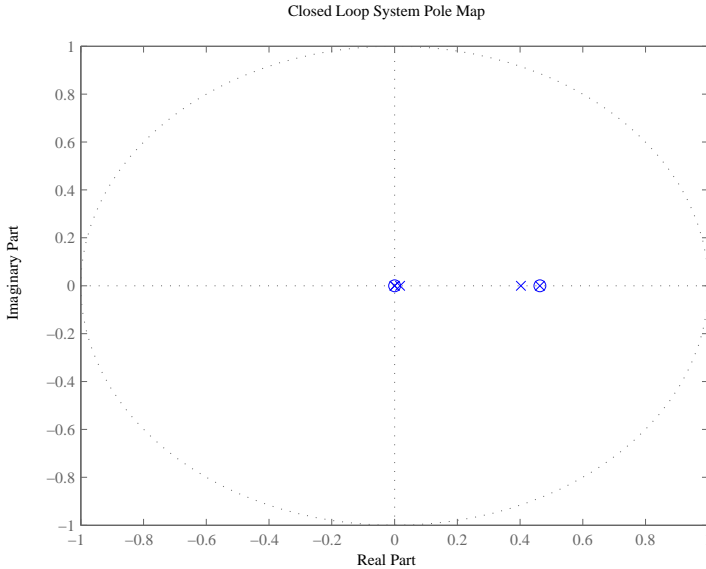
Figure 5.30   Polemap of the closed loop system.

compensator. This should be compensated for by filtering the input signals connected to the feed-forward.

LQG Control of The Real Engine

A corresponding control structure as demonstrated for the simulation was implemented in the ECM and tested on the real engine.

The rise time for CA50 gives some indication of the performance of the controller. Fig.5.33 illustrates the step responses at 4 bar NMEP. The mean rise time for a CA50 step is about 3 cycles.

Fig.5.34 shows the response to stepwise changes in the NMEP between 3 and 5.2 bar and how the phasings of the four cylinders match the reference value. Note how the controller advances EVC over the high to low load transient compared to steady state. This is needed since the intake pressure lags over the transient. EVC is compensated to achieve the right mixture temperature. However, it overcompensates a bit. The lowest subplot of the figure focuses on the data for cycles 350 to 470 . There is some deviation from the reference during cycles 390 to 410, but the controller settles fairly rapidly. A
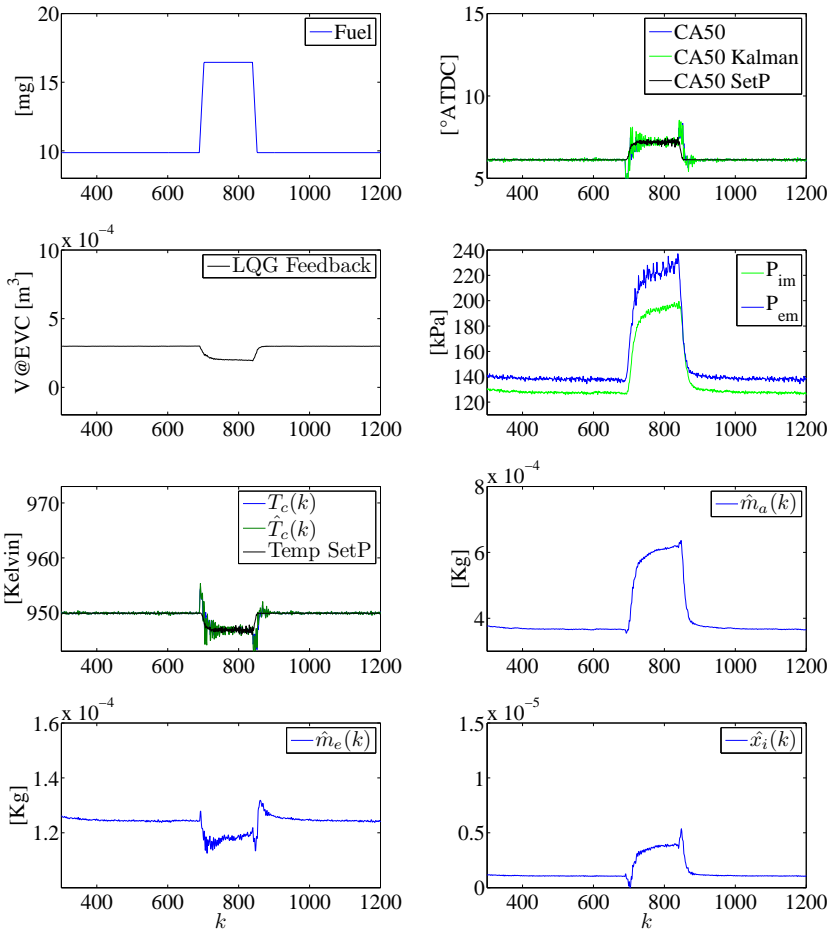
Figure 5.31   A simulation using the LQG controller without feedforward. The intake and exhaust pressure (P_{im} and P_{em}) are taken from the relevant transient measurements. The controller maintains the combustion phasing at the reference value by manipulating the EVC. Some deviation of the CA50 setpoint occurs over the transients. Some of this behavior can be compensated for through feedforward.

challenge of running the engine at higher load is that it can only be operated within a relatively narrow range. CA50 timings later than 8 to 9 CAD ATDC result in an elevated risk of misfiring. This means that the engine is operating very close to the misfire limit. Misfires will upset the controllers and can easily cause instabilities.
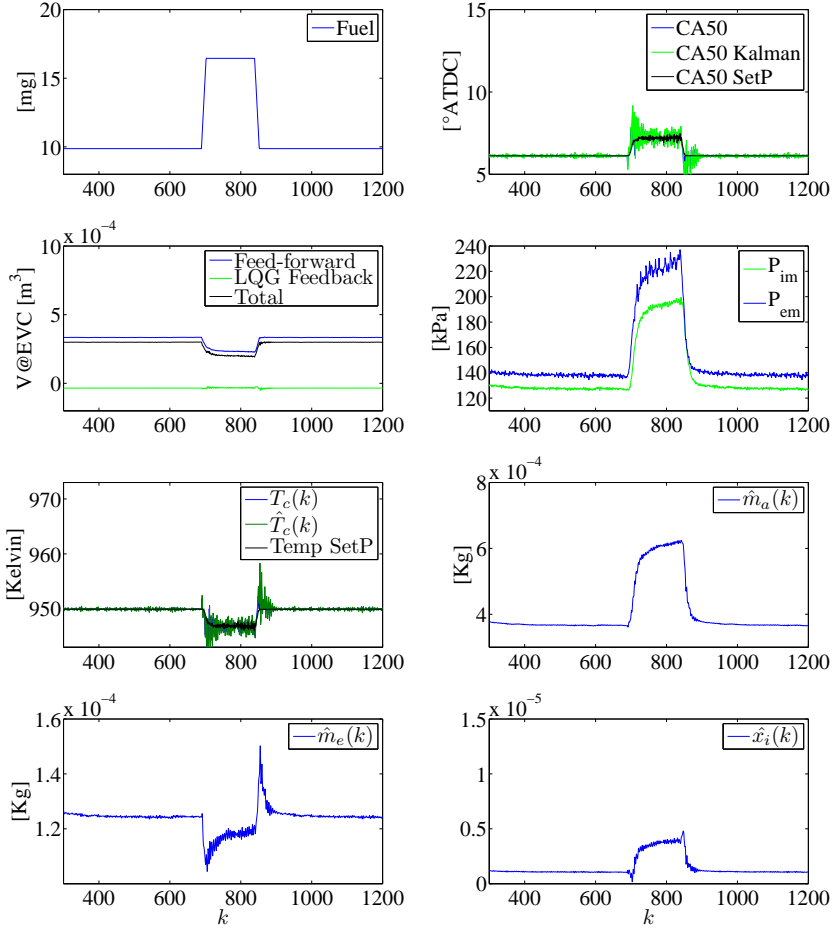
Figure 5.32 Example of a simulation using the LQG controller with feedforward. This figure should be compared to Fig. 5.31 The use of feedforward provides an improvement compared to the pure feedback experiment, but also propagates the noise present in the measurements.

Summary

Experiments with a real engine have shown that the proposed model-based controller approach can handle control at load transients. The controller could be improved in a number of ways; notably, the engine model used in designing the controller only considers events occurring inside the cylinders. Ideally, events occurring in the intake and exhaust manifolds should also be considered. This could for example be achieved by using linearized mean value

Figure 5.33 CA50 step responses using the real engine at 4 bar NMEP.

engine models. Another alternative would be to use models derived using data-driven system identification processes. The models so obtai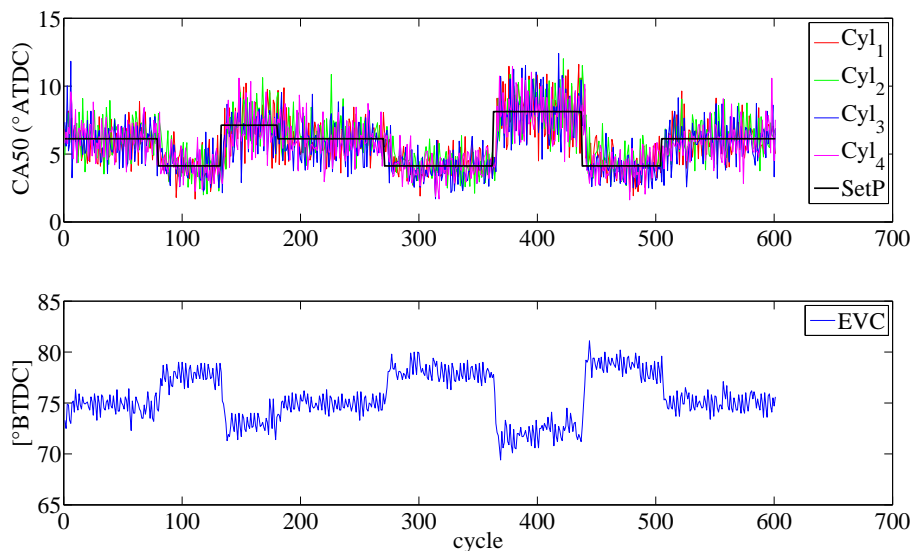ned could be used to augment the HCCI model. This would provide the controller with more data on the plant as a whole and may afford improved control.

5.7 Conclusions

The EVC timing is the most effective tuning knob for the combustion timing control. Two injections should be used for operation; one small injection, INJ1, during the negative valve overlap and one main injection, INJ2, during the intake stroke (see Fig. 5.2).

With equal injection actuator settings for all cylinders, high Ringing Intensity may occur in some cylinders while others may be close to misfiring. The stability of the engine can be improved by balancing these differences using active controllers for both load and combustion phasing.

The main controller sees the engine as a single cylinder engine and acts on measurements from the mean of the four cylinders. Map based feed forward for valve timing, injection pulse timing and CA50 reference maps improves transient performance.

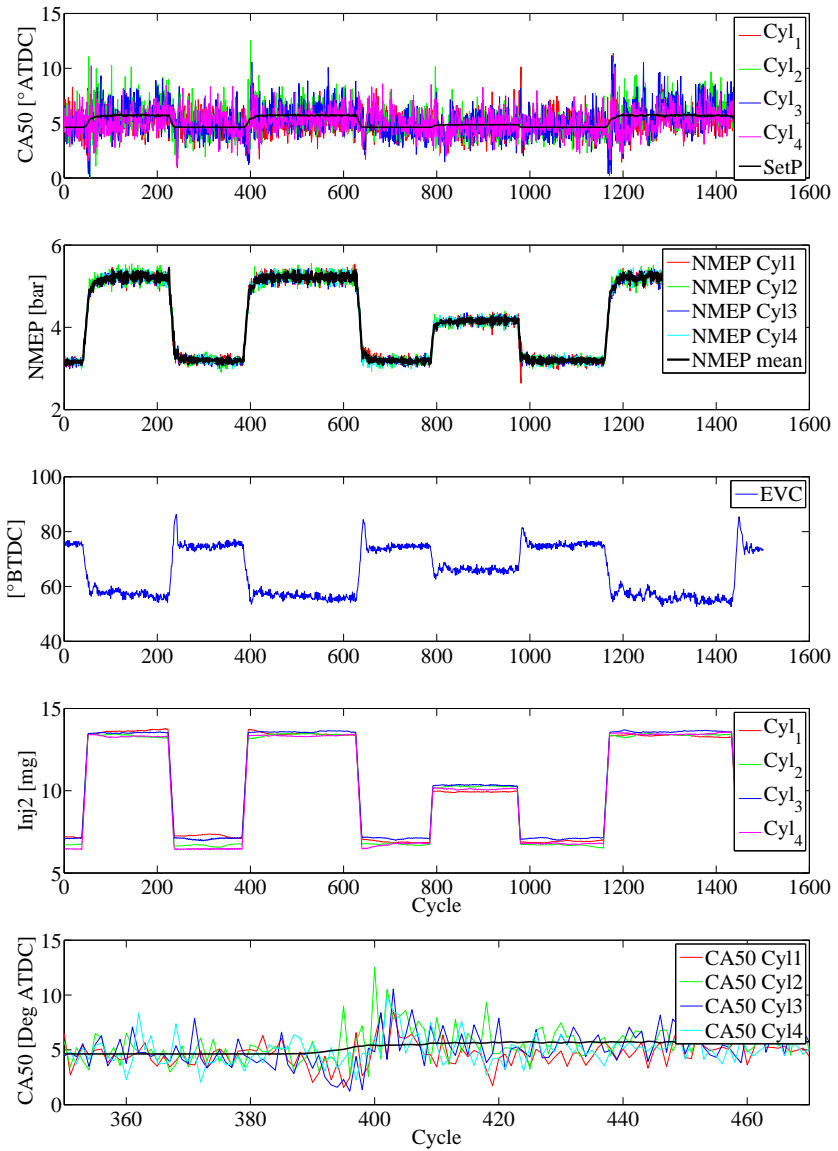**Figure 5.34**   The response of the CA50 to incremental adjustments of the load. Note how the controller advances EVC over the high to low load transient compared to steady state. This is needed to compensate for the turbo lag over the transients.

The combustion is to a large extent depending on the combustion from the previous cycle since the residuals are used to heat up the mixture. The main ignition trigger is the mixture temperature and there seems to be little or no correlation between CA50 and fuel air ratio. The stability of the combustion is decreased with lowered intake manifold temperature. It seem to be due to the need of earlier EVC for maintaining the combustion phasing, leading to a larger fraction of internal residuals and hence larger temperature fluctuations.

The exhaust valve timing directly affects the mixture temperature for the next cycle in a NA NVO HCCI engine. This is also the case when using a turbo but EVC also has a great impact on the volumetric efficiency of the engine. This controls the mass flow through the engine which affects the turbo and hence both the intake and the exhaust pressure. This is one of the reasons why turbo charging adds to the complexity of the engine dynamics

An HCCI model has been developed and linearized to give a state space model of the engine. A number of generalizations have been made but still, the model manages to capture the general trends and dynamics of the engine. The model takes the intake and exhaust pressures into account. That is particularly important since these conditions are greatly affected by a turbo charger.

The model is used used for the controller design which can be divided in different parts namely the CA50 to temperature function, Kalman filter , feedforward, and feedback. The structure of the system reveals that it actually controls the mixture temperature instead of CA50. The concept of using temperature control agrees well with the results in the chapter Turbo HCCI dynamics indicating that the mixture temperature should stay constant for a specific combustion phasing. The controller was implemented in the ECM and tested on the real engine. Load transients with fairly small deviation of the reference CA50 were achieved using this approach. It is likely that improvments could be achieved if the engine model used for controller design would be augumented with the dynamics of the turbo charger.

6

Combined Combustion Concepts

The term Combined Combustion Concepts (CCC) refers to a multi-mode gasoline engine that is designed to be able to switch between three different combustion modes: CI, PPC and SI. Some of the challenges associated with this concept and their solutions are discussed in this chapter.

PPC is a compromise that does not suffer from many of the drawbacks associated with turbocharged NVO HCCI while retaining a good emissions profile and imposing lower demands on the controller. For details about PPC see Chapter 2.

The high efficiency and favourable emissions profile of PPC makes it preferable to the other operating modes available in CCC (SI and CI). Ideally, the engine would operate under PPC over the entire speed/load range; since this is not possible, SI and CI are used in situations where PPC is impossible to maintain. The operating ranges under which the different modes were intended to be used is shown in Fig. 6.1.

The difference between PPC and conventional CI or Diesel combustion is the ignition delay. In PPC, the delay decreases as the load rises, which means that there will be a natural mode switch when the load is increased to the point that the mixture ignites before the end of injection. Consequently, the most important control action to be taken during a significant load increase involves retarding the injection and/or changing the EGR ratio to avoid knock and to maintain beneficial combustion phasing.

The lower load limit of Gasoline PPC is highly dependant on the fuel used. However, the mode of operation should be switched to SI combustion well
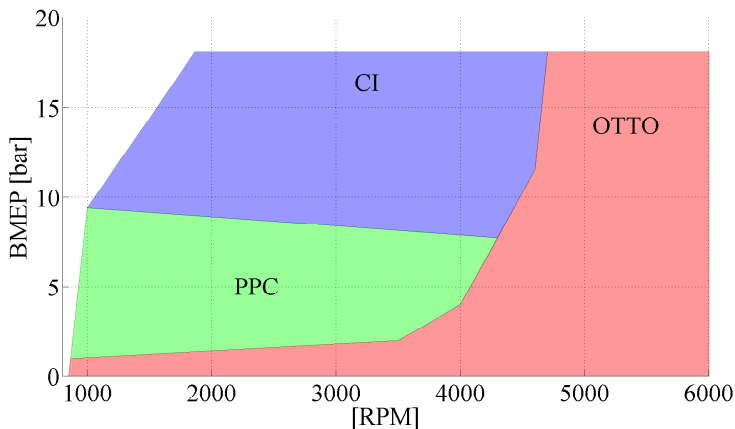
Figure 6.1 Speed/load map describing the different CCC modes and their expected operating ranges.

before reaching that limit. The high compression ratio under such circumstances should result in efficient combustion, at least by the standards of SI engines. SI combustion should also allow for higher engine speed and hence potentially higher specific power output.

The Engine

The modified SAAB A20DTH diesel engine was used in these experiments; for more details, see Chapter 3.

6.1 Properties of Gasoline PPC

This section gives a brief introduction of the properties of gasoline PPC and CI combustion. An understanding of this material is required in order to understand the methodological approach adopted in the sections discussing controller design. See [48, 4, 5, 49] for information regarding emissions and efficiency when using gasoline in diesel engines.

One of the basic differences when using gasoline instead of diesel is the ignition delay and combustion duration (see Fig. 6.2). When using gasoline, the latter is typically a factor of two shorter compared to the diesel. This results in high noise and NOx emissions if countermeasures are not employed.

The main way of dealing with these problems is to use EGR, which slows
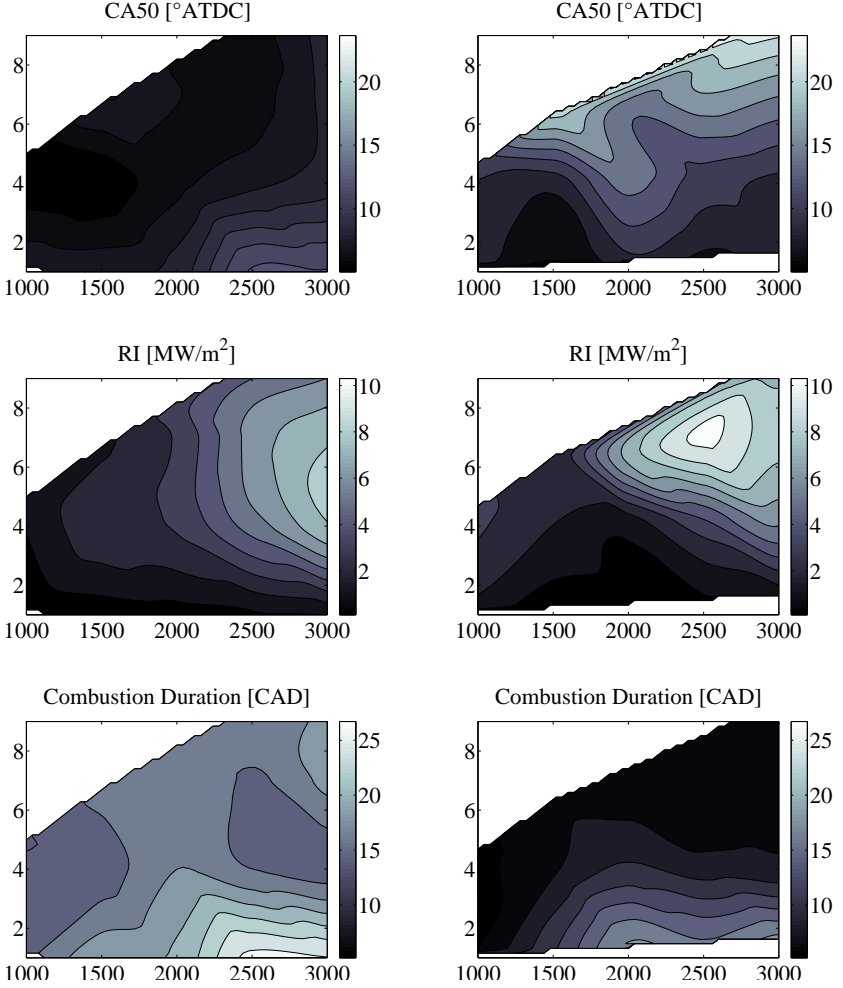
Figure 6.2   The difference in RI and combustion duration for diesel (left column) vs gasoline PPC (right column). The combustion of gasoline PPC is significantly faster.

down the rate of reaction and increases the duration of combustion. This has the effect of reducing NOx emissions and noise for both Gasoline and Diesel. However, it also results in increased soot production, although this is more severe with diesel than with gasoline and is one of the things that makes gasoline an attractive alternative to diesel. The average efficiency is similar for the both concepts.

Figure 6.3   Injection strategies for different engine loads in NMEP.

Fig. 6.3 illustrates the injection strategies and cumulative heat-release curves for loads between 1 and 10 bar NMEP at 2000rpm. The ignition delay is about 20 to 30 degrees for the single injection cases. EGR was used in the 6 bar case. At even higher loads, this alone is not sufficient, and dual injections must be used to suppress noise. This can be seen i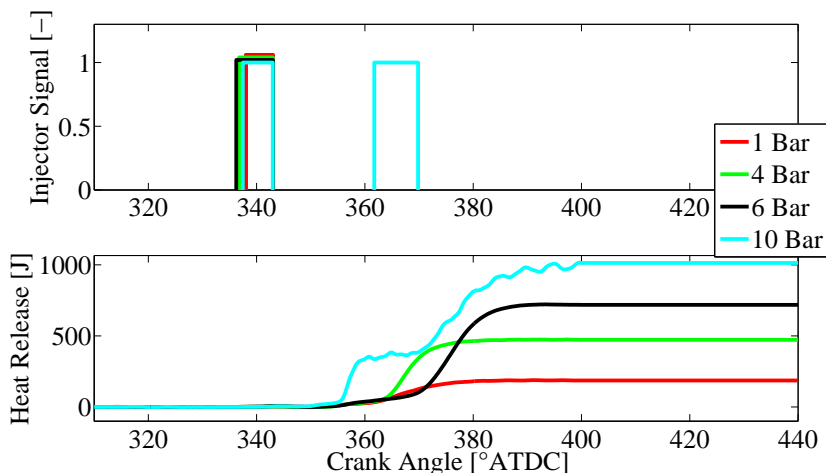n the data obtained under the 10 bar load case in the figure. This double injection strategy was tested for loads up to 18 bar NMEP, and resulted in a ringing intensity of less than 7 in all cases. Not all of the fuel is properly premixed in this double injection mode, and so the combustion process is more akin to conventional CI combustion although with gasoline.

6.2 PPC Transient Noise Control

Severe noise problems can appear during load transients. This section discusses techniques for dealing with transient load spikes in gasoline PPC mode without causing excessive noise by using a model-based approach

Excessively rapid combustion is harmful for the engine and unpleasant for the driver. Fig. 6.4 shows the ringing intensity during a gasoline PPC load transient while operating the engine using map based open loop injection control. The noise is extremely loud during the transient. The pressure traces for the corresponding load step are shown in Fig. 6.5 .
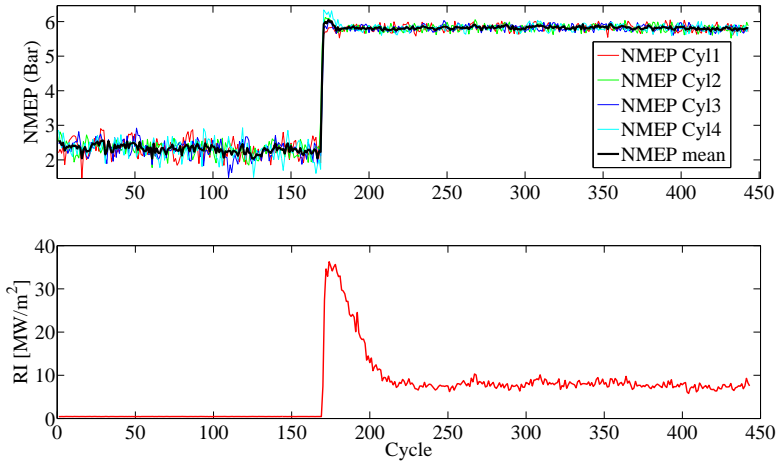
Figure 6.4 Ringing intensity during a load transient while operating the engine using map-based open loop injection control. The noise is very loud during the transient. The corresponding pressure trace is shown in Fig. 6.5.

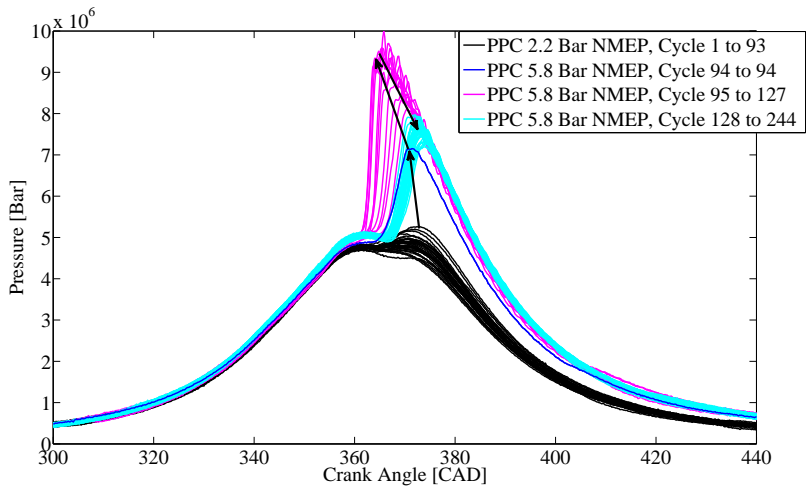**Figure 6.5** Cylinder pressure behavior for a load transient from 2.2 bar to 5.8 bar NMEP. The rapid pressure rise can be harmful for the engine. Note the oscillations on the pressure trace for the first higher load cycles (purple).

113

The main cause of the loud combustion noise is the absence of EGR and boost pressure over the transient. The noise is gradually suppressed as the intake pressure increases and the turbo spins up to settle at its new equilibrium point. The noise is also affected by the delay of the EGR which has to travel from the exhaust ports, pass through the turbine, mix with the fresh charge, and then pass through the compressor, intercooler, throttle, the intake valves before finally reaching the cylinders.

The most important outputs that need to be controlled in PPC mode are the engine load, combustion phasing, rate of pressure increase, and ringing intensity (Eq. 4.3). The last three measures are highly correlated and can to some extent be regarded as being equivalent; controlling one means controlling all of them. RI is suitable feedback for control of gasoline PPC because noise is a limiting factor for achieving high load.

A key advantage of using RI for feedback is that it will effectively result in automatic temperature correction. That is, the controller would advance the combustion in a cold engine so as to achieve the noise level expected for a hot engine. This will result in similar combustion duration and thus also similar stability for the both operating conditions. A CA50 based controller focus on maintaining the combustion phasing, meaning that the cold engine would operate with slower combustion and could potentially misfire. This could of course be dealt with by using a temperature-dependant mapping of reference CA50 value, but the RI approach requires less effort.

One way to handle the transient noise as described in Fig. 6.4 is to use double injections during the transient. This increases the combustion duration and reduces the noise. The drawback is increased soot production. A controller should therefore aim to reduce the amount of fuel in the second injection as soon as the boost pressure and EGR have been stabilized. The objective was to build a controller that could maintain an acceptable RI during the transient. The criteria for the controller was

- RI may not exceed 6 $\frac{MW}{m^2}$

- The total fuel request may not be disturbed.

- It should require little tuning

A control structure was implemented according to Fig. 6.6 . The "Total Fuel Req" shown in the figure is controlled by the main load controller.

The figure shows that a load increase would first act on the second injection, while the controller will start to rebalance the amount of fuel injected
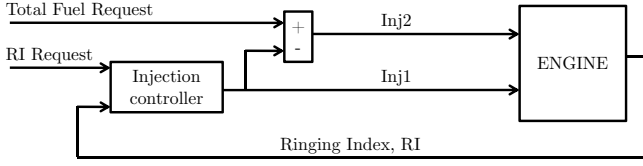
Figure 6.6   Basic structure of the RI Controller.

to achieve the desired RI-level. The injection controller was implemented as an Internal Model Controller (IMC) in order to fulfill the specified criteria.

System Identification for Controller Design

Designing an internal model controller requires a process model, $G_p(s)$ of the system to be controlled. However, the dynamics that relate the input data to engine output behavior are complex and not always easily modeled using a physical approach. Consequently, a system identification procedure was adopted to derive models describing the response of the RI, $y(k)$, to changes in the inputs, $u(k)$. The chosen inputs were the amount of fuel injected during the first and second injections. Boost pressure and EGR aside, these are the main factors that affect the noise output. The inputs were excited using Pseudo Random Binary Sequences (PRBS). The system identification process was then conducted using the N4SID script (in Matlab), which creates a dynamic model that fits the I/O data.

The model output is based on the mean RI for the four cylinders. The differences in the dynamics of the individual cylinders is not large enough to warrant the use of cylinder-specific models. The system identification process generated a statespace Multiple Input Single Output (MISO) model of the form

$$X(k+1) = AX(k) + Bu(k) \tag{6.1}$$

$$y(k) = CX(k) + Du(k) \tag{6.2}$$

System identification was conducted using two data sets. The first data set was used for model generation while the other was used to validate the data. The results of this validation can be seen in Fig. 6.7.

Internal Model Control - Introduction

The structure of the internal model controller is best described by Fig. 6.8

Measured and simulated model output
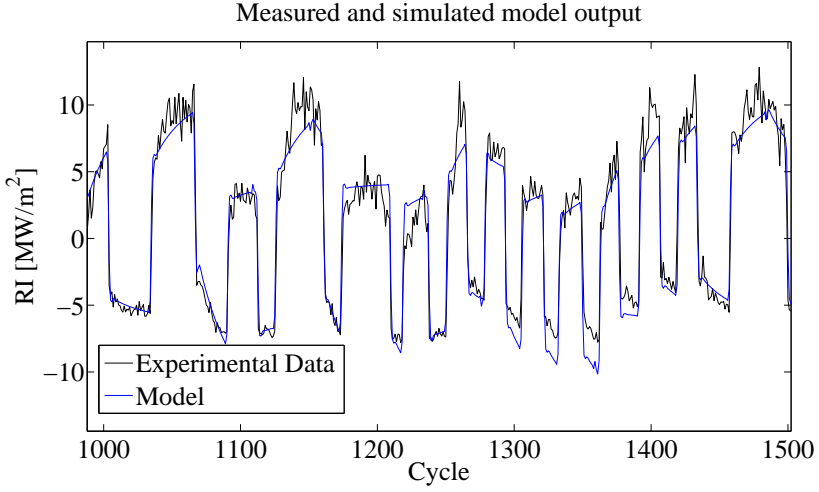
Figure 6.7   Comparison of the model's predictions and experimental data.
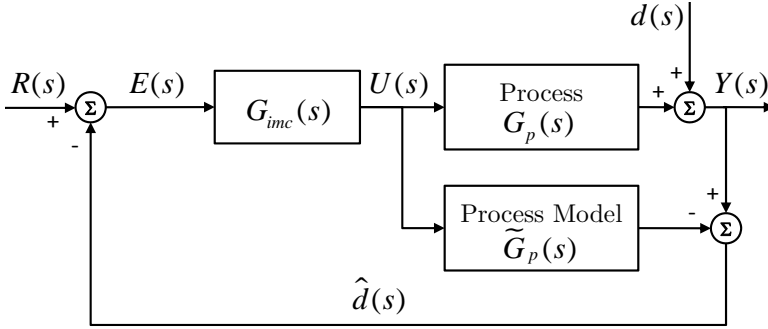
Figure 6.8   The structure of an Internal Model Controller.

or by the corresponding closed loop system equation

$$Y(s) = \frac{G_{imc}(s)G_p(s)R(s) + [1 - G_{imc}(s)\tilde{G}_p(s)]d(s)}{1 + [G_p(s) - \tilde{G}_p(s)]G_{imc}(s)} \qquad (6.3)$$

$G_{imc}(s)$ consists of the invertible part, $\tilde{G}_p^+(s)$, of the process model, $\tilde{G}_p(s)$ and a low-passfilter,$G_f(s)$ which is used for controller tuning.

$$G_{imc}(s) = \tilde{G}_p^+(s)^{-1}G_f(s) \qquad (6.4)$$

If it is assumed that $G_p(s) = \tilde{G}_p(s)$, Eq. 6.3 becomes

$$Y(s) = \tilde{G}_p^+(s)^{-1}G_f(s)G_p(s)R(s) + [1 - \tilde{G}_p^+(s)^{-1}G_f(s)\tilde{G}_p(s)]d(s) \quad (6.5)$$

which gives the following closed loop system

$$Y(s) = \tilde{G}_p^-(s)G_f(s)R(s) + [1 - \tilde{G}_p^-(s)G_f(s)]d(s) \quad (6.6)$$

where $\tilde{G}_p^-$ contains the parts of $\tilde{G}_p$ (such as timedelays) that cannot be inverted without introducing realisability problems or positive half plane zeros that would create unstable poles if inverted. One can from Eq. 6.6 see

- That the model's step-response behavior and disturbance rejection can be tuned using the low-passfilter $G_f(s)$

- That the controller provides time delay compensation. This is given by the fact that there is no extra term than $\tilde{G}_p^-$, which contans the time delay of the open loop system.

- That the controller will provide offset-free tracking. This is given by the fact that the steady state gain of $\tilde{G}_p^-(s)G_f(s)$ equals 1.

Internal model control is an intuitive and simple way of designing a controller that requires little tuning and has only one "control knob" in the form of the filter $G_f(s)$.

Designing G_{IMC}

The objective was to create a discrete time version of Eq. 6.3. This requires a transfer function, $\tilde{G}_p(z)$ derived from the statespace model obtained by the systems identification approach described above. The model describes the dynamics from the first injection to the output, RI.

$$\tilde{G}_p(z) = \frac{-0.27752(z - 4.33)(z - 0.5175)}{(z - 0.7324)(z^2 - 0.7749z + 0.412)} \quad (6.7)$$

The transfer function has a zero outside of the unit circle that would become an unstable pole if inverted. It also has timedelays that would provide realisability problems if inverted. These parts of the transfer function are collectively denoted by G_p^-

$$G_p^- = \frac{(z - 4.33)}{z^2} \quad (6.8)$$

The invertible part, G_p^+, is thus

$$G_p^+(z) = \frac{-0.27752(z - 0.5175)z^2}{(z - 0.7324)(z^2 - 0.7749z + 0.412)} \qquad (6.9)$$

As such, according to Eq. 6.4, G_{IMC} can be calculated as follows:

$$G_{IMC}(z) = \frac{(z - 0.7324)(z^2 - 0.7749z + 0.412)}{-0.27752(z - 0.5175)z^2} G_f(z) \qquad (6.10)$$

If it is assumed that $G_p(z) = \tilde{G}_p(z)$, the output of the closed loop system described by Eq. 6.6 becomes

$$Y(z) = \frac{(z - 4.33)}{z^2} G_f(z)R(z) + [1 - \frac{(z - 4.33)}{z^2} G_f(z)]d(s) \qquad (6.11)$$

It is apparent that the closed loop system retains the dynamic behavior of the non-invertible part of $\tilde{G}_p(z)$ and that its dynamic response can be tuned by adjusting the frequency of the lowpass filter $G_f(z)$. The cutoff frequency was increased until a level just before unstable conditions was starting to occur.

Noise Control Experiments using Internal Model Control

The internal model controller was incorporated as the "injection controller" in Fig. 6.6. The engine was operated with and without injection control; the use of the injection controller was found to afford significantly improved noise levels. As can be seen in Fig. 6.9 , under the noise-controlled regime, load increases do not cause the engine to exceed the specified noise level whereas under the map-based regime, load increases generate noise that greatly exceeds acceptable limits (Fig. 6.4). The pressure traces for the RI-controlled load increase are shown in Fig. 6.10 . Note how the double injections affects the combustion behavior and how it changes after the switch to single injection.

Double injection is a powerful tool for suppressing noise and should be used. However, it is not obvious how best to implement it. For example, it would be possible to manage noise during the transient by mapping the compensatory double injection instead of using a feedback controller, although this would be more labor-intensive.

6.3 Switching between PPC and SI modes

This section discusses strategies for switching between PPC and SI modes.
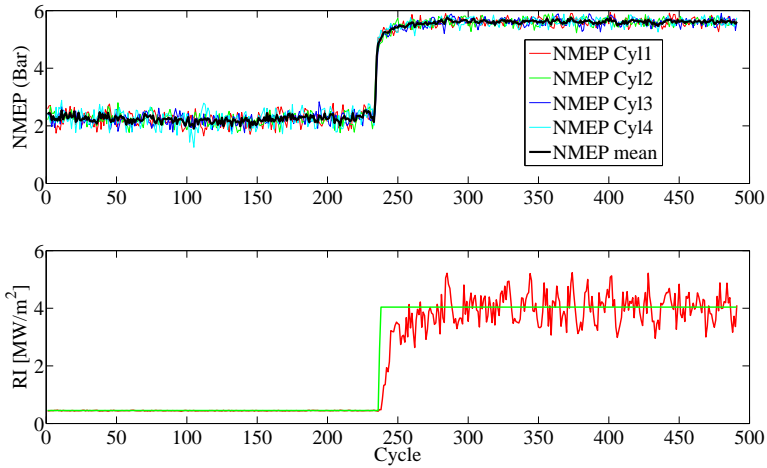
Figure 6.9   The noise remains within reasonable limits during the transient when using internal model control of RI. The improvement over the load transient shown in Figure. 6.4 is obvious.
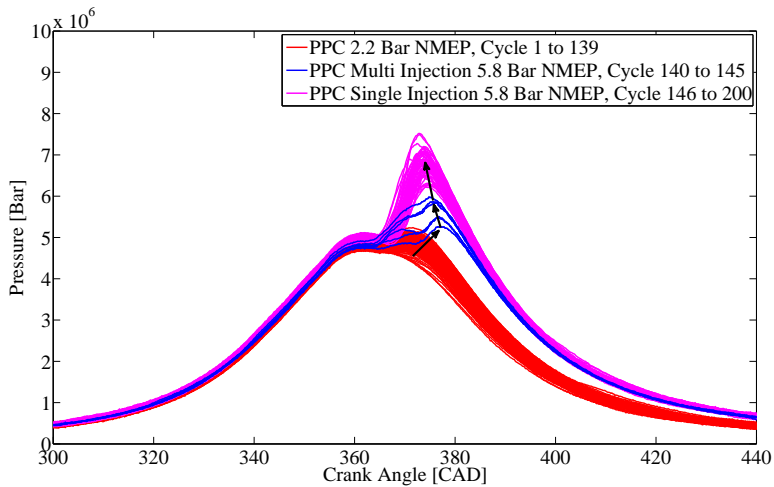
Figure 6.10   Cylinder pressure during a load transient from 4 to 6 bar when using RI-control. Each cycle is shown. Note the two combustion peaks that occur during the first cycles. These are due to the double injections used to maintain low noise levels. The figure should be compared to Fig. 6.5, which shows an analogous load step without noise control.

If the engine is heated, it is possible to operate in PPC mode using 70 Octane gasoline at all loads including idling, but it is difficult to initiate the combustion if the engine is cold or if a fuel with a higher octane rating is used.

This problem can be eliminated by operating in SI mode under circumstances where PPC combustion would be difficult to achieve. This requires the ability to switch between PPC and SI as appropriate. However, the two combustion concepts differ in some fundamental respects, which makes such switching difficult. PPC requires conditions that favor self ignition, but self ignition (or knock) is not at all desired during SI combustion. Another difference is the timing of the injections. The fuel is injected during the intake stroke in SI mode but during the compression stroke in PPC mode.

PPC requires that the throttle is fully open, while SI mode requires stoichiometric conditions and thus imposes restrictions on the acceptable air mass flow. There is unfortunately a zone between these concepts where the gas temperature and air massflow will be too high for SI but the mixture temperature and pressure will be too low for PPC. Since the engine is unable to operate in this "dead zone," the change from high to low intake pressure and back must be achievable at a rate corresponding to 1/4 of a cycle for a four cylinder engine.

The Modeswitching Algorithm and Experiments

Mapped control schemes were implemented in an attempt to achieve a mode switch. The first cycle-to-cycle SI to PPC switch was achieved by fully opening the throttle while simultaneously changing the timing of injection from the intake stroke to the compression stroke. This did work, but extreme rates of pressure increase were noted in a few cycles during the switch. During these cycles, HCCI-like combustion took place at a far too early stage because fuel was injected during the intake stroke while the throttle was open.

A smoother way of achieving the mode switch is to introduce stratified SI combustion in between the conventional SI and PPC modes. In this way, a more PPC-like injection timing is introduced, and cycles with extremely early HCCI combustion can be avoided when the throttle opens. Typical results obtained using the later switching scheme are shown in Fig. 6.11. This figure also shows how the most important signals behave during the switches. It is interesting to note the increase in NMEP that occurs for the PPC mode. The amount of fuel injected is constant for the two modes, illustrating the higher efficiency achieved in PPC mode.

Fig. 6.12 shows the pressure traces for a mode switch using 70 octane gasoline. The first, "red" cycles are those observed during conventional SI combustion,
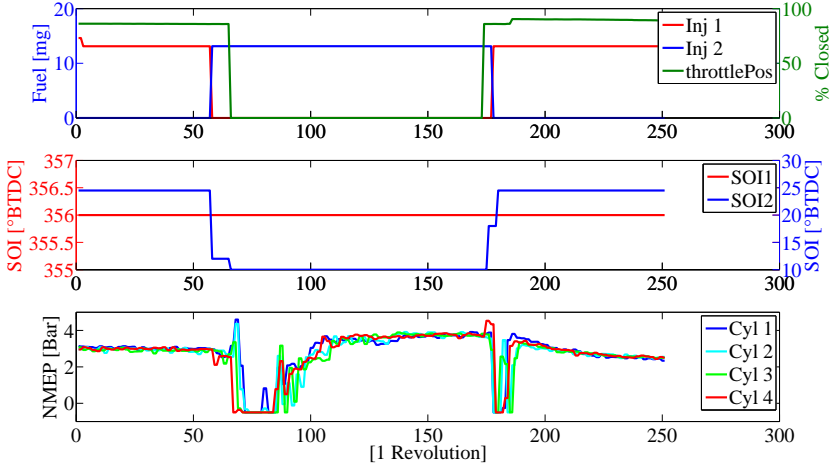
Figure 6.11   The NMEP during mode switches from SI to stratified SI to PPC to stratified SI and finally back to SI).

The following two "green" cycles represent stratified SI. The throttle is fully opened after these cycles. Although combustion is successfully initiated in the cycles immediately after the opening of the throttle (as shown by the blue pressure trace), a series of misfires occurred. The first PPC cycle was however initiated because of the hot residuals from the previous SI cycle.

The residual gas temperature is lower for PPC, resulting in a reduced mixing temperature after the first PPC cycle. This is the reason for the series of misfires observed (the yellow traces). As the inlet pressure gradually increases, the mixture achieves semi-beneficial conditions and the engine enters into an unstable PPC-type mode with misfires every second cycle (as shown by the magenta traces). As the boost pressure increases, the combustion stability increases until it eventually reaches a stable equilibrium point, shown by the black traces.

It is possible that the misfires could be minimized if the injection were advanced for the first couple of cycles in which they occurs. However this would also expose the engine to a high risk of early combustion, which could be highly damaging. The best solution would be to achieve a higher intake pressure at an earlier point in the transition. Unfortunately, this would not be straightforward to accomplish. Another solution, which would be easier to implement, would be to use controllable negative valve overlap, which cap-
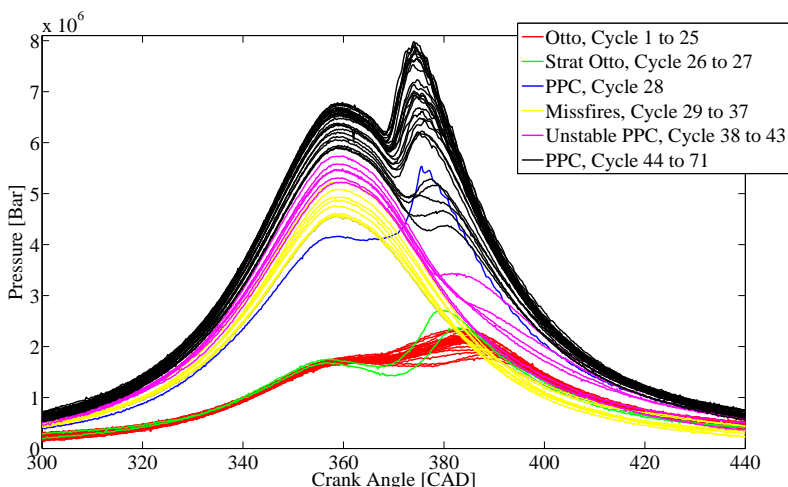
Figure 6.12 A mode switch from SI to PPC, showing the changes in cylinder pressure as the engine switches between the different modes.

tures hot residuals that can heat up the mixture. To achieve this, the timing of EVC should be advanced after the first PPC cycle and then gradually decreased so as to avoid premature early combustion.

A mode switch from PPC to SI is easier and should be possible to achieve without misfires or hardware modifications, although a higher degree of tuning is required. The pressure traces for this switch are shown in Fig 6.13. The intake pressure falls when the throttle closes and the combustion conditions enter what was previously described as the dead zone (green color). Combustion is initiated in the following (blue) cycle. This event is due to the accumulated fuel from the two previous misfires. The next, yellow cycle is excessively lean, and a misfire occurs. There are then two (magenta) cycles that are more lean than would be ideal but are rich enough to enable combustion. After this, the engine attains a steady state and operates under stoichiometric conditions, represented by the black cycles. A dump valve would make it easier to reduce the intake pressure more quickly.

6.4 Discussion

Most of the gasoline experiments discussed in this chapter were performed using 70 octane gasoline. Using this fuel, it is possible to operate in PPC
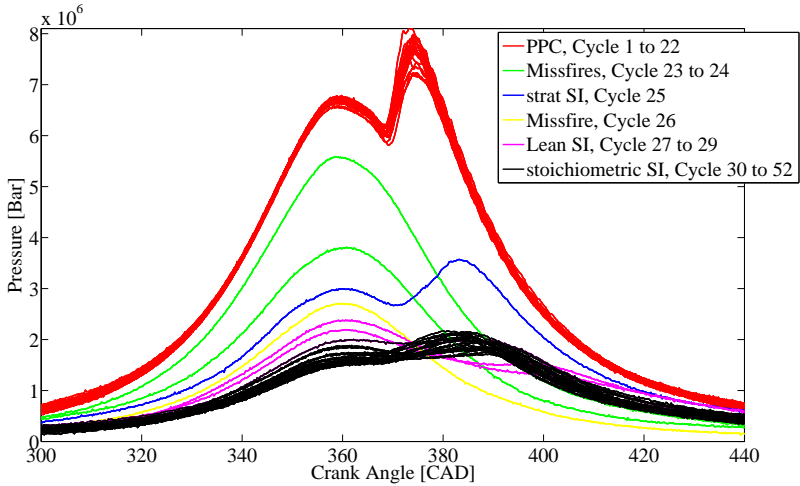
Figure 6.13   A PPC to SI mode switch demonstrating the cylinder pressure associated with the different modes that the engine has to go through.

mode while idling provided that the engine is heated. Fig. 6.14 shows what happens when the engine is started up at a temperature of 20 °C. A fuel mass corresponding to 4 bar NMEP is required to initiate the combustion. The first 400 cycles exhibit large cycle to cycle variation, which stabilises as the wall temperature increases. After around 2000 cycles, the engine was operated at a load of 0.1 bar, which is less than that which would be imposed by idling.

95 octane gasoline is a more demanding fuel, and it is almost impossible to initiate the combustion with a cold engine at any fueling level. This difficulty can be avoided by heating the engine, in which case a quantity of fuel corresponding to around 8 bar NMEP is needed to initiate combustion. The lower load limit for sustainable operation with this fuel is around 4 bar NMEP at 2000 RPM. This can be seen in Fig. 6.15 ; combustion gradually starts to fail when the load falls below 4 bar NMEP at cycle 1200.

As described above, controllable Negative Valve Overlap could probably be used to extend the operating range of PPC down to idle even with 95 octane gasoline. Another alternative would be to increase the compression ratio. However, this would increase the peak pressure, NO_x emissions, and also limit the peak load, which is not desired.

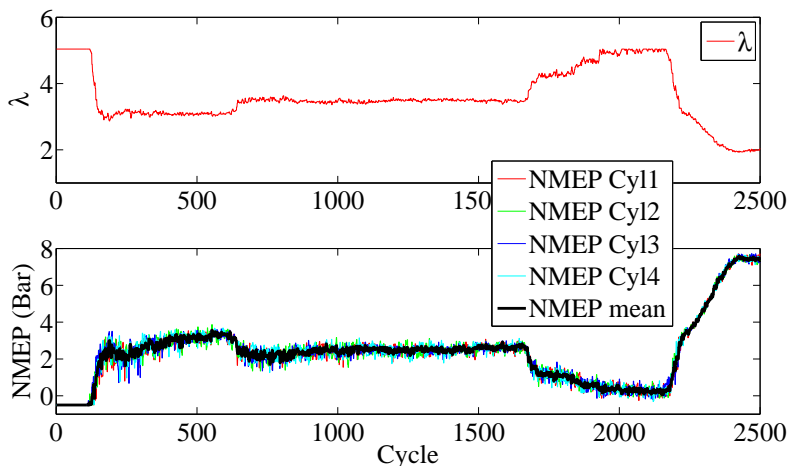The negative valve overlap strategy relies on residuals from the previous

Figure 6.14 Startup of the engine with an engine temperature of 20 °C. The first 400 cycles exhibit large variation which stabilises as the wall temperature rises. The engine is operated at a load below that which would be encountered when idling after approximately 2000 cycles.

cycle to initiate combustion. This is not possible in the first cycle since no residuals exists. A potential solution to this would be to crank the engine with high Negative Valve Overlap, inject fuel corresponding to $\lambda \approx 0.8$ just after EVC, and ignite the mixture over the NVO using a sparkplug. This would create hot residuals that would mix with the fresh charge during the intake stroke. The combination of NVO for low load PPC and SI over the first recompression event during cold starts could make it possible to completely eliminate the need for SI under low loads.

Another alternative solution to the cold start problem would be to use a more suitable fuel, such as diesel. A reasonable estimate of the mean heat up period that would be necessary using diesel would be the first 500 cycles (depending on load), after which 70 octane gasoline could be used. The engine would then be able to idle. A 5-liter tank of diesel would suffice for up to 800 cold starts using this strategy. Similar results should be possible with 95 octane gasoline if NVO were also used.

An alternative way of implementing CCC (Fig. 6.1) is shown in Fig. 6.16 . This approach could conceivably prove superior because it would allow for higher efficiency without using SI combustion. The maximum speed attainable under this concept would be lower since SI isn't used. It might however
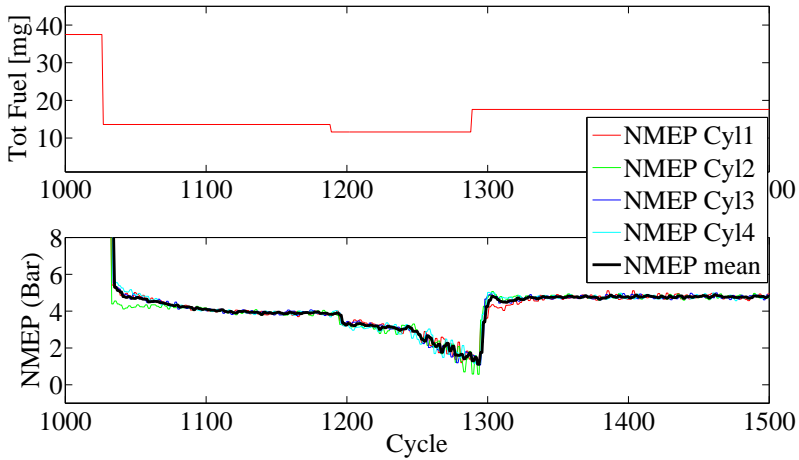
Figure 6.15   Combustion gradually starts to fail as the load falls below 4 bar NMEP at 2000 RPM when using 95 octane gasoline.
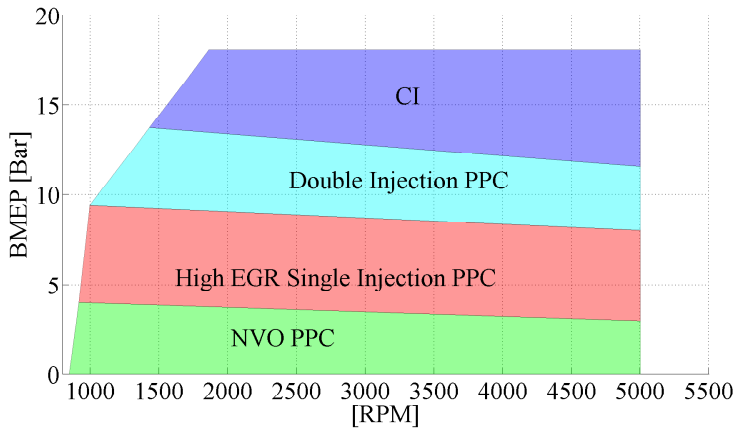
Figure 6.16   Speed/load profiles for the revised CCC structure, showing under what conditions the different combustion modes would be used.

be higher than is possible with conventional diesel engines because of the short duration of PPC combustion. It should therefore be possible to achieve higher specific power output using gasoline.

6.5 Conclusions

With the large amount of EGR that is required for PPC, load transients can cause excessive combustion noise (see Fig. 6.4) unless action is taken to handle the time delay associated with the movement of the residuals through the long-route EGR system. The approach adopted for dealing with this issue was to use double injections during transients. These double injections are managed using Internal Model Control. Using this controller, smooth progress through load transients was achieved without excessive or disturbing combustion noise.

If SI combustion is to be used in CCC, the engine must be able to smoothly switch between different modes of operation. Attempts were made to achieve this without excessively rapid pressure increases by using 2-3 cycles of stratified combustion as a buffer between the PPC and SI modes. This did work, but did not eliminate the problem of misfiring. A successful mode switch from SI to PPC will necessarily be associated with a sharp increase in the intake pressure and/or mixture temperature. Going from a throttled mode of operation to one in which the intake pressure is higher than atmospheric pressure is not easy. It is therefore important to be able to achieve PPC combustion with an atmospheric intake pressure. This could be achieved by increasing the mixture temperature, for example by using NVO. Mode switches from PPC to SI are less problematic and should be possible to achieve without misfires.

Ideally, it would not be necessary to use SI at all. Using 70 octane gasoline, the engine can be operated in PPC mode even while idling. It is extremely difficult to initiate the combustion if the engine is cold and using 95 octane gasoline . However, because of its widespread availability, it is important that an engine is able to run on 95 octane. The preferred way of achieving this would be to operate the engine in different modes as shown in Fig. 6.16. A large difference between NVO PPC and NVO HCCI is that in the former, the primary function of the negative valve overlap would be to heat the mixture enough to allow full and direct control of the combustion process through the injection timing. In the HCCI case, the negative valve overlap is the main "control knob" and precise temperature control is needed, which makes it difficult to operate without feedback. However, for PPC, even with valve overlap control, it would be hard to initiate combustion because no hot residuals are available during the first cycle. Three solutions to the cold start problem were considered. The first focused conventional SI combustion. The second focused on using spark-initiated combustion over the gas exchange TDC in the first cycle and NVO PPC in the following cycles. The third solution involves using dual fuels in combination with NVO.

Gasoline PPC with high dilution of the recirculated exhaust gas seems to generate favourable emissions profiles relative to diesel combustion and merits further investigation to establish its true potential. Future work should be focused on the development of engines and controls suitable for use with regular 95 octane gasoline. A number of ways by which this could be achieved have been outlined. Gasoline PPC represents a potentially very significant advance over HCCI in terms of combustion stability, which makes it very attractive from a control perspective.

7

Conclusions and Future Work

7.1 Conclusions

Solutions for modeling and control of a Turbo NVO HCCI and a CCC engine have been presented and tested experimentally. Closed loop combustion control is a powerful tool for achieving low emissions and noise as well as high reliability and efficiency. The limiting factors that make these goals hard to achieve are the bandwidth of the HCCI controllers and the engine's physical constraints. The work described in this thesis generated contributions to the following areas.

Feedback Sensors

A series of ion current experiments were performed; it was found that the shape of the signal was similar from cycle to cycle and was not significantly affected by variation in either Air-Fuel Ratio or speed. This opened up for the possibility of using a matched filter to maximize the SNR and detect ion currents at conditions where no useful data would otherwise be obtained. Some feedback experiments using ion currents demonstrated that sensors of this kind could be useful alternatives to pressure sensors at loads above 2.4 bar NMEP. At low loads, the SNR from an ion current sensor is too low which results in unreliable control.

Experiments with a torque sensor demonstrated that the pressure traces in each cylinder could be reconstructed using a combination of measurements of the physical torque, combustion models, and black box models. It was possible to determine the CA50 from the procedure used to reconstruct the pressure traces. While the CA50 values estimated in this way were promisingly accu-

rate, the limited scope of the experiments does not allow any firm conclusion regarding the reliability of this approach to be drawn. The method must be evaluated over a wider range of operating conditions at different speeds and loads in order to fully assess its performance and robustness. The proposed algorithm is not suitable for real-time implementation and should be further refined so as to be less computationally demanding.

A Physical approach to HCCI Modeling and Controller Design

A combustion model of the engine was developed that successfully reproduces some of the engine's behavior. The model operates in a cycle-to-cycle fashion, using the simulated data for a complete cycle to estimate the residual mass, cylinder air charge, and temperature at TDC. This temperature is mapped against experimental CA50 data to determine when combustion should begin. Experimental results shows good correlation against experimental transient data. The model was used to design a Kalman state estimator and an LQR feedback controller. In addition, the nonlinear combustion model was inverted to create a feedforward compensator. Transient improvements could be achieved using this approach.

Combined Combustion Concepts

It was demonstrated how a modified diesel engine was able to operate according to multiple different combustion concepts - Diesel, SI and PPC. To the author's knowledge, the multi mode engine concept articulated in this thesis has no predecessors elsewhere.

It is preferable to operate the engine with large amounts of EGR in PPC mode. However, this means that transient load steps can give rise to excessive combustion noise if action is not taken to mitigate the time delay associated with the movement of the exhaust through the long-route EGR system. The approach adopted for solving this problem involves using double injections during transients. These double injections are managed by an internal model controller that applies just enough double injection in order to limit the fuel penalty associated with it. Using this controller, the engine was able to handle load transients smoothly and without excessive or disturbing combustion noise.

Strategies for switching the engine's mode of operation from SI to PPC and back were tested. These are the first such switches ever reported in the literature.

7.2 Future Work

The natural next step in the search for high efficiency engines would be to further develop the PPC concept. To make the concept suitable for use in mass production engines, attention should be focused on identifying ways to allow PPC engines to handle low loads using regular 95 octane fuel. This could be done by operating the engine with negative valve overlap at low loads. As is the case with HCCI engines, this would increase the mixture temperature and facilitate self ignition. One of the drawbacks of using HCCI in combination with NVO is that NVO is the primary actuator for achieving the required temperature at the start of combustion. In the PPC case, NVO would play a secondary role, with the primary actuator being the injection timing. Combustion in such an engine would therefore be easier to control. However, if this strategy were adopted, it would be necessary to use some kind of ignition trigger to initiate combustion in the first cycle of the startup process. This could be achieved by using SI combustion for the first couple of cycles. In conjunction with NVO, this mode switch would be less problematic than those attempted experimentally because PPC combustion would be achievable without the need for elevated intake pressure.

It is possible that gasoline PPC engines could be operated without combustion feedback if they were better understood. However, data on combustion feedback events would allow for improved control of the process. Ion current experiments similar to those performed with HCCI should be performed in PPC engines. It is possible that ion current could be used across the entire speed load range, generating useful input data for the ECM.

8

Bibliography

[1] M. Fischer, M. Werber, and P. Schwartz, "Batteries: Higher energy density than gasoline?" *Elsevier*, vol. Energy Policy 37, 2009.

[2] S. Kook and C. Bae, "The influence of charge dilution and injection on low-temperature diesel combustion and emission." *SAE Paper No. 2005-01-3837*, 2005.

[3] P. M. Najt and D. E. Foster, "Compression-ignited homogeneous charge combustion." *SAE Paper No. 830264*, 1983.

[4] G. Kalghatgi, L. Hildingsson, and B. Johansson, "Advantages of a fuel with high resistance to auto ignition in late-injection, low-temperature, compression ignition combustion." *SAE Paper No. 2006-01-3385*, 2006.

[5] G. T. Kalghatgi, P. Risberg, and H. Ångström, "Partially pre-mixed auto-ignition of gasoline to attain low smoke and low nox at high load in a compression ignition engine and comparison with a diesel fuel." *SAE Paper No. 2007-01-006*, 2007.

[6] J. Hyvönen, "The performance of a multi cylinder hcci engine using variable compression ratio and fast thermal management." Ph.D. dissertation, Lund Institute of Technology, Lund, 2005.

[7] G. Haraldsson, "Closed-loop combustion control of a multi cylinder hcci engine using variable compression ration and fast thermal management." Ph.D. dissertation, Division of Combustion Engines, Lund institute of Technology, Sweden, 2005.

[8] L. Cummins, *Internal Fire.* Carnot Press, 1976.

[9] Four-stroke-cycle engine. (downloaded 110225). http://visual.merriam-webster.com/transport-machinery/road-transport/types-engines/four-stroke-cycle-engine.php. Visual Dictonary Online.

[10] T. Johansson, H. Aulin, B. Johansson, and P. Tunestål, "Hcci operating range in a turbocharged multi cylinder engine with vvt and spray-guided di.." *SAE Paper No. 2009-01-0494*, 2009.

[11] J. Hyvönen, G. Haraldsson, and B. Johansson, "Super charging hcci to extend the operating range in a multi cylinder vcr-hcci engine." *SAE Paper No. 2003-01-3214*, 2003.

[12] M. Christensen, B. Johansson, P. Amnéus, and F. Mauss, "Supercharged homogeneous charge compression ignition." *SAE Paper No. 2000-01-1835*, 2000.

[13] H. Aulin, T. johansson, P. Tunestål, and B. Johansson, "Control of a turbo charged nvo hcci engine using a model based approach." *IFAC Workshop on Engine and Powertrain Control, Simulation and Modeling*, 2009.

[14] M. Lewander, B. Johansson, P. Tunestål, N. Keeler, N. Milovanovic, and P. Bergstrand, "Cloosed loop control of a partially premixed combustion engine using model predictive control strategies." *AVEC 08 Proceeding 006*.

[15] *Communication from the commission to the european parliament and council, A Competitive Automotive Regulatory Framework for the 21st Century Commission's position on the CARS 21 High Level Group Final Report.*, Commission of the european communities Std.

[16] P. Tunestål, "Estimation of the in-cylinder air/fuel ratio of an internal combustion engine by the use of pressure sensors." Ph.D. dissertation, Lund Institute of Technology, 2001.

[17] P.Tunestål, "Self-tuning gross heat release computation for internal combustion engines." *Control Engineering Practice*, 2009.

[18] J. B. Heywood, *Internal Combustion Engine Fundamentals.* London: McGraw-Hill International, 1988.

[19] N. Collings, S. Dinsdale, and D. Eade, "Knock detection by means of the spark plug." *SAE Paper No. 860635*, 1986.

[20] P. Strandh, M. Christensen, J. Bengtsson, R. Johansson, A. Vressner, P. Tunestål, and B. Johansson, "Ion current sensing for hcci combustion feedback.." *SAE Paper No. 2003-01-3216*, 2003.

[21] A. Franke, "Diagnostics of electrical phenomena in gases for the monitoring of spark-ignited combustion." Ph.D. dissertation, Division of Combustion Physics, Lund Institute of Technology, Lund, 2000.

[22] R.Reinmann, "Theoretical and experimental studies of the formation of ionized gases in spark ignition engines." Ph.D. dissertation, Lund Institute of Technology, Lund, 1998.

[23] L. Sörnemo and P. Laguna, *Bioelectrical Signal Processing in Cardiac and Neurological Applications.* Lund: Academic Press, 2005.

[24] C. Wallin, L. Gustavsson, and M. Donovan, "Engine monitoring of a formula 1 racing car based on direct torque measurement." *SAE International*, vol. 2002-01-0196, 2002.

[25] I. Andersson and T. McKelvey, "Torque ratio concept for combustion phasing detection of a spark ignited engine." *IEEE Conference on Decision and Control*, 2004.

[26] I. Andersson and S. Larsson, "Self-optimising control of an si-engine using a torque sensor." *Control Engineering Practice*, 2005.

[27] R. B. GmbH, *Bosch Automotive Handbook, 5th Edition.*, 2000.

[28] B. Johansson, *Förbränningsmotorer.* Lund: Lund University Faculty of Engineering, 2003.

[29] A. Bjerhammar, *Theory of errors and generalized matrix inverses.* Stockholm: Elsevier publishing company, 1973.

[30] G. Colin, P. Giansetti, Y. Chamaillard, and P. Higelin, "In-cylinder mass estimation using cylinder pressure." *SAE Paper No. 2007-24-0049*, 2007.

[31] D. S. Stanglmaier and E. Roberts, "Homogenous charge compression ignition (hcci)." *SAE Paper No. 1999-01-3682*, 1999.

[32] P. Strand, "Hcci operation - closed loop combustion control using vva or dual fuel." Ph.D. dissertation, Lund Institute of Technology, Lund, 2006.

[33] G. Haraldsson, P. Tunestål, B. Johansson, and J. Hyvönen, "Hcci combustion phasing with closed-loop combustion control using variable compression ratio in a multi cylinder engine." *SAE Paper No. 2003-01-1829*, 2003.

[34] F. Agrell, H. Ångström, B. Eriksson, J. Wikander, and J. Linderyd, "Transient control of hcci through combined intake and exhaust valve actuation." *SAE Paper No. 2003-01-3172*, 2003.

[35] J. Hyvönen and B. Johansson, "Hcci operating range with vnt turbo charging." *Haus der Technik*, 2005.

[36] J. Souder, "Closed-loop control of a multi-cylinder hcci engine." *Homogenus Charge Compression Ignition Symposium*, 2004.

[37] G. M. Shaver, M. J. Roelle, and J. C. Gerdes, "Modeling cycle-to-cycle dynamics and mode transition in hcci engines with variable valve actuation." *Control Engineer Practice 14*, pp. 213–222, May 2006.

[38] F. Agrell, H.-E. Ångström, B. Eriksson, J. Wikander, and J. Linderyd, "Control of hcci during engine transients by aid of variable valve timings through the use of model based non-linear compensation." *SAE Paper No. 2005-01-0131*, 2005.

[39] M. Shahbakhti, R. Lupul, and C. R. Koch, "Predicting hcci auto-ignition timing by extending a modified knock-integral." *SAE Paper No. 2007-01-0222*, 2007.

[40] D. Blom, M. Karlsson, K. Ekholm, P. Tunestål, and R. Johansson, "Hcci engine modeling and control using conservation principles." *SAE Paper No. 2008-01-0789*, 2008.

[41] W. Fischer, R. Karrelmeyer, A. Loffler, A. Kulzer, and J.-P. Hathout, "Closed-loop control of a multi-mode gdi engine with cai." *5th IFAC Symposium on Advances in Automotive Control*, 2007.

[42] J. C. Gerdes, "Cycle-to-cycle control of hcci engines with variable valve actuation." *Homogenus Charge Compression Ignition Symposium*, 2004.

[43] N. Ravi, M. J. Roelle, H.-H. Liao, A. F. Jungkunz, C.-F. Chang, S. Park, and J. C. Gerdes, "A physically based two-state model for controlling exhaust recompression hcci in gasoline engines." *Paper IMECE2006-15331*, 2006.

[44] J. Bengtsson, P. Strandh, R. Johansson, P. Tunestål, and B. Johansson, "Multi-output control of a heavy duty hcci engine using variable valve actuation and model predictive control." *SAE Paper No. 2006-01-0873*, 2006.

[45] *Matlab Help, Control System Toolbox - Kalman.*

[46] *Matlab Help, Control System Toolbox - LQRY.*

[47] H. Aulin, T. Johansson, P. Tunestål, and B. Johansson., "Thermodynamic modeling and control of a turbo hcci engine," *Iasted Controls and application*, 2009.

[48] G.T.Kalghatgi, L.Hildingsson, and B.Johansson, "Low nox and low smoke operation of a diesel engine using gasoline-like fuels." *Internal Combustion Engine Division (ICED) 2009 spring technical conference. Paper No. ICES2009-76034*, 2009.

[49] L. Hildingsson, B. Johansson, N. Tait, G. Kalghatgi, and A. Harrison, "Fuel octane effects in the partially premixed combustion regime in compression ignition engines." *SAE Paper No. 2009-01-2648*, 2009.

A

T_{ivc} Estimation Method

From the experiments in the chapter "Turbo NVO HCCI Dynamics" it was noted that the start of combustion temperature remains constant for a specific combustion timing, independent of the fuel mass. The method for estimating the temperature is based on the assumption that the system can be consider as a closed system. There are two gases in the cylinder that are assumed to be ideal gases, the residuals and the fresh air charge. If it is also assumed that there is no energy transfer to or from the cylinder can the temperature at IVC be estimated as.

$$T_{ivc} = \frac{m_r T_r C_{vr} + m_{in} T_{in} C_{vf}}{m_r C_{vr} + m_{in} C_{vf}} \tag{A.1}$$

Where C_{vr}, C_{vf} is the specific heats for the residuals and air. $m_r T_r$ is the product of the mass and temperature of the residuals at intake pressure. During very slow changes in operating point can m_{in} and T_{in} can be measured by the mass flow meter and thermocouples placed in the inlet. T_r could be estimated using the temperature readings from the exhaust manifold but m_r is not possible to measure directly. One way to estimate m_r is to use known volume and cylinder pressure readings from the negative valve overlap and use it together with the ideal gas law according to

$$m_r = \frac{P_{evc} V_{evc}}{R T_{evc}} \tag{A.2}$$

In a similar way the temperature of the residuals at manifold pressure can be described by

$$T_r = \frac{P_{ivo} V_{ivo}}{R m_r} \left(\frac{P_{im}}{P_{ivo}} \right)^{\frac{\gamma-1}{\gamma}} \tag{A.3}$$

To improve the measurements of $P_{ivo} V_{ivo}$ or $P_{evc} V_{evc}$ should a least squares estimate similar to Eq. 4.39 be used

B

Abbreviations

AM	Amplitude Modulation
ATDC	After Top Dead Center
BTDC	Before Top Dead Center
CA	Crank Angle
CA50	Crank Angle of 50% Heatrelease
CAD	Crank Angle Degree
CA_{ionMax}	Crank Angle for peak ion current
CI	Compression Ignition
COV	Coefficient of variation
DI	Direct Injection
ECM	Engine Control Management
EGR	Exhaust Gas Recirculation
EVC	Exhaust Valve Closing
EVO	Exhaust Valve Opening
HCCI	Homogeneous Charge Compression Ignition
IVC	Intake Valve Closure
IVO	Intake Valve Opening
LQG	Linear-quadratic Gaussian (controller)
LTC	Low Temperature Combustion
mfb	mass fraction burnt
MISO	Multiple Input Single Output
NVO	Negative Valve Overlap
PID	Proportional Integral Derivative (controller)

PM	Particulate Matter
PPC	Partially Premixed Combustion
SCR	Selective Catalytic Reduction
SI	Spark Ignition
SISO	Single Input Single Output
SNR	Signal to Noise Ratio
SOI	Start Of Injection
TDC	Top Dead Center
TDC_f	Top Dead Center firing
TPU	Time Processing Unit
TWC	Three Way Catalyst